The Impact of WH/TS Codes in Implementing Incoherent OCDMA System

By

Siti Khadijah Idris @ Othman

A thesis submitted for the Degree

Of

Doctor of Philosophy

Centre for Intelligent Dynamic Communications (CIDCOM)

Department of Electronic & Electrical Engineering

University Of Strathclyde

Glasgow G1 1XW

United Kingdom

August 2014

This thesis is the result of the author's original research. It has been composed by the author and has not been previously submitted for examination, which has led to the award of a degree. The copyright of this thesis belongs to the author under the terms of the United Kingdom Copyright Acts as qualified by University of Strathclyde Regulation 3.50. Due acknowledgement must always be made of the use of any material contained in, or derived from, this thesis.

Signed: Date:

Committee in-charged:

Chair : Dr. Vladimir Stankovic

External Examiner : Prof Dr. Jarmila Mullerova

Internal Examiner : Dr. Pawel Niewczas

Preface

This thesis is submitted to the University of Strathclyde for partial fulfilment of the requirements for the degree of Philosophies doctor.

This doctoral work has been performed at the Department of Electronic and Electrical Engineering, Centre for Intelligent Dynamic Communications (CIDCOM), with Prof Ivan Glesk as main supervisor and with co-supervisor Prof Ivan Andonovic.

This PhD has been funded by the Ministry of Higher Education Malaysia.

Abstract

A viable last-mile solution for high-speed high-capacity optical networks capable of securely supporting a large number of simultaneous users by minimal hardware requirements is needed. Optical code division multiple access (OCDMA) is an advanced multiplexing scheme which provides a more efficient and fairer division of available bandwidth among users in comparison to other techniques such as wavelength division multiplexing (WDM) and optical time division multiplexing (OTDM). As a result, OCDMA has become a very attractive multi-access technique that can be used in local area networks (LAN) and last-mile application. I have built an incoherent OCDMA system, whose performance I investigated, including the influence of chromatic dispersion, timing jitter and the effect of ambient temperature fluctuations on data transmission over a 17-km bidirectional fibre link (a testbed) I designed between Strathclyde and Glasgow University. The OCDMA system is based on two-dimensional wavelength-hopping time-spreading (2D-WH/TS) incoherent OCDMA codes which use multiwavelength picosecond pulses. The encoders/decoders are based on fibre Bragg gratings (FBG) technology and the investigations were carried out at OC-48 (2.5 Gb/s) data rate. The testbed was built to be a fully chromatic dispersion compensated with sub-picosecond accuracy. Synchronisation and timing jitter effects were investigated on OCDMA signal transmitted over 17-km distance. A receiver that incorporates an all-optical clock recovery (AOCR) for synchronisation in incoherent OCDMA systems was developed and demonstrated. The all-optically recovered clock signal was then used to drive optical “time gate” to control a switching window (“a time gate”). This is to pass the autocorrelation peak while blocking the MAI noise to improve system power budget and overall performance.

Acknowledgements

It would not have been possible to write this doctoral thesis without the help and support of the kind people around me, to only some of whom it is possible to give particular mention here.

Foremost, I would like to express my sincere gratitude to my supervisor Professor Ivan Glesk for the continuous support of my PhD study and research, for his patience, motivation, enthusiasm, and immense knowledge. His guidance helped me in all the time of research and writing of this thesis.

My sincere thanks go to my second supervisor, Professor Ivan Andonovic. Also my fellow labmates in Broadband laboratory, Tolulope Osadola, for the stimulating discussions while working together. Also I thank my friends in University of Strathclyde.

Last but not the least; I would like to thank my husband Khuzairi Mohzan, my lovely daughters, Batrisyia and Numa Eshal, and my newborn Khalis Rizqi for their personal support and great patience at all times, for always there cheering me up and stood by me through the good times and bad. For my parents, family and extended family who pray for my success and encouraging me with their best wishes throughout my life.

I would like to dedicate my thesis to my beloved friend, the late Mardiana Bidin who pass away after submitting her PhD thesis. Her words really inspire me to finish my PhD.

Contents

List of Figures

List of Tables

List of Abbreviations

1D	one-dimensional
2D	two-dimensional
2D-OOC	two-dimensional optical orthogonal codes
2D-WH/TS	two-dimensional wavelength-hopping/time-spreading
3D	three-dimensional
AOCR	all-optical clock recovery
AOTG	all-optical time gate
ASE	amplified spontaneous emission
AWG	array waveguide grating
BER	bit error rate
BPF	band-pass filter
BRFL	Brillouin/Raman fibre laser
CD	chromatic dispersion
CDMA	code division multiple access
CDR	clock data recovery
CFBG	chirped fibre Bragg gratings
CFG	chirped fibre grating
CHPC	carrier-hopping prime code
CMG	chirped Moiré gratings
CW	continuous wave
DARPA	Defence Advanced Research Projects Agency
DCF	dispersion compensating fibre
DCM	dispersion compensating module
DDF	dispersion decreasing fibre
DFDF	dispersion flattening and decreasing fibre
DFF	dispersion flattening fibre
DSF	dispersion shift fibre
DSL	digital subscriber lines
DWDM	dense wavelength division multiplexing
EAM	electro absorption modulator
EDFA	erbium doped fibre amplifier

EPC	extended prime codes
FBG	fibre Bragg gratings
FEC	forward error correction
FH/TS	frequency-hopping/time-spreading
FP	Fabry Perot
FWHM	full width at half maximum
FWM	four-wave mixing
GPS	global positioning system
GVD	group velocity dispersion
HBR	holographic Bragg reflector
IL	insertion loss
ISI	inter-symbol interference
ITU	International telecommunication unit
LAN	local area network
LED	light emission diode
LiNbO3	lithium niobate
MAI	multi-access interference
MAN	metropolitan area networks
MCM	multi-code modulation
MLL	mode locked laser
MPC	modified prime codes
MUD	multiuser detection
MZI	Mach–Zehnder interferometer
NOE	nonlinear optical effects
O/E	optical to electrical
OAC	optical autocorrelator
OBI	optical beat interference
OBN	optical beat noise
OC	optical circulator
OCDMA	optical code division multiple access
ODL	optical delay lines
OHL	optical hard limiting

OOC	optical orthogonal code
OOK	on-off keying
OPC	optical phase conjugation
OSNR	optical signal to noise ratio
OTDM	optical time division multiplexing
OTDR	optical time-domain reflectometer
OTN	optical transport network
PC	prime codes
PCF	photonic crystal fibre
PD	photodetector
PLC	planar lightwave circuit
PLC	polarisation loop controller
PM	polarisation-maintaining
PMD	polarization mode dispersion
PMF	polarisation-maintaining fibre
PPM	pulse-positioning modulation
PRBS	pseudo random binary sequence
RF	radio frequency
SBS	Stimulated Brillouin scattering
SC	supercontinuum
SHG	second harmonic generation
SMF	single mode fibre
SOA-MZI	semiconductor optical amplifier based –Mach-Zehnder Interferometer
SPM	self-phase modulation
SRS	Stimulated Raman scattering
SSFBG	super structured fibre Bragg grating
SSMF	standard single mode fibre
T/W	time/wavelength
TDC	tuneable dispersion compensator
TDM	time division multiplexing
TF	tuneable optical filter
TFF	thin film filter

TOAD	terahertz optical asymmetric demultiplexer
TPA	two photon absorption
VIPA	virtually imaged phased arrays
WDM	wavelength division multiplexing
WH/TS	wavelength hopping time spreading
XPM	cross-phase modulation

List of Publications

The work reported in this thesis has produced the following publications:

Journal

1. S. K. Idris, T. B. Osadola, and I. Glesk, "Investigation of All-Optical Switching OCDMA Testbed under the Influence of Chromatic Dispersion and Timing Jitter," *Journal of Engineering Technology (JET)*, Vol. 4 (1), pp.41-53, (2013).
2. S. K. Idris, T. B. Osadola, and I. Glesk, "Towards self-clocked gated OCDMA Receiver," *Journal of European Optical Society Rapid Publication (JEOS:RP)*, Vol. 8, (13013), pp. 1-6, (2013).
3. S. K. Idris, T. B. Osadola, and I. Glesk, "OCDMA Receiver with Built-in All-Optical Clock Recovery," *Electronic Letters*, Vol. 49 (2), pp. 143-144, (2013).
4. T. B. Osadola, S. K. Idris, I. Glesk, "Improving Multi Access Interference Suppression in Optical CDMA by using All-Optical Signal Processing," Telfor Journal, Vol. 5(1), (2013).
5. T. B. Osadola, S. K. Idris, I. Glesk, and W. C. Kwong, "Effect of Variations in Environmental Temperature on 2D-WH/TS OCDMA Code Performance," *Journal of Optical Communications and Networking*, Vol. 5, pp. 68-73, (2013).
6. T. B. Osadola, S. K. Idris, I. Glesk, and W. C. Kwong, "Network Scaling Using OCDMA over OTDM," *IEEE Photonics Technology Letters*, Vol. 24 (5), (2012).
7. T. B. Osadola, S. K. Idris, I. Glesk, K. Sasaki, and G. C. Gupta, "In situ Method for Power Re-Equalization of Wavelength Pulses Inside of OCDMA Codes," *IEEE Journal of Quantum Electronics*, Vol. 47 (8), pp. 1053-1058 (2011).

Conference

8. T. B. Osadola, S. K. Idris, and I. Glesk, "Novel power saving architecture for FBG based OCDMA code generation," *Proc. SPIE 8915*, Photonics North 2013, 89150H (October 11, 2013); DOI: 10.1117/12.2037500; http://dx.doi.org/10.1117/12.2037500.

9. S. K. Idris, T. B. Osadola, and I. Glesk, "Experimental Investigation of 2D-WH/TS Codes based on PS Multi-Color Pulses," *21th Telecomm.Forum*, pp. 903-906, TELFOR 2013.

10. S. K. Idris, T. B. Osadola, S. Shaukat, and I. Glesk, "All-Optical Clock Recovery for OCDMA Systems with optical time gating," *20th Telecomm. Forum*, pp. 903-906, TELFOR 2012.

11. T. B. Osadola, S. K. Idris, and I. Glesk, "Novel Method for multi access interference suppression in multiwavelength FBG-encoded OCDMA", *20th Telecomm. Forum*, pp. 907-910, TELFOR 2012.

12. S. K. Idris, T. B. Osadola, and I. Glesk, "OCDMA Receiver with built-in All-Optical Clock Recovery," Post-deadline submission, *4th European Optical Society Annual Meeting*, EOSAM 2012 , 25-28 September 2012, Aberdeen, Scotland.

13. T. B. Osadola, S. K. Idris, I. Glesk, and W. C. Kwong, "Improving Network Scalability Using OCDMA over OTDM" *Optical Fibre Communication Conference and Exhibit, 2012, OFC 2012.*

14. I. Glesk, T. B. Osadola, S. K. Idris, K. Sasaki, and G. C. Gupta, "Demonstration and Analyses of a Hybrid Multiplexing Scheme for Scaling-Up the 'Last Mile'," *14th International Conference on Transparent Optical Networks,* Invited paper, *(ICTON)*, 2012.

15. I. Glesk, T. B. Osadola, S. K. Idris, K. Sasaki, and G. C. Gupta, "Evaluation of OCDMA system deployed over commercial network infrastructure,"*13th International Conference on Transparent Optical Networks (ICTON), 2011*, pp. 1-4, 26-30, June 2011.

16. I. Glesk, M. N. Mohd Warip, S. K. Idris, T. B. Osadola, and I. Andonovic, "Towards Green High Capacity Optical Networks," *7th International Conference on Photonics, Devices and Systems,* ARTEMIS Olympik Hotel-Congress Centre, Prague, Czech Republic, August 24 - 26, 2011.

17. T. B. Osadola, S. K. Idris, I. Glesk, I. Andonovic, C. Michie, A. E. Kelly, and M. Sorel, "Strathclyde-Glasgow fibre-optic testbed for testing ultra-high speed

communications," Poster presentation in Scottish Research Partnership in Engineering (SRPe) Conference-Showcasing Engineering Research. Dynamic Earth, Edinburgh, 15th February 2011.

18. S. K. Idris and I. Glesk, "Investigation of OCDMA System Performance under Influence of Transmission Link Chromatic Dispersion," Poster presentation GRPE conference, Ross Priory, June 2012.

19. S. K. Idris and I. Glesk, "Receiver with Built-in All-Optical Clock Recovery and Optical Time Gating," Poster presentation GRPE conference, SECC, Glasgow, 19th June 2013.

Chapter 1

1.1 Introduction

With the growing needs for ultrahigh transmission speeds, optical fibre technology is becoming the replacement technology for the copper cable. The past 30 years have seen enormous strides in the fields of fibre optics and various device integrations. Many fibre optic devices are ready today for use in system applications and as commercial products [1] within communication networks.

In recent years, there has been a rapid increase in the capacity of transmitting high-rate data based on both time division multiplexing (TDM) and wavelength division multiplexing (WDM) technologies within the optical domain. Optical fibre will inevitably become the dominant transmission medium of metropolitan area networks (MANs). The performance of optical transport networks (OTNs) is continually being upgraded by using new fibre optic techniques, but access networks – called the 'last mile' – are still mostly based on copper and have many problems such as low transmission bandwidth, high failure rate, and high cost of operation and maintenance. They cannot efficiently support new services and applications based on multimedia and broadband services [2]. The access networks constructed with twisted wires and coaxial cables have become the bottleneck in providing larger bandwidth to users.

The expansion of the Internet has already increased the demand for bandwidth in access networks. Although some access technologies – such as digital subscriber lines (DSL), or even cable modems – may be sufficient for certain applications, such as web surfing or email, one can see an increasing demand for more bandwidth. Applications such as streaming media, video on demand and video telephony (Skype), to name a few, drive up the demand for a larger bandwidth [3]. But access networks face more challenges than other parts of transmission networks. Here, protocols, multi-service capability and cost are dominant issues. Fibre optics technology has a number of advantages in addressing the above issues, and optical code division multiple access (OCDMA) is a technology [4], [5] that can help. OCDMA is a solution for multiple accesses (others are TDM [6] and WDM [7]),

which can implement the transmission, switching and routing signals over the optical networks on its own, or in a combination with the optical time division multiplexing (OTDM) and WDM.

Figure 1.1 illustrates multiple access technique for TDM, WDM and CDMA. An analogy of multiple access is a room (channel) in which people wish to talk to each other simultaneously. To avoid confusion, people could take turns speaking (time division), speak at different pitches (frequency division), or speak in different languages (code division). CDMA is analogous to the last example where people speaking the same language can understand each other, but other languages are perceived as noise and rejected. Each group of users is given a shared code. Many codes occupy the same channel, but only users associated with a particular code can communicate.

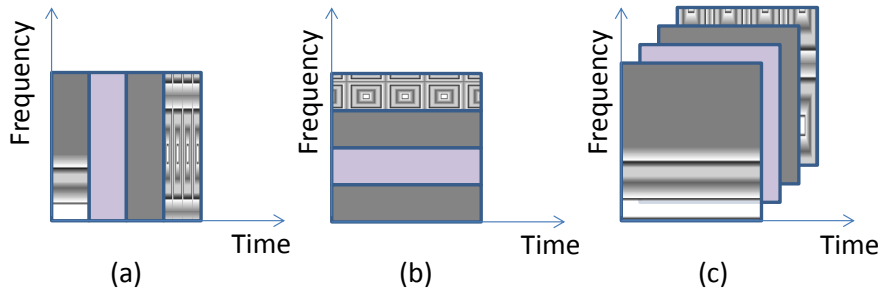

Fig. 1.1 Multiple access techniques. (a) TDM, (b) WDM and (c) OCDMA

The development of OCDMA began with two technical papers, and these form the foundation for most developments in OCDMA [8], [9]. Further and rapid development of OCDMA continued with publications by Prucnal, Santoro and Fan in 1986 [8], and by Weiner, Heritage and Salehi in 1988 [9]. The significance of the first seminal paper [8] is that it showed that pseudo-orthogonal direct sequences, such as prime sequence codes, could readily be implemented as tapped delay lines in optical fibre. The correlators, or decoders, for the encoded data could similarly be implemented as tapped delay lines. This meant that, in a system sense, an optical network could share the transmission channel in a ‘multiple access’ sense. Furthermore, it meant that the mechanisms that imposed the codes on the data (by the OCDMA encoder), and those for recovering a particular set of coded data (by the

OCDMA decoder), could be designed to operate without requiring any form of electronics. Nevertheless, generating the data flow in the optical domain did require electrical-to-optical conversion, but optical data encoding/decoding was now an all-optical process. This is an important breakthrough and it triggered new research into the physical implementation of coding schemes.

For the second paper [9], the key findings were that coherent coding and decoding of optical pulses could be used in communication networks. In particular, the spectra could be encoded with phase codes. Soon after, bipolar and spectral encoding schemes, that mimic the codes used by radio frequency (RF) communication, were added to the knowledge base of coherent OCDMA [9].

It can be said that the emergence of OCDMA as a viable technology started when agencies, such as the American DARPA (Defence Advanced Research Projects Agency), provided the funding to support research of OCDMA-related technologies, device integration, and system implementations towards commercialisation.

1.2 Early History

Apart from the first technical papers mentioned earlier, Salehi's research on incoherent OCDMA focussed on obtaining unipolar codes with good auto and cross correlations such as OOC (optical orthogonal / pseudo-orthogonal codes) [10], [11], [12]. Prime codes (PC) were then introduced [8]. In order to improve the code performance, Kwong proposed the extended prime codes (EPC) and modified prime codes (MPC) [13], [14]. The two-dimensional optical orthogonal codes (2D-OOC) were formed by Tancevski and Andonovic using both wavelength and time dimensions [15] – leading to the wavelength-hopping/time-spreading (WH/TS) family of codes. To increase the number of users, unipolar codes with larger capacity needed to be designed. Mendez, Andonovic, and Chen have transferred their interest from the study on 1D codes to 2D codes [15], [16], [17], [18], which helped to increase the capacity of the OCDMA systems and improved their performance. There followed a wealth of literature on the design of 2D-WH/TS codes with various code properties such as cardinality and correlation values [1], [19], [20].

It was recognised early on that the performance of OCDMA was limited by multi-access interference (MAI), so schemes such as optical hard limiting (OHL), and multiuser detection (MUD), and other techniques to improve OCDMA performance, were also proposed and developed [21], [22], [23], [24]. Also of interest has been research into all optical means of signal processing in hybrid systems and providing security in the physical layer [6], [25]. It is expected that optical processing can help to overcome the limitation imposed by a bandwidth limited electronic signal processing. Optical encoding/decoding, which refers to the process of assigning OCDMA codes to user information (data) at the transmitter side and intelligently extracting this information from coded signals in the presence of MAI at the receiver side, is an important aspect of optical signal processing. Various encoding and decoding methods exploring different technologies and approaches were demonstrated for use by the incoherent two-dimensional OCDMA encoder and decoder [26].

American DARPA has been a great supporter of OCDMA which resulted in numerous research achievements such as new coding algorithms and schemes, advanced encoding and decoding hardware, network architectures and OCDMA technologies [27], [28], [29], [30]. Great progress has been made in encoding algorithms, hardware implementations of encoders/decoders of coherent and incoherent OCDMA, and network protocols.

Chen designed algorithms [31] that can generate codes with ideal correlation properties (i.e. a cross-correlation less than or equal to one, for any arbitrary time shift between two different codes). However, many of these algorithms could only generate a limited number of codes. Therefore, the research has been focussed on the use of depth-first search algorithms in order to generate a large number of 2D codes satisfying the ideal correlation properties [32]. The significant advantage of this approach is the increased number of codes that can be generated. Thus, when used in conjunction with FEC algorithms, the potential to support a larger number of users with low BER can be designed, and this allows the support of higher data rates.

Glesk and Prucnal recognised for the Terahertz Optical Asymmetric Demultiplexer (TOAD) [33], as an ultrafast all-optical switch – has done seminal research in the areas of all-optical photonic switching [34], [35] and the investigation of linear and nonlinear optical signal processing techniques to provide high-speed data confidentiality in communications networks [24], [36] and OCDMA. Mendez researched optical communication modulation and coding as well as OCDMA avionic integration. He introduced a concept in which WDM and OCDMA share a set of discrete wavelengths and components with similar modulation formats [37], [38].

Kitayama et al. have focussed their research on coherent OCDMA systems [39], [40], [41]. Error-free transmission of bandwidth-symmetric full-duplex, using hybrid multi-port and super structured fibre Bragg grating (SSFBG) encoder/decoder without the optical thresholding, polarisation multiplexing and FEC, was achieved [42]. In the inline-dispersion-compensation-free coherent OCDMA transmission, using the bandwidth optimisation of OC's spectrum was proposed. With this scheme, 10 Gb/s, 4-user, OCDMA transmission over 59 km of the standard single mode fibre (SMF), without inline dispersion compensation, was experimentally demonstrated for the first time.

To improve system performance in incoherent OCDMA, a number of research were done conceptually and experimentally. A significant experimental application in optical signal processing was ultrafast all-optical time-gating using TOAD, which improved performance of the incoherent OCDMA system – namely its efficiency, scalability, and maximisation of the number of simultaneous users – which also resulted in the improved power budget [43]. To suppress MAI, an incoherent OCDMA receiver was designed with an all-optical time gate (AOTG) [44]. Theoretical analysis and experimental demonstration was performed based on (3, 11) frequency-hopping/time-spreading (FH/TS) OCDMA codes with a chip size of 73 ps and using a receiver with 2 ps AOTG. An error-free operation with BER less than 10^{-12} was achieved. The experimental results demonstrated that such a receiver will

not only eliminate the MAI (thus, increase system scalability), but at the same time, will improve the system power budget.

The effect of beat noise in an incoherent OCDMA has also been evaluated experimentally at a data rate of 2.5 Gb/s, for the carrier-hopping prime code (CHPC) family of 2D time/ wavelength (T/W) OCDMA codes, with and without time gate [45]. Results indicate that beat noise can introduce as much as a 10 dB power penalty, and time gating improves performance by reducing the power penalty by approximately 5 dB. The performance of incoherent multi-wavelength OCDMA was analysed under the impact of four-wave mixing (FWM) [46] with MAI, optical beat interference (OBI) and receiver noise included in the analysis. The numerical results show that the impact of FWM on the system performance is relatively strong – when transmitted power is high, frequency spacing is small, or dispersion shift fibre (DSF) is used, the system performance is severely degraded.

A tuneable 2D T/W OCDMA encoder was proposed and demonstrated [47] to be capable of creating 2D codes with variable code weight. This architecture uses ultrafast optical delay lines and all-optical sampling, operating at 115 Gchips/s, and allows differentiated service provisioning through variable code weight. Another technique is the use of chirped Moiré grating (CMG) to demonstrate incoherent wavelength-encoding/time-spreading OCDMA [48]. Holographic Bragg reflector (HBR) technology was also used for incoherent OCDMA encoders/decoders [49], [50]. Simultaneous encoding/decoding operation of two WH/TS codes was successfully performed at OC-24. The technology enables inexpensive small footprint multiport designs, making possible multiple code generation – a very attractive approach in building cost-effective, robust and lightweight systems.

Chromatic dispersion in long-haul fibre optic communication systems, which results in temporal widening of optical pulses, has also been investigated. In particular, intersymbol interference (ISI) [51], pulse width and peak power limitation [23], and pulse distortion [52] have been examined. In multi-wavelength OCDMA, dispersion also presents unconsidered dispersion-induced temporal skewing among wavelength

channels [53], and this paper provides the first detailed quantitative consideration of the performance consequences of temporal skewing in multi-wavelength OCDMA systems. Through the simulation, two novel methods for combatting the deleterious effects of temporal skewing are proposed: optimum threshold detection and code-pattern pre-skewing. It is shown that, for a practical 2D-codes system configuration with optimum threshold detection, multi-wavelength OCDMA networks can maintain design bit error rate performance within an order of magnitude for link lengths of up to approximately 500 m. Code-pattern pre-skewing presents the possibility of completely eradicating the impact of temporal skewing; however, further investigation is needed.

Chromatic dispersion can have a severe effect on incoherent OCDMA. An analytical study presented the impact of chromatic dispersion on the performance of the 2-D WH/TS OCDMA system [54]. The investigation also considered noise and interferences, including MAI, optical beat interference (OBI), and receiver's noise. The results show that, for single mode fibre (SMF) under the impact of chromatic dispersion, the number of supportable users is extremely decreased and the transmission length is remarkably shortened. The main factor that limits the system performance is time skewing of the autocorrelation peak. Although the impact of pulse broadening and peak power reduction is almost compensated by DSF, the impact of time skewing remains still relatively strong. This suggests that alternative techniques, such as pre-skewing at encoder and post-skewing at decoder, are desired so that the systems can use low-cost SMF.

Investigation into the reduction of the dispersion effects in multi-wavelength OCDMA systems, by using multi-code modulation (MCM) signalling, was done numerically [55]. The major advantages of the proposed system are the abilities of simultaneously mitigating chromatic dispersion, MAI, and OBI. The numerical results reveal that the proposed system outperforms the conventional on-off keying modulation (OOK) and pulse-positioning modulation (PPM) in terms of the number of supportable users, user's bit rate, and the required power.

In terms of system synchronisation, demonstration of all-optical clock recovery in incoherent OCDMA is very limited [56]. A self-clocked all-optical add/drop multiplexer for asynchronous OCDMA ring networks was demonstrated in an incoherent OCDMA system; however, the clock extraction is not performed all-optically, but rather uses electrical clock data recovery (CDR) [57].

State-of-the-art research can predict that future development will enable all-optical CDMA to accommodate requirements for Tb/s networks combined with asynchronous access capability and a degree of security in transmission [58]. As the device technology has matured, so has the field of OCDMA. Researches throughout the world have extensively investigated new OCDMA codes, suitable hardware, as well as architectures, which can make OCDMA networks a reality. Most of the simulations and experiments were done in the laboratory environment. However, out-of-laboratory experimental demonstrations investigating the capabilities of OCDMA are still limited. The purpose of this thesis is to make contributions in this area, conducting out-of-laboratory demonstrations and experiments.

Another goal of my research was also to investigate the implementation and application of optical switching in order to improve the incoherent OCDMA system. In the big picture, this I achieved by improving techniques and methods used in optical switching so that the received signal is free from noise and, at the same time, the system can accommodate more simultaneous users – hence, the system scalability can be increased. All-optical signal processing is the most promising scheme to achieve such goals because of its potential of ultrahigh-speed response.

The use of 2D-WH/TS families of codes [59] has also been widely researched for use in different OCDMA applications. These codes are characterised by the combination of time spreading and wavelength hopping of picosecond pulse patterns, which spreads optical pulses in both the time and wavelength domain simultaneously, thus achieving code flexibility as well as better performance [60], [61]. Widely studied has been the family of prime codes employing multi-wavelength short pulses for codes generation [1], [54], [62], [63].

When it comes to incoherent OCDMA, not much study has been done in terms of learning the extent to which a small, or even residual, amount of chromatic dispersion in a transmission link can affect performance of OCDMA systems that utilise multi-wavelength picosecond pulses for 2D-WH/TS code creation. In communications systems, there is always a need to extend the reach of the existing fibre link or to relocate the user terminals. In this event, a simple addition of an extra length of fibre would mean also adding some amount of dispersion. Therefore, it is necessary to understand how chromatic dispersion accumulated over fibre link may affect the overall OCDMA system performance [64].

Besides the chromatic dispersion impairments, the OCDMA performance is also influenced by multi-access interference (MAI) and the influence of timing jitter on synchronisation. This is even truer for the coding schemes using 2D-WH/TS OCDMA codes with multicolour picosecond pulses [20]. Optical time gating using an electro absorption modulator (EAM) can be used to suppress MAI to increase incoherent OCDMA system scalability and to improve system power budget. In the laboratory environment, local synchronisation is used to mitigate the effect of the timing jitter [65]. However, inaccurate synchronisation and timing jitter will strongly affect incoherent OCDMA systems at longer transmission distances. In [66] I demonstrated the use of a self-synchronised OCDMA receiver with built-in all-optical clock recovery to mitigate the effect of the timing jitter and shown that an incoherent OCDMA receiver with incorporated all-optical clock recovery for self-synchronisation will be required for this type of systems.

1.3 Contributions from Thesis

- To the best of my knowledge, no reports have been published on high-precision dispersion compensation of out-of-laboratory fibre optic transmission link to support a picosecond-based optical data transmission.
- Design and implementation of incoherent OCDMA testbed with 2D-WH/TS codes for use in the testbed in and out-of-laboratory experiments.
- Investigation of 2D-WH/TS codes with multicolour picosecond pulses has been analysed and demonstrated for the first time in an out-of-laboratory

environment and under real-time environmental conditions over longer distances.

- The obtained research data from the evaluation of FBG encoders/decoders and the 10G / 40G -tuneable chromatic dispersion compensators were shared with OKI, Japan and OSAKI, Japan, respectively to help improving their products.
- Investigation of physical impairments of the transmission fibre link on prime codes based on picosecond multicolour pulses was reported for the first time.
- First all-optical clock recovery demonstration from an incoherent OCDMA signal in the field trials.
- First demonstration of the optical sampling gate synchronisation derived all-optically from an incoherent OCDMA signal on the receiver end.

1.4 Organisation of the Thesis

The thesis is organised with the background study and theory being discussed in the first section of each chapter, and the summary presented at the end of each chapters, with experiments as follows. Chapter 2 reviews the OCDMA concept. From the review, the discussion is then moved to the theory on OCDMA codes including multi-colour pulses and the code generation techniques. These generation techniques then lead to 2D-WH/TS coding. However, the implementation of 2D-WH/TS using multicolour picosecond pulses increases the effect of chromatic dispersion.

In Chapter 3, the transmission impairment is discussed. This is then narrowed to the dispersion in the fibre optic system. The theory and the effect of chromatic dispersion, as well as the effect of chromatic dispersion on the multi-wavelength OCDMA system, is highlighted. The different compensation techniques are also discussed here.

Chapter 4 deals with transmission impairment due to the implementation of a testbed over a certain distance. First, the testbed itself is verified for chromatic dispersion. Experimental investigation is conducted to see the effect. An outgoing laser pulse width is compared to the received pulse width to measure the pulse broadening with

respect to the distance. Then 2D-WH/TS code based on multicolour pulses is launched and code's received autocorrelation signal is investigated for distortion due to chromatic dispersion effects. The proper chromatic dispersion (CD) compensation using a fibre-based dispersion compensator module, plus fine tuning to achieve sub picosecond accuracy, is implemented.

In Chapter 5, the OCDMA testbed – starting from assembly of the OCDMA transmitter and receiver, up to the establishment of the bidirectional fibre optic testbed between the University of Strathclyde and Glasgow University – is discussed. Theory of supercontinuum, and supercontinuum generation for use in the testbed, is also discussed here.

In Chapter 6, the experiment is followed with an investigation of the effects of residual chromatic dispersion on transmission channels used by advanced OCDMA system and the impact of varying chromatic dispersion on system performance in a multiuser environment is investigated.

Chapter 7 deals with other important issues when implementing code with multi-colour pulses over longer distances. The synchronisation issue is discussed. The theory of clock recovery and all-optical based clock recovery implementation, to overcome synchronisation issues, is also discussed here. The experimental investigation of the implemented all-optical clock recovery on OCDMA is conducted.

Chapter 8 addresses time gating issues in order to eliminate MAI and increase system performance. The experiment is continued with a combination of time gate and all-optical clock recovery implemented on the OCDMA system. An all-optical recovered clock is used to drive the semiconductor optical amplifier –Mach Zehnder Interferometer (SOA-MZI) optical switch used as the time gate. The result is discussed.

In Chapter 9, the University of Strathclyde and Glasgow University transmission testbed is reconfigured for testing of 10 Gb/s and 40 Gb/s tunable dispersion compensators (TDC) provided by OSAKI Japan. The results are discussed.

The conclusion and future work are discussed in Chapter 10. Please note here references to my publications are highlighted in bolt.

Chapter 2: ODCMA Concept

2.1 Introduction to CDMA

Code division multiple access (CDMA) principles have been investigated in the context of satellite and mobile radio communications [67], [68], [69], [70]. In the late 1970s, CDMA technology was aimed at military communication, which was a spread frequency technique increasing the robust security of information transmission [71]. Spread frequency communication has been used in military communications for a long time in order to resist intended interference and implement low probability of detection. With the emergence of satellite and mobile communications, 'spread-spectrum' was considered as the basis of a CDMA technique [72]. Since then, CDMA has been successfully deployed in cellular telephony networks along with the global positioning system (GPS) satellite broadcast link. These days, CDMA is widely used in the field of wireless communication, especially the third generation wireless communication systems.

CDMA is a spread spectrum multiple access technique. A spread spectrum technique spreads the bandwidth of the data uniformly for the same transmitted power. A spreading code is a pseudo-random code that has narrow ambiguity function, unlike other narrow pulse codes. In CDMA a locally generated code runs at a much higher rate than the data to be transmitted. Data for transmission is combined via bitwise XOR (exclusive OR) with faster code. Figure 2.1 show how the spread spectrum is generated.

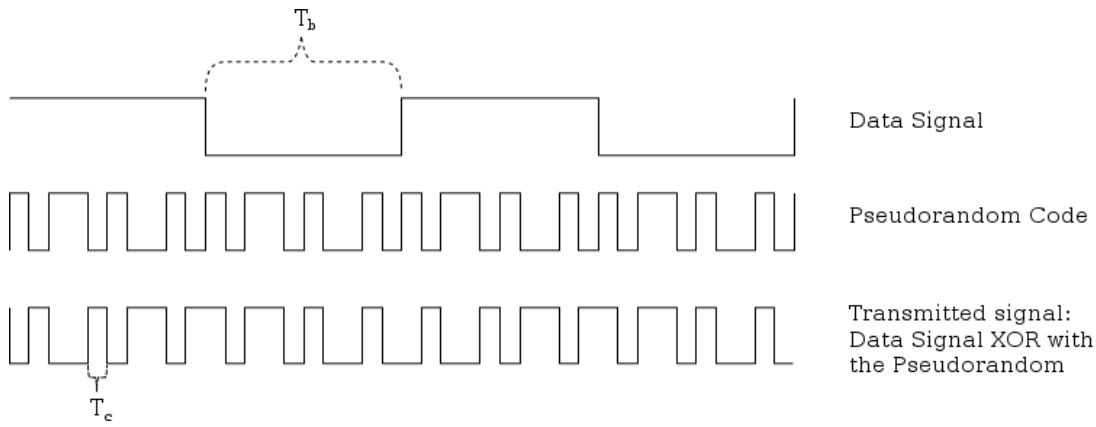

Fig. 2.1 Generation of CDMA signal

The data signal with pulse duration of T_b is XOR with the code signal with pulse duration of T_c (chip period). Since bandwidth is proportional to $1/T$, where T is bit time, therefore the bandwidth of the data and spread spectrum signal is $1/T_b$ and $1/T_c$ respectively. Since T_c is much smaller than T_b the bandwidth of the spread spectrum signal is much larger than the bandwidth of the original signal.

2.2 History of OCDMA

The Optical CDMA story begins with the hope that the key benefits of CDMA in radio frequency systems will pervade it. This means that OCDM is an alternative multiplexing technique that has its origins in RF communications [67], [68] but has been since applied to the optical domain due to a number of inherent advantages that the technique offers. These advantages include flexible access to wide bandwidth, code-based dynamic reconfiguration, decentralised networking, passive code translation and a measure of security through data obscurity [28]. Unlike WDM, which provisions a dedicated wavelength per communication channel, or OTDM, which offers a dedicated time slot per communication channel and therefore requires strict synchronisation between channels [73], OCDM provides an equal access to the used spectrum for all its channels. This spread-spectrum-based technology shows advantages such as asynchronous access capability with low latency to the available bandwidth, soft capacity on demand [74], high spectral efficiency, high simultaneous user allocation, ability to support variable bit rates and bursty traffic. It offers increased data privacy using various platform against unauthorised eavesdropping [49], [51], [75], [76]. These benefits are particularly advantageous in optical access networks that need flexibility, scalability, reconfigurability and cost-efficiency. In other words, OCDMA provides more efficient use, and a fairer division of bandwidth between the users, in comparison to other multiplexing techniques. As a result, OCDMA became a very attractive multi-access technique that can be used for local area network (LAN) and last-mile applications [77], [78].

The first task for OCDMA was to develop fibre delay lines for optical “code processing” [79]. Such a demonstration was given in 1986 [8]. In that demonstration,

CDMA concepts from RF communications were directly applied to the optical domain by using fibre delay lines to construct a temporal coding sequence. This forms the basis for a range of modern CDMA approaches based on incoherent and coherent optical matched filtering using fibre delay lines. Since the publication of this paper, there has been significant progress in OCDMA in terms of the number of coding schemes that have been demonstrated [9], [15], [80], [81] as well as the development of the all-optical technologies that enable such coding operations [82], [83], [84]. New families of optical code sequences were also developed to provide greater discrimination between the desired code and unwanted codes [10], [32].

The OCDMA technique spreads the message signal to a relatively wide bandwidth by using a unique code, rather than a specific wavelength or time slot, that reduces interference, enhances system processing and differentiates users. The optical code is impressed upon the data to be transmitted with each optical code being unique to a given transmitter (user). Optical code requires a bandwidth larger than that required by WDM or OTDM. The spectrum of the OCDMA signal is broadened – hence the term 'spread-spectrum'. By assigning each transmitting channel its own unique optical code, OCDMA systems allow all transmitting channels to overlap both temporally and spectrally (in time and wavelength domains). Each user channel modulates a set of optical pulses with the data for a transmission. The data signals from all channels are multiplexed asynchronously and transmitted over the network. At the receiver side, a copy of all transmitted data signals is passed to each decoder (user). With the knowledge of the code used to encode the optical signal, a receiver extracts the desired data from the signal. If the code matches, the original data is recovered – while codes that do not match are rejected. This approach allows the same available bandwidth to be shared among various users and the code assignments can be flexibly and dynamically changed [1], [2].

2.3 OCDMA Systems Classification

Various types of OCDMA systems have been proposed as the result of intensive research in the past 30 years. Since the initial efforts [8], [10], [85], different approaches have been proposed for OCDMA implementation. These systems can be

categorised into two dominant approaches. The first is based on the coding principle and it can be divided into coherent and incoherent OCDMA systems. Each has their own merits and drawbacks. The two approaches can be compared based on the maximum size of the code space and the feasibility of the optical technology required, as well as the effect of transmission impairments on them [4]. The second method of categorisation is based on the coding domain. The coding process can be realised in either the spectral domain or temporal domain using one-dimensional (1D) code sequences [1], [86] and in both domains using two-dimensional (2D) code sequences [45], [61], [87], [88], [89].

2.3.1 Coherent OCDMA

The coherent OCDMA system encodes/decodes the optical signal by manipulating the phase of the optical signal (pulse) of a highly coherent source, and coherent schemes are based on modulation detection of the signal optical phase [90]. This means that in coherent OCDMA systems, a given user's code is generally applied via phase coding of the optical signal field, which is often derived from a highly coherent wideband source such as mode-locked laser. The receiver for a coherent OCDMA system relies on a coherent reconstruction of the signal field to recover the decoded user's data. The coding process is performed in the bipolar manner, which is similar to that in the wireless CDMA systems. Because the "negative" components exist in the bipolar codes, they have ideal correlation properties and large cardinalities. The technologies for the implementation of the coherent OCDMA system are relatively complex and challenging to realise. Coherent systems achieve higher performance due to their coding correlations being better than the incoherent ones, but they require high-precision control of the optical path within the encoder and decoder. The practical application of the coherent OCDMA system depends on the maturity of technologies. The bipolar codes are also applicable to the incoherent OCDMA systems by using differential detection.

2.3.2 Incoherent OCDMA

Incoherent OCDMA has also been investigated as a promising candidate for the next generation of optical access networks [1], [75], [91]. OCDMA is called incoherent

when the coding is done on an optical power basis (on/off keying). In contrast to coherent OCDMA, incoherent OCDMA systems typically rely on amplitude-modulated codes rather than directly manipulating the optical phase. Schemes use standard techniques of intensity modulation and detection [90]. Since the code processing is done using optical amplitude of pulses, the frequency, phase and spectral content of the pulse are not considered [71]. A number of incoherent OCDMA system architectures utilise wideband incoherent sources, such as broadband amplified spontaneous emission (ASE), while other incoherent architectures utilise pulsed laser sources as part of their implementation. The incoherent OCDMA code is a unipolar code. Therefore, the orthogonality between any two code words is difficult, even impossible, to implement. Incoherent systems are regarded as more practical because the light sources and encoding and decoding techniques have a low complexity and are cost effective. In comparison to coherent systems, incoherent OCDMA systems are therefore relatively simpler.

2.3.3 One-dimensional (1D) Code

The coding can be performed in either a time or frequency domain as one-dimensional (1D) OCDMA. 1D coding is mostly used due to its simplicity, and it can be realised in both incoherent and coherent systems by different schemes. In the OCDMA systems with temporal coding, each data bit is divided into several short time periods called chips, and intensities or phases of these chips are changed according to a designed code sequence. Similarly, spectral coding is done by dividing the spectrum of each data bit into several narrow bandwidths called frequency bins, and controlling the intensities of these frequency bins. In 1D incoherent OCDMA codes, although the constructions of the algebraic congruence codes are simple and easily realised in hardware, they have poor correlation properties and small cardinalities. Meanwhile, their cardinalities are confined to prime numbers. Despite a lot of effort, their performances still cannot satisfy practical requirements. The biggest limitation of 1D incoherent OCDMA codes is that the code cardinality is proportional to the length of spreading [71]. Also, from the practical point of view, in optical fibre communication systems it is difficult to make the width of optical pulse narrower than the order of picoseconds. Furthermore,

narrow optical (picosecond) pulses are more affected by fibre nonlinearity, dispersion, etc.

2.3.4 Two-dimensional (2D) Code

Because of the easy implementation of incoherent OCDMA systems, the coding theory for 1D incoherent OCDMA codes establishes the basis for the implementation of 2D incoherent OCDMA coding and networks, which are more promising for practical applications. Most 2D coding processes are predominantly in an incoherent manner (very few coherent 2D coding schemes were reported). Compared to 1D coding, 2D coding can support more users in a network and significantly improve the system performance because the size of the 2D code set is larger, and the correlation properties of 2D code sequences are better than 1D code sequences. The common approaches to incoherent OCDMA can be further classified into temporal spreading, spectral-amplitude coding, spatial coding and two-dimensional wavelength-hopping/time-spreading (2D-WH/TS), depending on how exactly the intensity modulated code is applied [92]. In my research, I was focussed on 2D-WH/TS coding.

2.4 Two-dimensional Wavelength-Hopping/Time-Spreading (2D-WH/TS) Codes

Use of the 2D-WH/TS family of codes has been widely researched [50]. These codes are characterised by the combination of time spreading and wavelength hopping of picosecond pulse patterns which spreads optical pulses in both the time and wavelength domain simultaneously, thus achieving code flexibility as well as better performance [15], [61], [60]. Among the advantages are reduced cross correlation, increased cardinality and nonexistence of autocorrelation side lobes [54], [93], and this improves the code performance [92]. A big advantage of 2D codes is the significant increase of the code cardinality, which increases the number of users in the network. While the reduced code length helps to increase the user data rate.

Practically speaking, in the 2D-WH/TS coding scheme in the time domain, each user data bit (see Fig. 2.1) is encoded with a sequence of multicolour pulses placed in

time slots referred to as (time) chips. These multicolour pulses are obtained in a frequency domain in which the source has bandwidth spectrally divided into several sub-band frequencies, with a central wavelength λ_i, by frequency filtering.

Figure 2.2 illustrates the concept of incoherent 2D-WHTS OCDMA code. The 2D-WH/TS code is represented by a 2×2 matrix with time and wavelength as its two orthogonal axes. As indicated, the wavelength domain is divided into *w* wavelength bands each occupied by wavelength λ_w and the time domain is divided into *N* chips. The optical pulses are then positioned within this matrix [59]. Coloured boxes in Fig. 2.2 represent short optical pulses of different wavelength λ_j, $j = 1, w$ of τ duration. In 2D-WH/TS OCDMA, all users share the same wavelength spectrum.

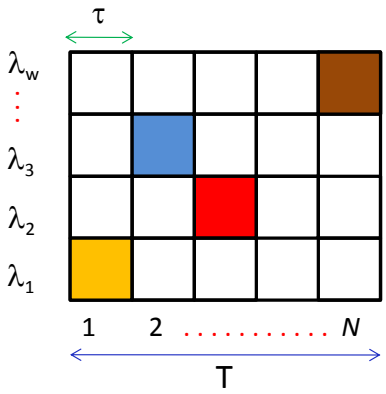

Fig. 2.2 Concept of incoherent OCDMA in which each colour represents a short optical pulse of different wavelength λ_i; (T: bit width, *N*: number of chips, τ: pulsewidth)

It is well known that an increase in the number of chips results in an improvement in the number of simultaneous users, and thereby improves scalability [19]. In order to increase the number of chips within a 2D-WH/TS incoherent OCDMA code, if the data rate is fixed, the chip width must be reduced. In practical terms, this requires a reduction of the duration of each "wavelength" pulsewidth. Theoretically, it is possible to obtain large code sets for the incoherent OCDMA systems provided that short pulses are used to form the 2D-WH/TS codes. It is shown that in the implementation of such 2D-WH/TS code-based incoherent OCDMA systems, the environmental factors must be considered to ensure an effective and robust data transmission [20].

2.4.1 WH/TS Coding Algorithm to Generate Codes

The formula to generate the code parameters for positioning multicolour wavelength pulses λ_i within the 2D matrix, shown in Fig. 2.2, is given below:

w = code weight
N = code length = number of chips
i = code order
for j =0: w−1
*code(i +1, j +1) = mod(j * i, p) + 1*
End

where *i* and *j* are integer numbers and *p* is prime number integer. Using the above algorithm, the generated (4,101) codes are shown in Table 2.1.

Table 2.1 (4,101) Code generation positioning

λ_1	λ_2	λ_3	λ_4
...	...	...	...
1	85	68	51
1	86	70	54
1	87	72	57
1	88	74	60
1	89	76	63
1	90	78	66
1	91	80	69
1	92	82	72
1	93	84	75
1	94	86	78
1	95	88	81
1	96	90	84
1	97	92	87
1	98	94	90
1	99	96	93

1	100	98	96
1	101	100	99

Figure 2.3 is an illustration of one code from the (4,101) family of codes.

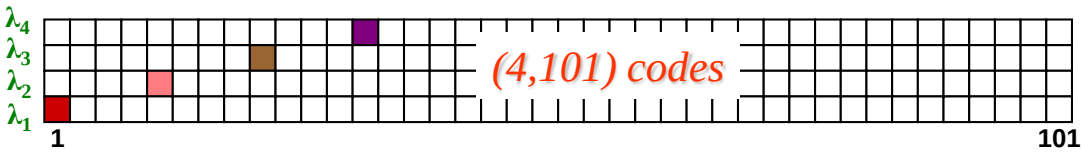

Fig. 2.3 Illustration of one code from the family of (4,101) 2D-WH/TS codes

2.5 2D-WH/TS Code-Generation Techniques

Consequently, an OCDMA network can support real-time, multiuser, high-speed data communications. OCDMA encoders and decoders are key components for the design of OCDMA networks. In effect, their architectures and implementation can significantly affect the complexity and cost of optical transmitters/receivers, the power loss, the number of users in a network and the reproducibility of the encoder/decoder [3].

The two main elements of the transmitter are the optical source and the encoder, while the receiver consists of the decoder and the photo receiver. Various encoding methods exploring different technologies and approaches exist and were demonstrated for use with incoherent OCDMA encoders. These include the use of thin-film filters (TFF) in combination with optical delay lines (ODL) [91], holographic Bragg reflector (HBR) [49], and fibre Bragg gratings (FBG) [94].

A WH/TS encoder based on array waveguide grating (AWGs) and TFFs first creates a wavelength-hopping pattern followed by a time-spreading pattern. The individual wavelength of the code sequence is independently delayed, allowing the use of a rapidly tuneable timeslot tuner for dynamic variation of codes. However, an encoder based on HBRs firmly combines the formation of the wavelength-hopping and time-spreading patterns, thus forbidding independent control and delay of each wavelength. Encoders based on a linear array of FBGs allow independent control of

the wavelengths but require a complex scheme for independent delay of each wavelength [95].

2.5.1 Arrayed Waveguide Gratings (AWG) OCDMA Encoders

Arrayed waveguide gratings (AWGs) on silicon and lithium niobate technologies have attracted much attention since the early 1990s due to their potential for low insertion loss [96], [97], [98]. Figure 2.4 shows a phased array of optical waveguides that acts as a grating. The input signal is coupled into an array of planar waveguides. The waveguides are at different lengths to provide different phase shifts to the signal in each waveguide. These phase shifts are also wavelength dependent because of the frequency dependence of the mode-propagation constant [99].

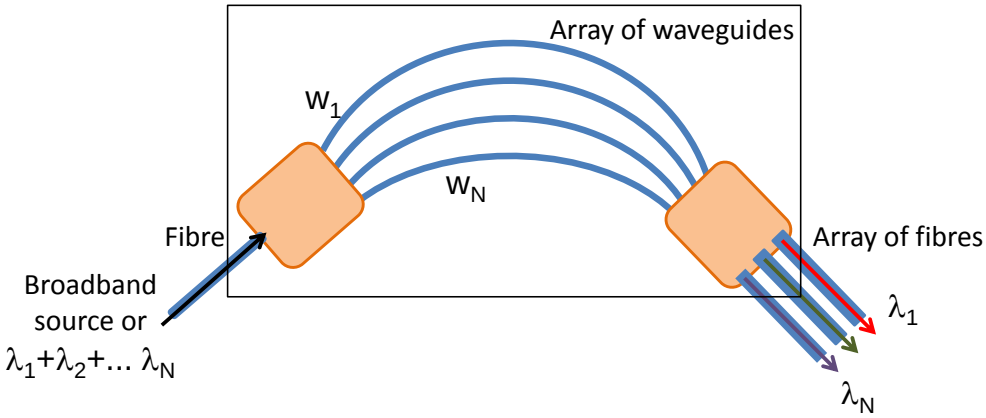

Fig. 2.4 AWG schematic

Typical characteristics of AWGs are polarisation dependence, temperature sensitivity, good flat spectral response and insertion loss less than 3 dB [95]. They have better than −35 dB cross talk threshold and can be easily integrated with a photodetector. Applications of AWGs include their use in WH/TS encoders/decoders [100]. Today, the AWG is a mature technology offering the advantage that the entire WH/TS encoder/decoder is integratable, thus resulting in a smaller footprint [95]. The application of two AWGs in a 2D-WH/TS encoder is shown in Fig. 2.5 with $D_1 - D_N$ are the delay length.

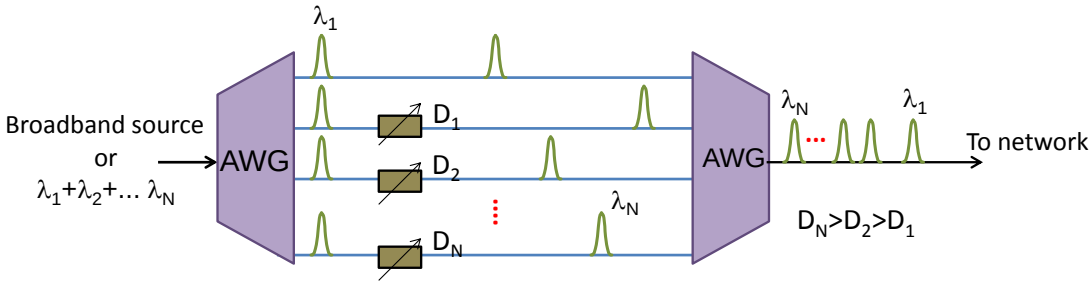

Fig. 2.5 Schematic of 2D-WH/TS encoder with four wavelengths in the code using AWG

2.5.2 Thin-Film Filters (TFFs) OCDMA Encoders

Thin-film filters (TFF) can be considered as Fabry-Perot (FP) etalons with multiple reflective dielectric thin-film layers used to form the mirrors surrounding the etalon cavity. Similar to a FP etalon, TFFs can act as bandpass filters. The principles of thin-film optics [101], which govern the performance of TFFs, have been studied for a variety of applications such as edge filters, anti-reflection coatings and high-reflectance coatings [102].

A TFF-based WDM multiplexer and demultiplexer can be used to form a 2D-WH/TS encoder/decoder, as depicted in Fig. 2.6, by cascading a number of these filters and controlling delay length D_i. The first filter in the cascade passes wavelength λ_0 and reflects all the others into the second filter. The second filter passes wavelength λ_1 and reflects those remaining, and so on. The filters on the right side multiplex λ_i back together after that exposure to different delays D_i.

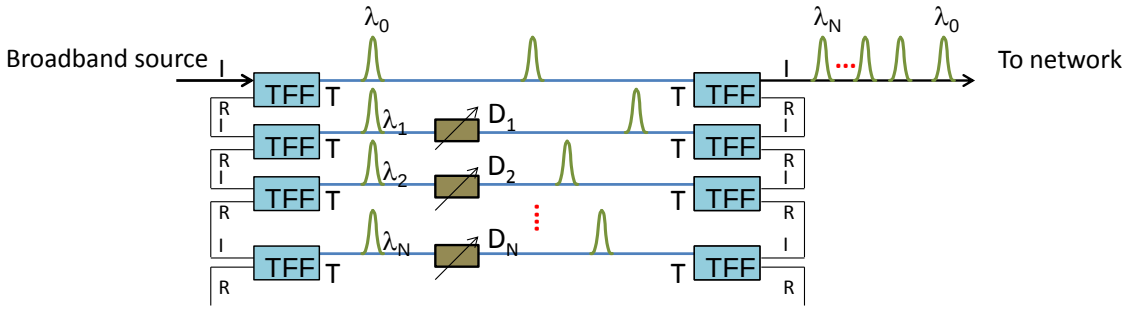

Fig. 2.6 Schematic of a 2D-WH/TS encoder with four wavelengths in the code using TFF (I: input port, T: transmitted port, R: reflected port)

TFFs have emerged as a dominant filter technology in commercial markets due to their flexibility, low loss, low cost and passive temperature compensation. They provide the lowest-loss solution at low channel counts, and similar loss to AWG at high channel counts. In addition, the device is insensitive to the polarisation of the signal and extremely stable to temperature variations. TFFs have been used for various optical networking applications such as optical switches [103] and switchable add-drop filters [104].

The use of TFFs in a WH/TS system implies that the chip size is limited only by the optical pulse width. This contrasts with FBG-based encoders/decoders in which the spacing between adjacent gratings imposes an additional constraint. The resulting increase in code matrix size can thus be used for better system performance. TFFs have been used recently for WH/TS encoders/decoders in various experiments [29], [30].

2.5.3 Fibre Bragg Gratings (FBGs)-based OCDMA Encoders

Recently, fibre Bragg gratings (FBGs) have been used for various applications in optical networks [105], [106]. The applications include add/drop multiplexing and wavelength routing in WDM networks, dispersion compensation and wavelength stabilisation techniques in fibre lasers. FBGs have also been used to implement various OCDMA encoding schemes such as spectral amplitude coding [107], spectral phase coding [108], temporal phase coding [109] and WH/TS [110], [111]. The use of FBG-based approaches in OCDMA provides the advantages of all-fibre encoding/decoding for increased efficiency and the potential to support reconfigurable systems using tuneable devices. The use of FBGs for encoding and decoding of WH/TS optical codes in OCDMA systems, by spreading multiple wavelengths within a bit period and placing them into time chips at the transmitter end and reciprocally de-spreading them and forming an autocorrelation peak at the receiver end, is a widely known technique [94].

Figure 2.7 illustrates the schematic representation, and principle of operation, of a fibre Bragg grating. In its simplest form, FBG consists of a periodic modulation of

the refractive index in the core of an SMF. The fundamental building blocks for most FBGs are structures having uniform grating planes with a constant period, where the phase fronts are perpendicular to the fibre's longitudinal axis [112]. Fibre gratings can be classified into two types: those that couple counter propagating waves (typically operating in a reflection mode and referred to as short-period grating) or couple co-propagating waves (typically operating in transmission mode and referred as long-period grating) [113].

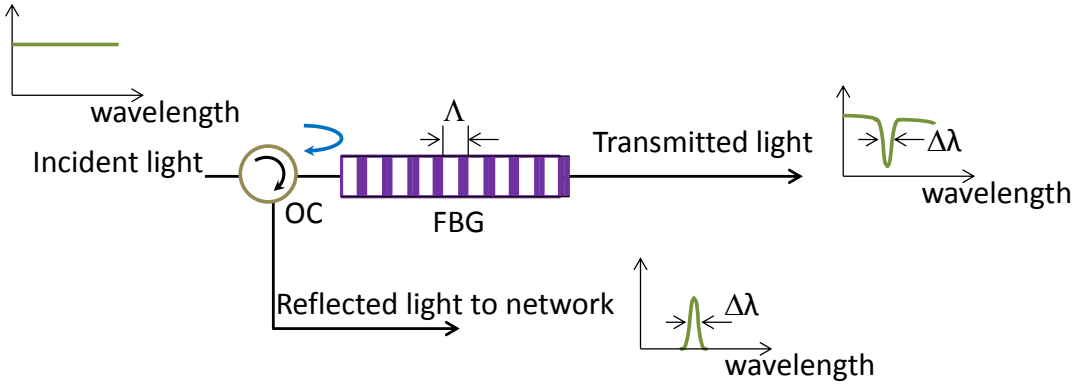

Fig. 2.7 Schematic representation of an FBG and its operation

Let's consider FBG written into optical fibre, the input light will be reflected by the refractive index perturbation if the wavelength of the incident light satisfies the Bragg condition [105] – Eq. 2.1,

$$\lambda = 2n_{eff}\Lambda \tag{2.1}$$

where λ is the wavelength of incident light, n_{eff} is the effective refractive index of the propagating mode, and Λ is the grating period – then the reflected waves will add coherently. Otherwise, it will become progressively out of phase with each reflection and cancel out. This means that if the Bragg condition is satisfied, coherent reflection of input light occurs (otherwise it is mostly transmitted). Some tunability of the FBG centre wavelength can be achieved by using strain.

Implementations of FBGs for WH/TS code generation are based on two structures: the linear array of FBGs or chirped Moiré gratings (CMGs) [93], [111], [114], [115].

CMGs structures are composed of superposed linearly chirped FBGs that enable the use of a single passive grating structure to implement WH/TS encoding/decoding [48]. However, the linear relationship between wavelengths and time, and the associated inherent coupling of the wavelength-hopping and time-spreading patterns in CMGs, implies that the number of codes that can be implemented is limited. It is worth noting that FBG, while inexpensive, provides a very promising approach towards miniaturisation and complexity, as the function of wavelength filtering is combined with desired time delays in one single fibre device [26].

Figure 2.8 illustrates a schematic of a FBG-based WH/TS encoder. Here an optical pulse from the broad band source such as supercontinuum (SC) source is sent to four consecutive Bragg gratings written into optical fibre via an optical circulator (OC) to generate a 2D-WH/TS OCDMA code.

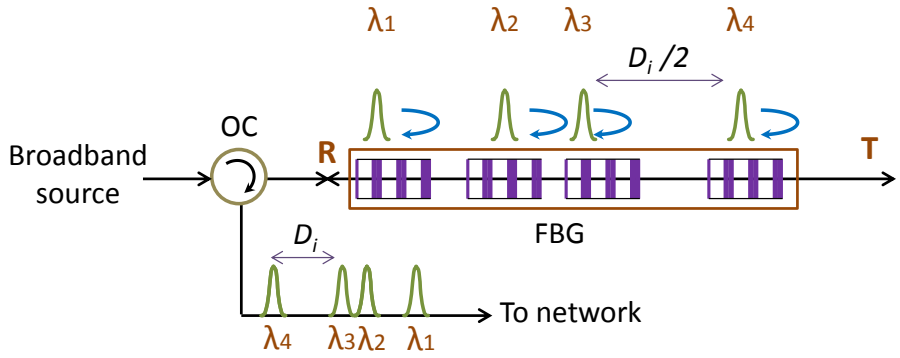

Fig. 2.8 Schematic of a WHTS encoder with four wavelengths λ_i in the code using FBG technology, OC – optical circulator, D_i – delay

2.5.4 Holographic Bragg Reflector (HBR)

A new integration technology platform has been recently developed based on the principle of volume holography. Holography is a method of capturing phase and amplitude characteristics of a three-dimensional (3D) object on a 2D photographic plate using coherent light (laser light) [99]. The end result is an incomprehensible image of dense stripes and whorls on the plate – known as a hologram. Thus, essentially perfect 2D volume holograms can be constructed to interact with specific signal beams and provide signal routine and wave–front transformations with

powerful spectral control. Photonic crystals form a subset of such volume holograms [116]. The technology has been demonstrated for applications in coarse and dense WDM systems and for spectral comparison using silica as the substrate [117].

The basic building block of this platform is the HBR [50], [118]. An HBR images the signal from an input port to an output port while applying a specific spectral filtering function. It provides excellent channel-specific pass-band control like TFFs and FBGs, and its spatially distinct input and output ports obviate the need for bulky circulators or loss power splitters to separate the input and output signals. The ability of HBRs to provide both spectral slicing and temporal delay simultaneously implies that the footprint of HBR-based WH/TS encoders/decoders can be made very small. Multiple HBRs can be superimposed, interleaved or overlaid to design multiport devices [119].

2.6 OCDMA Impairments

Despite the developments in related technologies to date, OCDMA systems suffer from a phenomenon known as multiple access interference (MAI), which limits the overall system performance as the number of active channels increases. MAI results from the "improperly" decoded codes passing through the unmatched decoder and being incident on the photodetector. This MAI limits system performance as it scales with the number of channels. MAI arises from the fact that a receiver receives a copy of all transmitted codes and not just the intended one. Although the decoder recovers the desired code (channel) the remaining channels are improperly decoded, they are also incident on the photodetector resulting in a background noise that scales as the number of users increases.

To combat MAI, various optical time-gating [44], [91] and optical-thresholding [89], [120] techniques have been experimentally demonstrated. Since all users share the same bandwidth, OCDMA also suffers from optical beat noise (OBN), which arises when all the incoming electrical fields are mixed in the photodetector. OBN is a severe limitation in OCDMA as it scales with the square of the number of users [23]. Beat noise has been studied in relation to coherent and incoherent OCDMA [74],

where it is determined that beat noise can be overcome through the use of a low-coherence source, longer optical codes or through the use of some form of synchronisation.

2.7 Implementation of 2D-WH/TS

Implementations of WH/TS have focussed on using multi-wavelength lasers for providing short pulses at multiple wavelengths. Multi-wavelength sources using an array of lasers are limited by the higher complexity in controlling large numbers of lasers [95]. System costs rise dramatically if a multi-wavelength source is required at each node. Spectral slicing of a broadband source is a promising approach for achieving a multi-wavelength source. Various broadband sources have been used such as light-emitting diode (LED), amplified spontaneous emission (ASE) noise from an erbium-doped fibre amplifier (EDFA) [114] and supercontinuum (SC) generation [115]. The generation of SC in optical fibres with spectral filtering has been used for multi-wavelength sources for applications in WDM/OTDM networks [121], [122] and in WH/TS OCDMA networks [88].

In this thesis, the effect of chromatic dispersion for 2D-WH/TS codes that utilise short picosecond pulses for code generation will be investigated in details. This is important especially because of the relative broadening (of the order of the pulse width) due to fibre chromatic dispersion [20], [53], even with relatively short propagation distance in a single-mode optical fibre. This makes control of chromatic dispersion one of the key factors for preventing significant degradation in the OCDMA system.

Chapter 3: Dispersion and Fibre Optic Systems

3.1 Introduction

Extending the reach of optical transmissions at higher bit rates becomes a major challenge. Transmission impairments will generally affect optical transmission and decrease the quality of the optical signal along the propagation path.

3.2 Transmission Impairments

The physical or transmission impairments affecting optical communications can be categorised into linear and nonlinear impairments [123], [124], [125]. The terms linear and nonlinear in fibre optics mean intensity independent and intensity dependent, respectively. When the degradation caused by an optical element does not depend on the optical power of the signals transported through the optical element, the impairment is said to be linear. In contrast, nonlinear impairments depend on the optical power of the signals transported, and therefore, the level of degradation strongly depends on the intensity of the optical signals [123], [124], [125]. Linear impairments are static in their nature, and nonlinear impairments are dynamic in their nature.

Some important linear impairments are attenuation, chromatic dispersion (CD), insertion loss (IL), etc. Nonlinear impairments basically include a nonlinear crosstalk [124], [125] – due to four-wave mixing (FWM), self-phase modulation (SPM), cross-phase modulation (XPM) (all resulted from the Kerr effect) – and stimulated Raman scattering (SRS), and stimulated Brillouin scattering (SBS) [123], [126]. Among these impairments, polarisation mode dispersion (PMD) and chromatic dispersion produce temporal dispersion, whereas attenuation mainly affects the optical-signal-to-noise ratio (OSNR) [124]. In practice, in optical fibre, the impairments which affect OSNR can usually be compensated using amplifiers such as an EDFA [123]. Figure 3.1 shows the summary of transmission impairments based on linear and nonlinear effects [123].

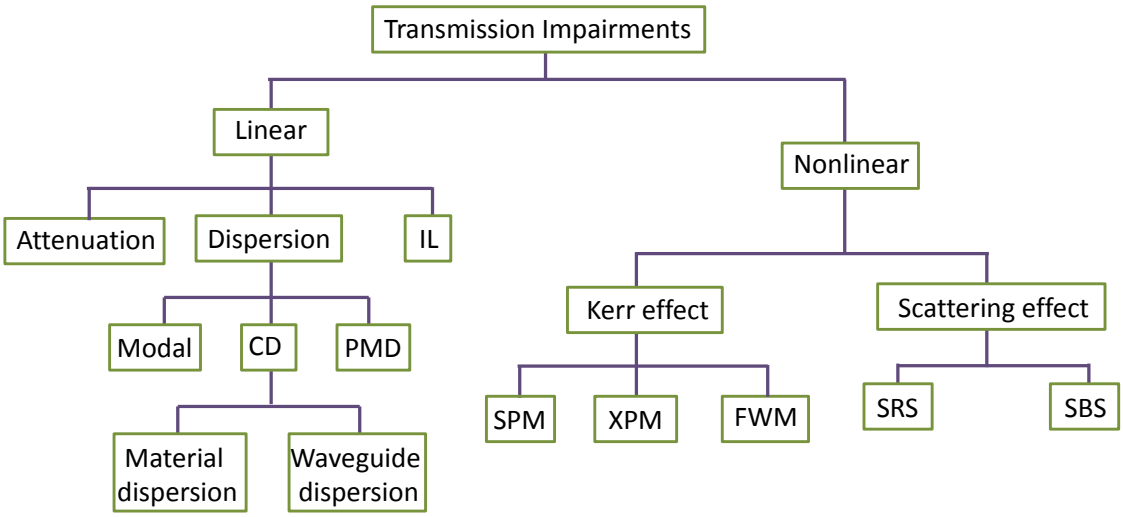

Fig. 3.1 Transmission impairments category; IL – insertion loss, CD – chromatic dispersion, PMD – polarisation mode dispersion, SPM – self-phase modulation, XPM – cross-phase modulation, FWM – four wave-mixing, SRS – stimulated Raman scattering, SBS – stimulated Brillouin scattering

There are three types of dispersion: modal, chromatic and polarisation mode. Chromatic dispersion is the combination of two components: material and waveguide dispersion [127]. The combined effect of material and waveguide dispersions for a particular mode alone is also called intramodal dispersion. Modal dispersion is caused by the variation in propagation constant between different modes; it is also called inter-mode dispersion [128].

Modal dispersion can be observed in multimode optical fibre where multiple modes of the same signal pulse propagate at different velocities along the optical fibre and cause pulse broadening. Generally, modal dispersion does not occur in a single-mode fibre because there is only one fundamental mode propagating [96], [129]. However, it exists even when chromatic dispersion disappears [128]. In contrast, if only one mode is excited in optical fibre, only intramodal chromatic dispersion needs to be considered – even when the fibre is a multimode fibre [128].

PMD in optical fibre is caused by imperfections in the circularity of the fibre's cross-section. External forces applied on the fibre, irregularities, or even heating, are all potential sources of PMD. Unlike chromatic dispersion, the dispersion introduced by PMD does not depend on the wavelength. PMD is also smaller in magnitude than

that of chromatic dispersion [124]. Overall, chromatic dispersion is considered one of the most harmful effects to system performance within the category of linear impairments [123], [124].

3.2.1 Dispersion in Single-Mode Optical Fibre

Dispersion is a phenomenon in which the phase velocity of a wave or group velocity depends on its frequency [130], [131]. Dispersion is sometimes called chromatic dispersion to emphasise its wavelength-dependent nature, or group-velocity dispersion (GVD) to emphasise the role of the group velocity. The group velocity difference occurs because the index of refraction (n) of the transmission media is wavelength dependent $n = n(\lambda)$. Chromatic dispersion causes pulses to spread in optical fibre, degrading signals over long distances. In SMF, the variation in these groups' velocities, with which spectral components propagate, results in a time broadening of the transmitted optical pulse.

Material dispersion comes from a frequency-dependent response of the material to propagating waves, caused by the wavelength dependence of the refractive index of glass in the fibre. Material dispersion is a dominant part of chromatic dispersion [132].

Waveguide dispersion is caused by frequency dependence of the propagation constant of a specific mode due to the waveguiding effect. Waveguide dispersion occurs when the speed of a wave in the waveguide (such as an optical fibre) depends on its frequency, in the distribution of light between the core and the cladding of an SMF. As a result, different wavelengths propagate at different velocities in core and cladding. More generally, waveguide dispersion can occur for waves propagating through any inhomogeneous structure, whether or not the waves are confined to a region. Waveguide dispersion is relatively small compared to material dispersion. In general, both types of dispersion may be present, although they are not strictly additive, but their combination leads to signal degradation in optical fibres. The chromatic dispersion phenomenon is illustrated in Fig. 3.2, indicating the pulse broadening due to dispersion.

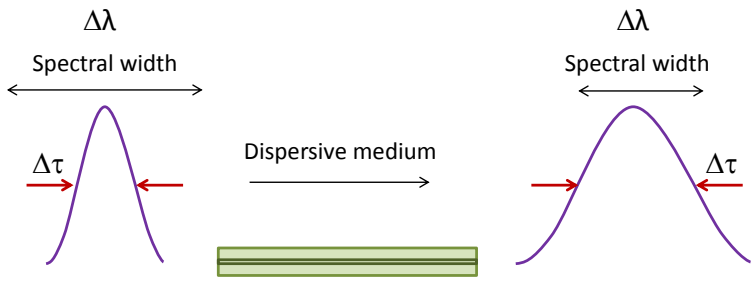

Fig. 3.2 Effect of chromatic dispersion, Δτ is temporal width, Δλ is spectral width

Because, in optical fibre, the pulse spectral components do not propagate with the same speed they will arrive at the receiver at different times, the phase velocity, v can be expressed by Eq. 3.1 [131],

$$v = \frac{c}{n(\lambda)} \tag{3.1}$$

where c is the speed of light in a vacuum, n is the refractive index of optical fibre and λ is the wavelength.

As a result, the optical pulse will broaden in time, decrease in peak power and change its pulse shape along the optical fibre. When the pulse becomes wider, it can overlap and interfere with adjacent pulses. This induces inter-symbol interference (ISI) at the destination. Eventually, this limits the maximum achievable data transmission rate and/or transmission distance [96], [127]. Figure 3.3 indicates the ISI effect due to pulse broadening. This interference will affect the BER.

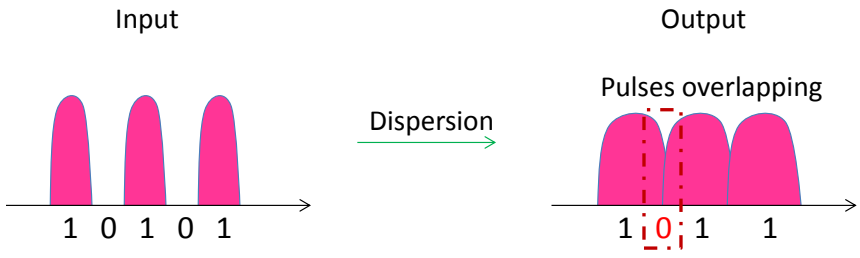

Fig. 3.3 Illustration of pulse broadening and ISI effect due to chromatic dispersion

Notably, in long-haul fibre optic communication systems, chromatic dispersion, if unchecked, will result in strong temporal widening of optical pulses. In particular, effects such as inter-symbol interference [51], pulsewidth and peak power limitation [23], and pulse distortion [52] due to chromatic dispersion were studied and are well understood.

3.2.2 Chromatic Dispersion Evaluation

Refractive index varies with wavelength, which can be shown by Eq. 3.2 [131], [133]. For visible light, refraction indices *n* of most transparent materials (e.g., air, glasses) decrease with increasing wavelength λ:

$$1 < n(\lambda_{red}) < n(\lambda_{yellow}) < n(\lambda_{blue}),$$

or alternatively:

$$\frac{dn}{d\lambda} < 0 \tag{3.2}$$

In this case, the medium is said to have normal dispersion. If the index increases with increasing wavelength, the medium is said to have anomalous dispersion.

The dispersion D, of standard SMF for a wavelength range from 1200 to 1625 nm can be calculated by using the following empirical formula [134]:

$$D \approx \frac{S_0}{4}\left(\lambda_c - \frac{\lambda_0^4}{\lambda_c^3}\right) \tag{3.3}$$

Where D is in ps/(nm.km), S_0 is zero dispersion slope in ps/(nm^2.km), λ_c and λ_0 is central wavelength and zero dispersion wavelength in (nm) respectively.

Zero dispersion wavelength λ_0 is wavelength where material and waveguide dispersion cancel each other out. Typically, zero dispersion wavelength of SMF (ITU G.652) is near the wavelength of 1310 nm.

As already mentioned, chromatic dispersion occurs as result of the fact that the different spectral components of the optical pulse travel in fibre at slightly different group velocities. The frequency dependence of the group velocity leads to a pulse

broadening because different spectral components of the pulse will disperse during propagation in optical fibre and do not arrive simultaneously. For pulse propagation distance L in a single-mode fibre (SMF), if $\Delta\omega$ is optical pulse spectral width, and v_g is the group velocity, the extent of the pulse broadening can be written [15], [16]

$$\Delta\tau = \frac{d\tau}{d\omega}\Delta\omega = \frac{d}{d\omega}\left[\frac{L}{v_g}\right]\Delta\omega = L\frac{d^2\beta}{d\omega^2}\Delta\omega = L\beta_2\Delta\omega \tag{3.4}$$

where β is wavenumber parameter in fibre (as K in free space) and β_2 is called group velocity dispersion (GVD) parameter in (ps^2/km) [3]. By substituting $\omega = 2\pi c/\lambda$, and using $\Delta\omega = (-2\pi c/\lambda^2)\Delta\lambda$,

$$\Delta\tau = \frac{d}{d\lambda}\left[\frac{L}{V_g}\right]\Delta\lambda = DL\Delta\lambda \tag{3.5}$$

where

$$D = -\frac{2\pi c}{\lambda^2}\beta_2 \tag{3.6}$$

D is dispersion expressed in (ps/nm.km) and varies with the wavelength. If D is less than zero, the medium is said to have positive dispersion. If D is greater than zero, the medium has negative dispersion. If a light pulse is propagated through a normally dispersive medium, the result is the higher frequency components travel slower than the lower frequency components.

The dispersion D defined above is obtained from the 'first' derivative of the group velocity. Higher derivatives are known as higher-order dispersion [7] and are simply a Taylor series expansion of the dispersion relation $\beta(\omega)$ of Eq. 3.4 to the medium or waveguide around a particular frequency [135].

3.2.3 Impact of Chromatic Dispersion on Multi-Wavelength OCDMA Codes

Advances in multiplexing technology have provided ways to increase the capacity of optical networks. Three significant trends became evident – namely the continual increase in the number of channels, increase in data rates from 2.5 Gb/s to 10 Gb/s to 40 Gb/s, and longer transmission distances [130]. These trends are now 'clashing'

with chromatic dispersion. The management of chromatic dispersion is one of the critical challenges for telecommunication systems, especially operating at data rates of 10 Gb/s and higher.

There have been a number of studies investigating the impact of fibre dispersion on OCDMA and 2D-WH/TS OCDMA systems [51], [53], [136], [137], [138]. 2D codes use multicolour pulses to achieve better code performance, in terms of both cardinality and correlation properties, in comparison to the 1D codes [10]. In 2D-WH/TS OCDMA systems to increase the bitrate, the chip size is designed to be smaller. Since a single user has its data spread across many discrete wavelengths, this approach presents a unique challenge that does not exist in conventional TDM or WDM telecommunication systems [136]. The system performance will therefore be more severely affected by fibre chromatic dispersion [133].

The impact of chromatic dispersion on 2D-WH/TS codes with multi-wavelength pulses includes pulses broadening, peak power reduction and time-skewing [55]. Any deviation from a transmission link chromatic dispersion compensation will result in a deteriorated of autocorrelation peak decoded by the user [136]. Therefore, fibre chromatic dispersion will have two deleterious effects: each short optical pulse in a given time-wavelength chip will broaden in time, similar to regular dispersion effects on data signal, and will also experience a different time-skew on the arrival depending on wavelength [53].

Figure 3.4 illustrated the time-skewing effect on the 2D-WH/TS codes and the resulting autocorrelation peak obtained. The first study of the impact of the time skewing on the 2D-WH/TS OCDMA system was reported in [53]. Based on coding theory, the authors did an investigation of the impact of temporal skewing on code autocorrelation and cross-correlation properties. However, the impacts of pulse broadening and peak power reduction were not included in the analysis.

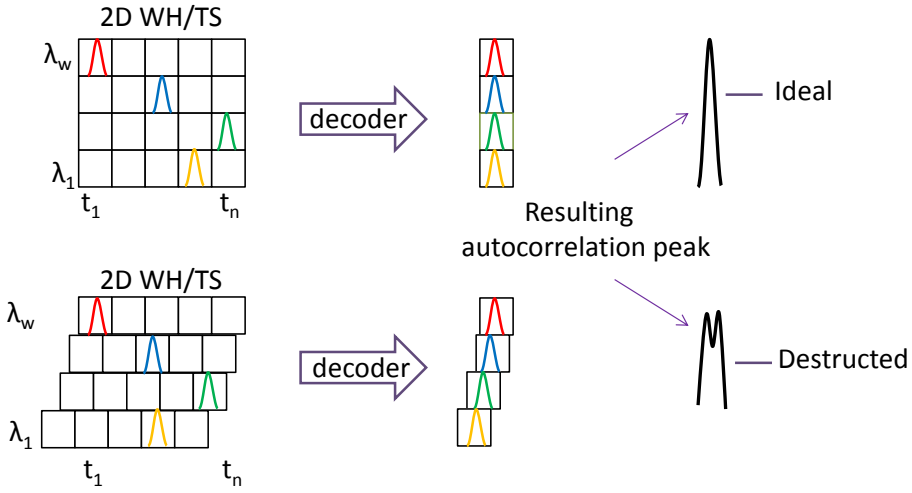

Fig. 3.4 Illustration of time skewing and the effect on the resulting autocorrelation peak for 2D-WH/TS codes for ideal (top) and destructed (bottom) cases

Later, a model of Gaussian pulse propagation in the optical fibre was proposed [54]. In this model, the impact of a GVD and chromatic dispersion effects on the performance of 2D-WH/TS OCDMA systems was analysed. Various parameters, such as maximum transmission length, number of supportable users, required power and power penalty, were also investigated in the analysis. Under the impact of chromatic dispersion, the number of supportable users is extremely decreased and the maximum transmission length is remarkably shortened in the case of SMF. The main factor that limits the system performance is autocorrelation time skewing. Although the impact of pulse broadening and peak power reduction can be significantly reduced when DSF is used, the impact of time skewing is still relatively strong [53], [54].

3.3 Chromatic Dispersion Compensation Technique

The result of chromatic dispersion in optical fibre, whether negative or positive, will ultimately affect the temporal width of the pulse. This makes dispersion management extremely important in optical communications systems based on short picosecond pulses, since if the dispersion is too high, a group of pulses representing an OCDMA bit will spread in time and merge/overlap, rendering the bit-stream unintelligible. This limits the transmissions length that a signal can be sent without regeneration.

One possible solution is to send a signal at a wavelength in which the chromatic dispersion is zero (e.g., around 1.3 μm in silica fibres), so pulses will suffer minimal spreading from dispersion. In practice, however, this approach causes more problems than it solves, because zero chromatic dispersion unintentionally creates conditions for other nonlinear effects such as four-wave mixing [54].

Dispersion compensation schemes [23], [139], [140] in spectrally encoded OCDMA systems have been proposed. Compensation for chromatic dispersion can be achieved by using techniques that utilise compensating elements such as dispersion compensating fibre (DCF) [141], optical phase conjugation (OPC) [142] or chirped fibre grating (CFG) [110]. Figure 3.5 illustrates the concept of chromatic dispersion compensation.

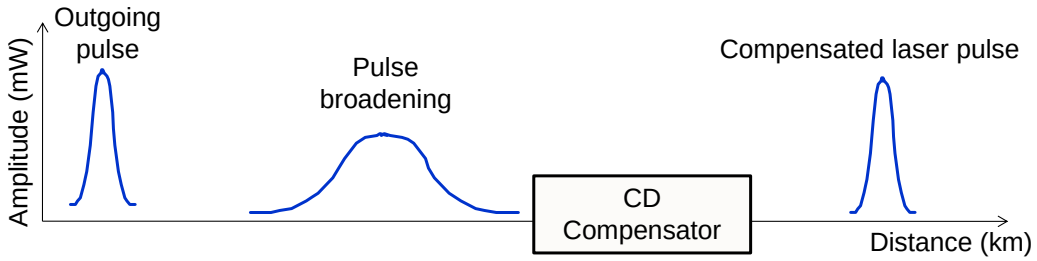

Fig. 3.5 Illustration of the concept of chromatic dispersion compensation

It is worth mentioning that dispersion control is also important in lasers that produce short pulses and EDFAs. The overall dispersion of the optical resonator is a major factor in determining the duration of pulses emitted by the laser. A pair of prisms can be arranged to produce net negative dispersion, which can be used to balance the usually positive dispersion of the laser gain medium. Diffraction gratings can also be used to produce dispersive effects; these are often used in high-power laser systems. Recently, an alternative to prisms and gratings has been developed: chirped mirrors. These dielectric mirrors are coated so that different wavelengths have different penetration lengths, and therefore different group delays. The coating layers can be tailored to achieve a net negative dispersion.

3.3.1 Fibre-Based Chromatic Dispersion Compensating Technique

Fibre-based chromatic dispersion is inherently robust and technically brings some advantages by restricting undesirable nonlinear effects (such as SPM and FWM) to acceptable levels. Eliminating chromatic dispersion is also possible using special devices [130]. In fibre optic transmission systems, dispersion compensating modules (DCM) are often used for chromatic dispersion compensation. These modules provide a fixed amount of compensating dispersion value. DCM is often placed between two fibre amplifiers (EDFA) [96], [132]. Dispersion compensating fibre (DCF), fibre Bragg grating (FBG) and optical phase conjugation (OPC) can be used in chromatic DCM. Typically, the DCM length is specified as the length (in km) of standard SMF it will compensate or by the total compensated value of dispersion, specified in ps/nm [132]. Table 3.1 shows typical dispersion and slope values for various types of nonzero dispersion shift fibres (NZDSF) and SMF that can be used for dispersion compensation.

DCM containing DCF typically has high fibre attenuation and insertion loss. This loss can be compensated by optical amplification [143]. The effective core area (A_{eff}) of DCF is much smaller than standard ITU-T G.652 SMF, thereby DCF may experience some optical signal distortions caused by nonlinear optical effects (NOE) [132]. Typical DCF has an effective core area A_{eff} = 12 μm^2, whereas the standard SMF has A_{eff} = 80 μm^2. DCF has an attenuation coefficient α = 0.6 dB/km whereas standard SMF has α = 0.2 dB/km. The nonlinear effects are stronger in fibres with smaller values of A_{eff}. The impact of nonlinear optical effects can be reduced by lowering optical power [127].

Table 3.1 Typical dispersion and slope values in various types of fibres [144]

Type of Fibre	Typical dispersion at 1550nm (ps/nm.km)	Typical slope at 1550nm ($ps/nm^2.km$)	C-Band dispersion range (1530 to 1565nm) (ps/nm.km)	L-Band dispersion range (1570 to 1620nm) (ps/nm.km)
Conventional SMF-28	17	0.057	15.9 – 17.8	18.1 – 21.0
NZDSF (early) Type-1	2.6	0.067	1.3 – 3.6	3.9 – 7.3
Type-2	3.5	0.067	2.2 – 4.6	4.8 – 8.2
NZDSF (large effective area)	3.8	0.1	1.8 – 5.3	5.8 – 10.8
NZDSF (reduced slope)	4.4	0.045	3.5 – 5.1	5.3 –7.5
NZDSF (new large eff. Area)	4.2	0.085	2.6 – 5.5	5.9 – 10.1
NZDSF (new light fibre)	8.0	0.057	6.8 – 8.9	9.1 – 12.0

DCF has a large negative dispersion $D = -80\ ps/(nm.km)$. It must be noted that DCF adds polarisation mode dispersion (PMD) to the fibre optic transmissions link, a typical value is 0.1 $ps/\sqrt{km}$ [132]. The reason for PMD is that different frequency components of pulses, which have different polarisation states, propagate with different velocities, resulting in pulse broadening. PMD becomes a significant limiting factor for high-speed optical communication systems [96].

DCM with chirped FBG for compensation of chromatic dispersion is also available. It has a grating period which is not constant, but changes linearly over the length of the grating with the shorter grating period located at the beginning of the grating [132]; however, over the length of the grating these periods linearly increase. Therefore, shorter signal wavelengths are reflected sooner and have less propagation delay through the FBG, but longer signal wavelengths travel further into the fibre grating before they are reflected back and accordingly have more propagation delay through the FBG. Typically, the length of the fibre grating is from 10 to 100 cm [132]. A significant advantage of using an FBG-based chromatic dispersion compensation module, over a DCF fibre module, is its relatively small insertion loss and very short length.

Commercial DCF, used to compensate accumulated chromatic dispersion of 100 to 120 km standard SMF span, has about 10 dB of insertion loss, whereas an FBG-based chromatic dispersion compensation module is capable of compensating the same fibre span length with an insertion loss only up to 4 dB [143]. In contrast to a DCF-based chromatic dispersion compensation module, an FBG-based chromatic dispersion compensation module can be used at higher optical powers without inducing any nonlinear optical effects [96].

Besides DCF-DCM and FBG-DCM, the accumulated chromatic dispersion can also be compensated by optical phase conjugation (OPC), which realises an inversion of the optical signal phase. OPC is sometimes referred to as spectral inversion, and it is a promising technology capable of compensating accumulated chromatic dispersion and impairments caused by nonlinear optical effects, such as Kerr nonlinearities (FWM) and SPM, in long-haul fibre transmission systems [145]. Since the dispersion accumulates linearly along the fibre optic transmission link, OPC-DCM must be placed exactly in the middle of the link in order to obtain full dispersion compensation. This is to ensure that the distortion that occurred in the first part of the transmission link, before the OPC-DCM, is cancelled by the distortion that occurs in the second part of the link, after the OPC-DCM. However, it is not always possible to place OPC-DCM exactly in the middle of the fibre transmission link. Therefore,

an extra DCF module can be employed to obtain full chromatic dispersion compensation [96], [145].

Good-quality dispersion compensation modules are offered with the parameters having low dispersion variations, low insertion loss, low nonlinearity, low cost and good temperature stability [146].

3.4 ITU Dispersion Tolerance Limits

As transmission data rates continue to increase, this determines the total amount of allowed residual dispersion in a data transmission system. For transmission rate's corresponding pulse duration, International Telecommunication Unit (ITU) recommends a dispersion tolerance of 10% of the total pulse duration – as shown in Table 3.2.

Table 3.2 ITU dispersion tolerance limit

Data transmission rate (Gb/s)	Duration of single pulse (ps)	Dispersion tolerance limit (ps)
2.5 (OC-48)	400	40
10 (OC-192)	100	10
40 (OC-768)	25	2.5

3.5 Summary

In this Chapter the significance of chromatic dispersion management was discussed. Intuitively it seems obvious that the residual chromatic dispersion of the transmission system should be near zero, or zero, in order for short picosecond pulses or high-data-rates to be successfully transmitted over long distances [147]. However when the chromatic dispersion of the optical fibre is zero for the signal wavelength band used, optical signals with slightly different wavelengths travelling in the optical fibre will experienced the nearly 'phase matched' conditions, resulting in the generation of nonlinear effects such as four-wave mixing (FWM) [147]. In order to suppress such detrimental nonlinear effects, the chromatic dispersion of the optical fibre needs to

be in the range close to zero. This requirement apparently contradicts the zero CD condition to avoid waveform distortions. These contradictory conditions can be met by introducing dispersion management schemes, in which optical fibre exhibits non-zero chromatic dispersion locally, and yet the overall (or average) dispersion is set small (close to zero) in the signal wavelength band used for data transmissions [147].

As shown in Table 3.1 the typical value for the standard SMF dispersion coefficient is approximately 17 ps/nm.km [148], [149], [150] but some use 16.5 ps/nm.km [147], or in the range between 15–17 ps/nm.km. This dispersion coefficient depends on many parameters including temperature. The temperature effect on ODMA transmission will be investigated in later chapters of my thesis.

Therefore the proper chromatic dispersion compensation is important in order to achieve reliable system performance from the testing. Since the DCF is used as part of the optical transmission link, the fibre is conveniently coiled and packaged into a small DCF module. DCFs are single-mode fibres whose chromatic dispersions in the 1.55 µm wavelength band are negative with relatively large absolute values per unit length [151]. Negative dispersion from the DCF can be balanced with positive dispersion from SMF-28 – as is illustrated in Fig. 3.6. In the next Chapter 4 I will implement this technique for the fine CD tuning.

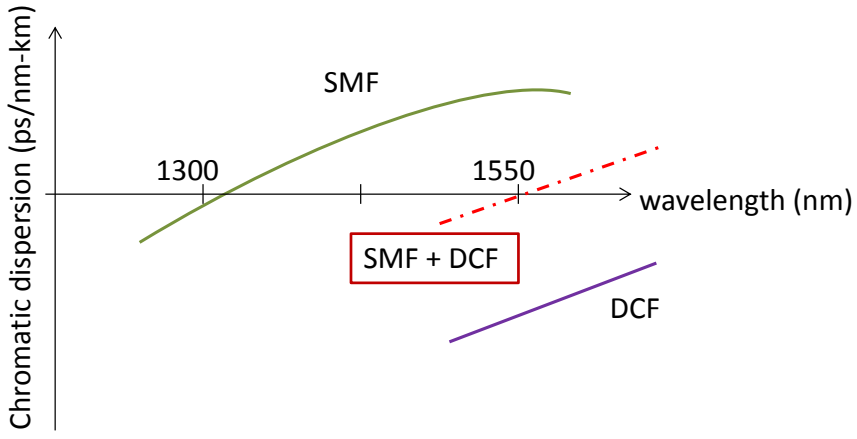

Fig. 3.6 Chromatic dispersion compensation approach when using dispersion compensating fibre (DCF) and SMF-28

Chapter 4: Construction of a Dispersion-Free Fibre Optic Link

4.1 Introduction

Testbeds are important tools to help verify and evaluate system design and performance [152]. This real link is essential for system testing under real environment with uncontrolled condition such temperature, humidity and other parameters. The outcomes will have a greater impact for any stakeholders and will be more significant in comparison to a laboratory arrangement with a spool of fibre shielded from the external environment.

In order to conduct an investigation of an OCDMA system under real environmental conditions, a fibre optic transmission link was built, between Glasgow University and the University of Strathclyde, over dark fibre. A bidirectional transmission length of this SMF-28 fibre link was measured using OTDR (see Fig. 4.1), and the distance recorded was 14.7 km. Using a dispersion coefficient of 16.5 ps/(nm.km), transmitting a narrow pulse over this distance generates a dispersion of approximately 242.55 ps/nm. To compensate for this amount of chromatic dispersion, dispersion compensation fibre (DCF) – known as a dispersion compensation module (DCM) – for a distance of 14.7 km is needed. The DCM I used was for a SMF length of 15 km, (ED7G043-30, G) and has a dispersion of −259 ps/nm.

DCF is presently the preferred solution for a fixed amount of chromatic dispersion compensation. DCF is engineered to have a high negative dispersion at 1550 nm. Due to its nearly constant dispersion slope across the large used spectrum in SMF-28, the chromatic dispersion in SMF cannot be exactly balanced by DCF. Thus, while DCF can neutralise the effect of chromatic dispersion at a single wavelength, at other wavelengths the chromatic dispersion will be either under or over compensated. This effect is known as dispersion slope mismatch [130].

Since DCF modules are available in fixed lengths of compensating fibre, it may be difficult to find a DCF that exactly compensates the chromatic dispersion introduced by the fibre, leading to residual chromatic dispersion. In my case, by comparing

positive and negative dispersion between the fibre link and DCF, a difference of −16.45 *ps/nm* is calculated. Thus, it is expected that the testbed is over compensated, and additional SMF-28 with positive dispersion is needed.

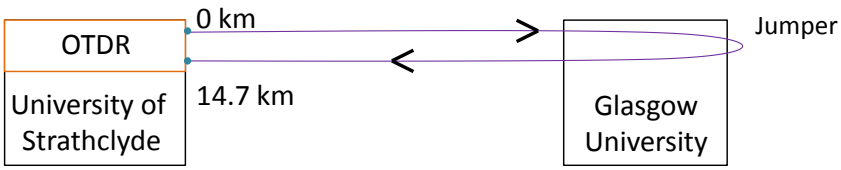

Fig. 4.1 OTDR measurements to determine the testbed length

To achieve sub-picosecond chromatic dispersion compensation accuracy, some additional tuning was necessary. Fundamental experiments needed to be conducted to verify the accuracy of performed chromatic dispersion compensation. The experimental setup to evaluate the effect of residual chromatic dispersion on laser pulse is illustrated in Fig. 4.2. The outgoing laser pulse is transmitted over the fibre link with the chromatic dispersion compensation module in place, and its pulse width is monitored.

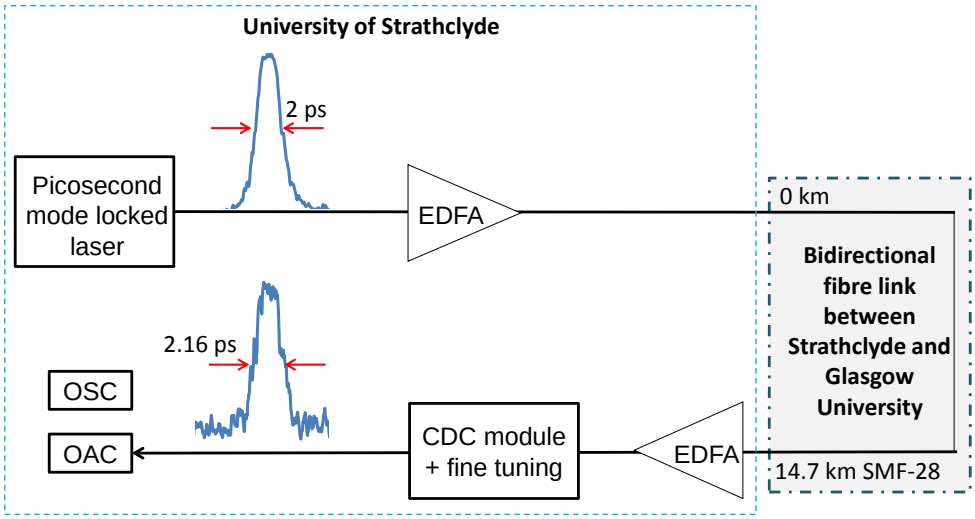

Fig. 4.2 Experimental setup demonstrating the effect of chromatic dispersion on laser pulse showing outgoing laser pulse and chromatic dispersion compensated laser pulse; EDFA – erbium-doped fibre amplifier, CDC Module – chromatic dispersion compensation module, SMF – single-mode fibre, OAC – optical autocorrelator, OSC – oscilloscope

To achieve sub-picosecond accuracy in chromatic dispersion compensation, the transmission link needed to be modified by adding an extra length of SMF-28. The tested extra lengths added were between 975 m and 1250 m. Figure 4.3(a) is the laser pulse generated by a mode-locked laser. The pulse width is approximately ~2 ps full width at half maximum (FWHM). This laser pulse was then sent through the transmission link and the return pulse was monitored using a bandwidth-limited Agilent oscilloscope with a 64 GHz optical sampling head (86105B). The effect of different added SMF-28 fibre lengths is depicted in Fig. 4.3(b to d).

Figure 4.3(b) is the returned laser pulse obtained after a 16.2 (14.7 + 1.5) km transmission (SMF-28 transmission link + DCM). Obviously, the pulse is broadened, which means the dispersion is not perfectly compensated and an extra length of SMF-28 is required. Figure 4.3(c and d) shows the laser pulses obtained with additional fibre lengths of 1000 m and 1250 m added, respectively.

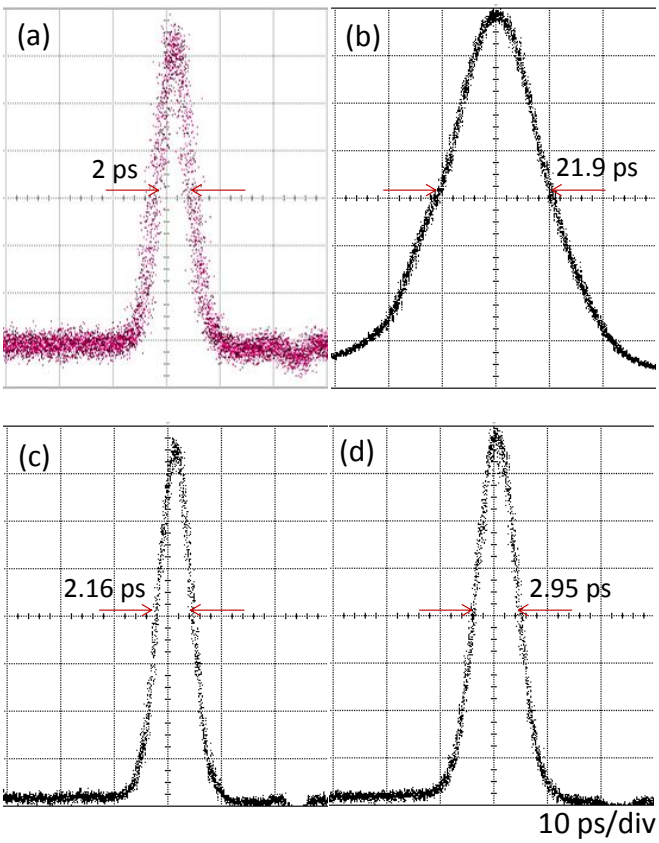

Fig. 4.3 Illustration of laser pulse width measurements to find a proper fibre length for complete dispersion compensation using a bandwidth-limited oscilloscope with a 64 GHz optical sampling head. (a) Input laser pulse and output laser pulse, (b) DCM only, (c) DCM + 1000 m, and (d) DCM + 1250 m was added to the bidirectional link, respectively

Since the pulse is monitored using a bandwidth-limited Agilent oscilloscope with a 64 GHz optical sampling head (86105B), the pulsewidth measured does not show the accurate reading. One should consider how such pulses can be measured experimentally since the shape and width of ultrashort pulses can change considerably. For pulses broader than ~20 ps FWHM, pulse characteristics can be measured directly by using oscilloscope with a 64 GHz optical sampling head (Agilent 86105B). Streak cameras can be used for pulses as short as 1 ps. However, most of them work best in the visible spectral region and cannot be used at wavelengths near 1.55 μm [133]. The obtained pulse width needs to be measured accurately in order to clarify the proper laser pulsewidth value.

A common technique for characterising ultrashort optical pulses is known as autocorrelation measurements and is based on the nonlinear phenomenon called

second harmonic generation (SHG). In this method, the pulse is sent through a nonlinear crystal together with a delayed replica of its own [153]. A second harmonic signal is generated inside the crystal only when two pulses overlap in time. Measuring the second harmonic power as a function of the delay produces an autocorrelation trace. The width of this trace is related to the width of the original pulse. The exact relationship between the two widths depends on the pulse shape. This technique can measure pulse widths down to a few femtoseconds but provides little information on details of the pulse shape. In fact, the autocorrelation trace is always symmetric – even when the pulse shape is known to be asymmetric. The use of cross correlation, a technique in which an ultrashort pulse of known shape and width is combined with the original pulse inside a second harmonic crystal, solves this problem to some extent. The auto and cross correlation techniques record intensity correlation and can also make use of other nonlinear effects such as two photon absorption (TPA) [154].

The autocorrelation technique is the most common method used to determine the laser pulse width characteristics on picosecond and sub-picosecond time scales. The basic optical configuration of the optical autocorrelator is similar to an interferometer. I used a Femtochrome optical autocorrelator (AOC) in all my experiments. An incoming optical pulse train generated by a mode-locked laser is split into two beams of equal intensity. An adjustable optical delay is inserted into one of the arms. These two optical pulse trains are then recombined within a nonlinear material - a second harmonic generation (SHG) crystal.

The emitted SHG signal is photodetected and observed by the “slow” oscilloscope. The amount of photocurrent as a function of a delay between interacting pulses is then measured and the autocorrelation function is called. The pulse width measured by the optical autocorrelator [155] can be calculated using Eq. 4.1 and it comprises three parts.

$$\Delta\tau = K\left(\frac{T}{t}\right)(\Delta T) \tag{4.1}$$

Where the first part constant *K* depends on the shape of the pulse – either sech, Gaussian or exponential – as shown in Table 4.1.

Table 4.1: The values of *K* for different pulse shapes

Pulse shape	*K*
Hyperbolic Secant	0.648
Gaussian	0.707
Single-sided exponential	0.5

The second part of Eq. 4.1 is the calibration factor which can be calculated using

$$\frac{T}{t} = \frac{2x\ (psec)}{0.3s\ (msec)} \tag{4.2}$$

where *x* (mm) is the distance between two mirror positions representing two delays, *s* is the distance between two pulse positions on the oscilloscope related to *x* (as illustrated in Fig. 4.4). When the rotator moves for distance *x*, the light has to travel double that distance, *2x*. 0.3 factor comes from displacement measurement

$$T = \frac{2x}{c} \tag{4.3}$$

where c is the speed of light and in vacuum it is $0.3\,\mu m/fs$. The last part in eq. 4.1, ΔT is the pulsewidth measured by the oscilloscope.

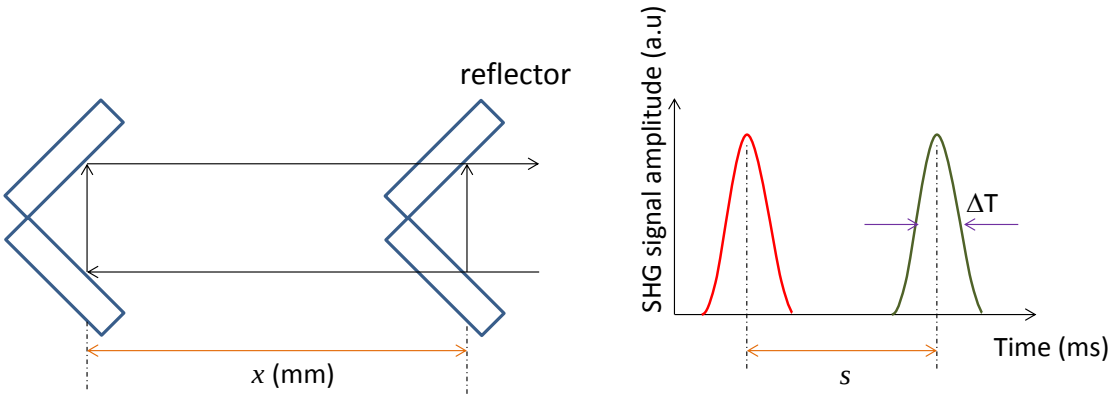

Fig. 4.4 Illustration of the procedure for obtaining autocorrelator calibration parameters. On the left – autocorrelator delay adjustment by the micrometre, on the right – corresponding shift of the autocorrelation peak observed on the oscilloscope

To calculate the laser pulse width, I assumed it to be a Gaussian pulse width. The distance x = 2.3 mm was read off the micrometre screw gauge on the autocorrelator and resulted, on the oscilloscope, to a corresponding time shift s = 0.8 ms. The measured autocorrelation width ΔT = 1.6 ms. This is the average from several measurements ranging from 1.55 ms to 1.65 ms. This average value is used in the equation. Therefore, the compensated laser pulse is 2.16 ps – as shown in Fig. 4.5.

$$\Delta\tau = K\left(\frac{T}{t}\right)(\Delta T) = 0.707\left(\frac{2(0.23)}{0.3(0.8m)}\right)1.6 = 2.168\,ps$$

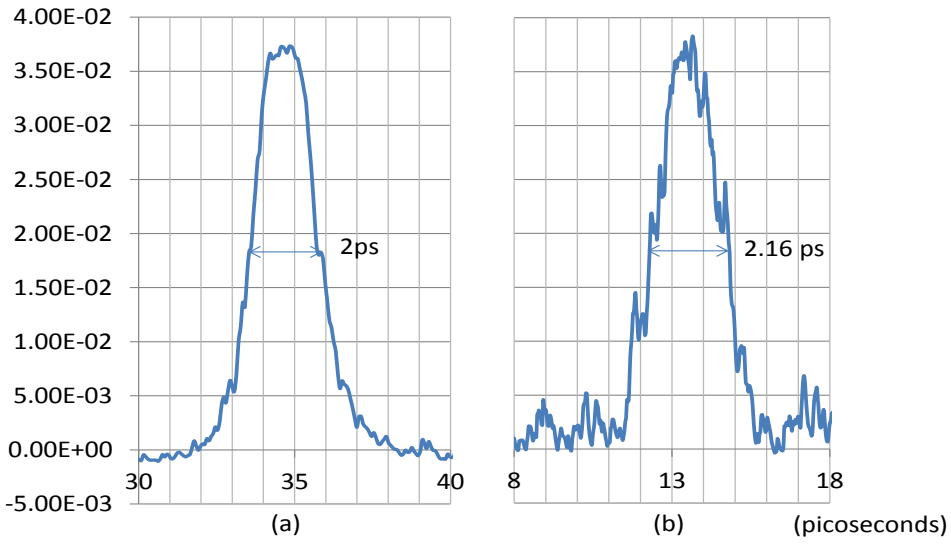

Fig. 4.5 Laser pulse width as measured using a Femtochrome optical autocorrelator. (a) Outgoing laser pulse, and (b) pulse obtained when DCM + 1000 m was added to the bidirectional fibre link

From the Agilent oscilloscope measurements, and by using the optical autocorrelator (Femtochrome), it was decided that adding 1000 m of SMF-28 to the DCM was needed to achieve the best result - the bidirectional link dispersion with residual chromatic dispersion of ~ 0.05 ps/nm.

4.2 Chromatic Dispersion Evaluation Using 2D-WH/TS OCDMA Code

This experiment was aimed at verifying if the bidirectional fibre link to be used as an OCDMA system testbed was properly compensated for the chromatic dispersion. In this set of experiments, a 2D-WH/TS OCDMA code, based on multi-wavelength picosecond pulses, is used instead of a single picosecond laser pulse. Figure 4.6 depicts the experimental setup, showing the OCDMA transmitter and receiver. Generated OCDMA code is sent through the transmission link and the return signal is monitored after passing the OCDMA decoder by using a bandwidth-limited oscilloscope with a 64 GHz optical sampling head (Agilent 86105B)

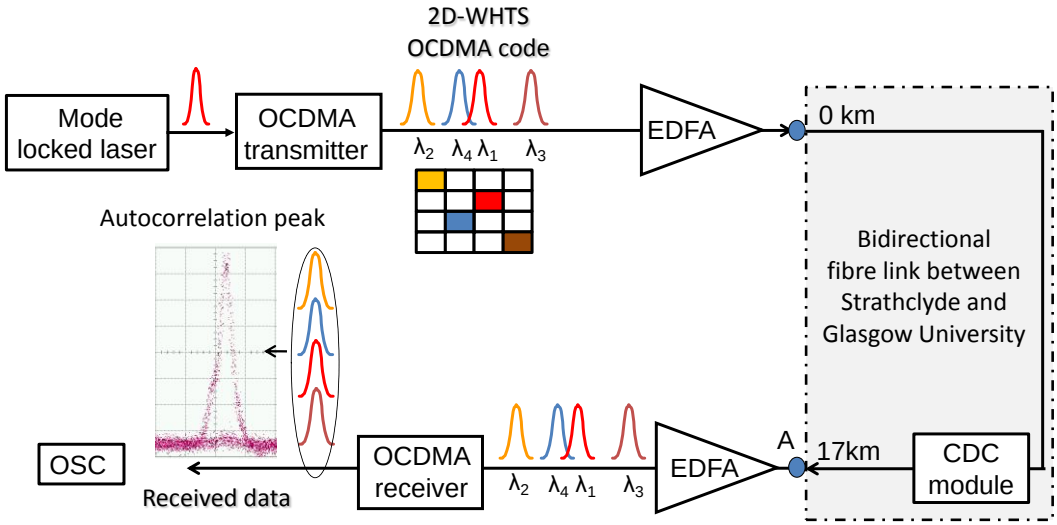

Fig. 4.6 Experimental setup to evaluate the impact of chromatic dispersion on 2D-WH/TS OCDMA code: OCDMA – optical code division multiple access, EDFA – erbium-doped fibre amplifier, CDC – chromatic dispersion compensation module, OSC – oscilloscope

Figure 4.7 illustrates the chromatic dispersion skewing effect on 2D-WH/TS OCDMA code in a case where chromatic dispersion compensation is not properly applied. Decoded OCDMA code results in an autocorrelation peak – shown in Fig.

4.7(a); however, chromatic dispersion causes the skew effect of the autocorrelation peak – Fig. 4.7 (b).

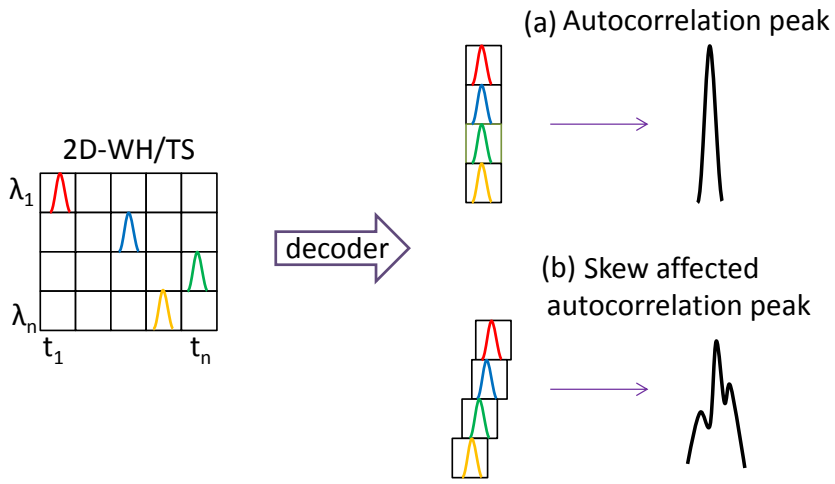

Fig. 4.7 Illustration of time skewing effect on 2D-WH/TS codes induced by the chromatic dispersion

The effect of the time skew illustrated in Fig. 4.7 can be seen on the results obtained by an oscilloscope shown in Fig. 4.8. These results are compared to autocorrelation peak from back-to-back measurements (Fig. 4.8a). Figure 4.8(b to d) shows recorded autocorrelation peaks for different combinations of chromatic DCM plus additional length of SMF-28 after the round-trip in the testbed.

The concept of the experiment is as follows:

(a) If complete chromatic dispersion compensation has been achieved, the decoded autocorrelation peak of a received OCDMA code, after propagation in the testbed, will not be time skewed and a pulse like that seen in Fig. 4.7(a) will be observed.

(b) If the link still has a residual chromatic dispersion, the received autocorrelation peak will be time skewed – see Fig. 4.7(b). The amount of skewing will depend on the amount of residual chromatic dispersion.

Figure 4.8(a) illustrates the autocorrelation peak obtained from the back-to-back measurements. Figure 4.8(b) is the autocorrelation peak obtained when only DCM is used to compensate for chromatic dispersion. This wide and skewed autocorrelation peak shows that the link is improperly compensated. The autocorrelation peak in Fig.

4.8(c) is identical to the back-to-back autocorrelation peak. Here, DCM plus additional SMF-28 of 1000 m is used to compensate for the chromatic dispersion compensation, and proper chromatic dispersion compensation is achieved. In Fig. 4.8(d), DCM plus 1250 m of extra SMF-28 was used. Improper chromatic dispersion compensation is observed. When the extra length of SMF-28 was increased, the obtained autocorrelation peak started to broaden and skewed again – Fig. 4.8(d).

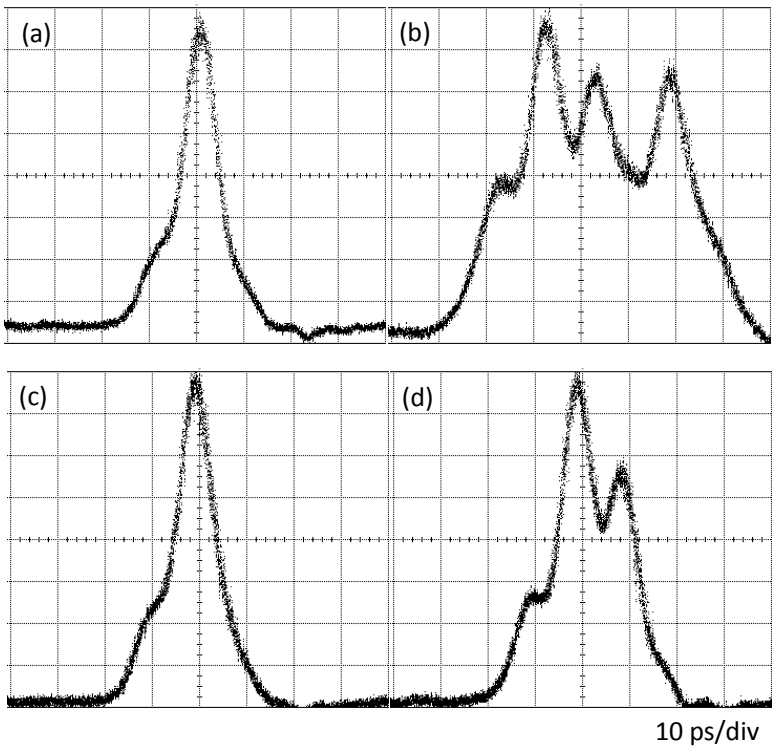

Fig. 4.8 Autocorrelation peak as seen on a bandwidth-limited oscilloscope (Agilent 86105B) with a 64 GHz sampling head. (a) Back-to-back, (b) DCM only added to the bidirectional link, (c) DCM + 1000 m added, and (d) DCM + 1250 m added

4.3 Summary

Fibre optic transmission links are the heart of every communication testbed and to know links dispersion properties is very important, especially if the fibre link will need to support data rates over 10 Gb/s or data transmissions using short multicolour ps optical pulses. Therefore, I verified the bidirectional transmission link built between University of Strathclyde and University of Glasgow for CD related transmission impairments. My contributions encompass conducting fundamental experiments over the fibre link to study and determine chromatic dispersion using a

short laser pulse from an erbium-doped fibre mode-locked laser and 2D-WH/TS OCDMA code based on multicolour picosecond pulses. From these experiments I measured the residual chromatic dispersion of this bidirectional link. The obtained experimental results confirmed that the Strathclyde-Glasgow bidirectional fibre link is compensated for chromatic dispersion with a sub-picosecond accuracy and the residual dispersion for the optical spectrum range (1550.12 nm -1552.52 nm) being used by the 2D-WH/TS OCDMA codes is near zero which will provide supressing conditions to generate FWM in my future experiments.

Chapter 5: OCDMA Testbed Construction

5.1 Introduction

The Strathclyde–Glasgow fibre optic testbed is shown as a block diagram in Fig. 5.1, and it consists of a transmitter, receiver terminal and a bidirectional fibre optic link – as described in Chapter 4. The transmitter and receiver terminals are based on OCDMA technology.

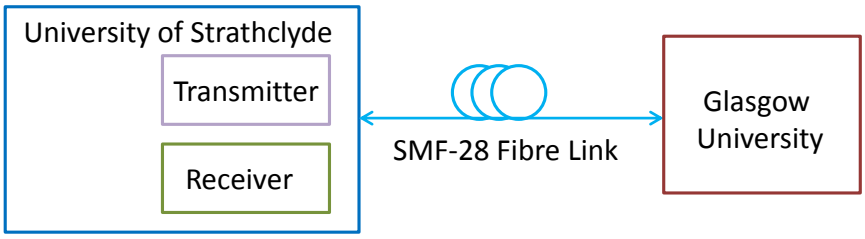

Fig. 5.1 OCDMA testbed block diagram

5.2 OCDMA Transmitter and Receiver Terminal

The schematic diagram of the OCDMA transmitter terminal is illustrated in Fig. 5.2. It is designed to support four OCDMA users. It consists of four optical circulators (OCs), four FBG-based OCDMA encoders, a 1×4 power splitter, and 4×1 combiner contained in a sealed housing. The individual components are inter-connected by FC/APC connectors.

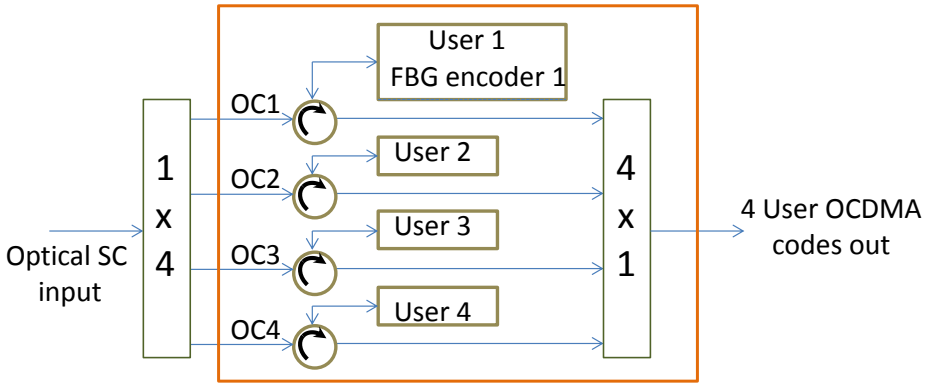

Fig. 5.2 OCDMA transmitter port design showing optical circulators (OC) with 1×4 and 4×1 power splitter and combiner; Optical SC – optical supercontinuum

The 4-user transmitter terminal is based on four OCDMA FBG encoders (FBG Enc) and is assembled as shown in Fig. 5.2. All four encoders are placed close to each other and properly attached to individual optical circulators (OCs) and, finally, to a 4×1 power combiner. FC/APC connectors are used on the box front face, and the box is sealed (See Fig. 5.3).

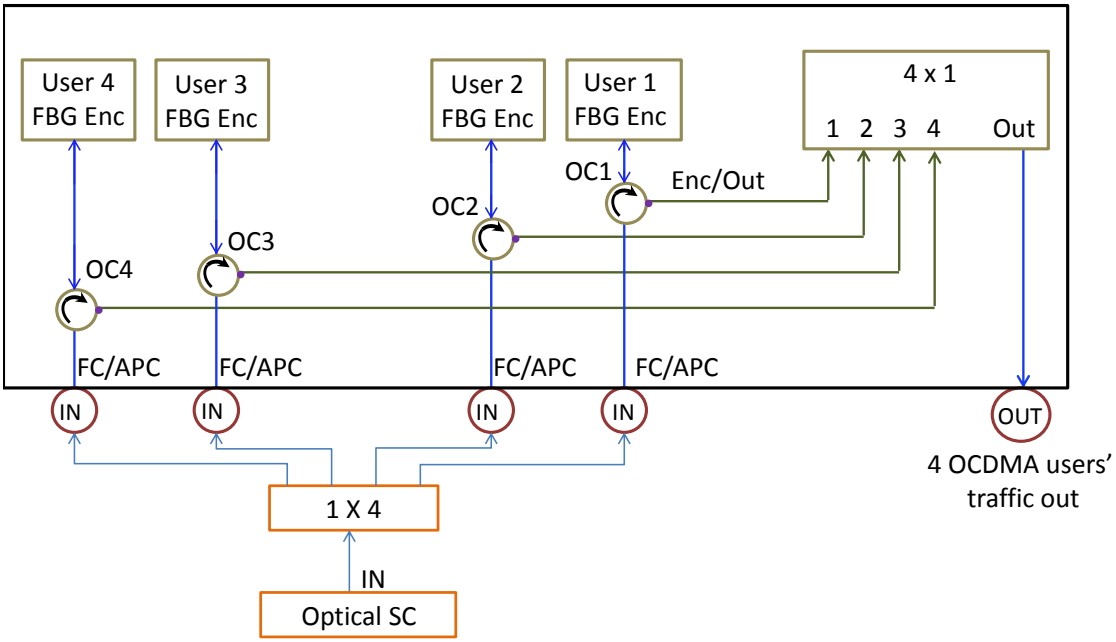

Fig. 5.3 The illustration inside the transmitter port. FBG Enc – FBG based encoder, OC – optical circulator, SC – supercontinuum, IN – input, OUT – output, 4×1 and 1×4 – power combiner and power splitter

Figure 5.4(a) depicts the inside of the OCDMA transmitter terminal box and Fig 5.4(b) shows its top view.

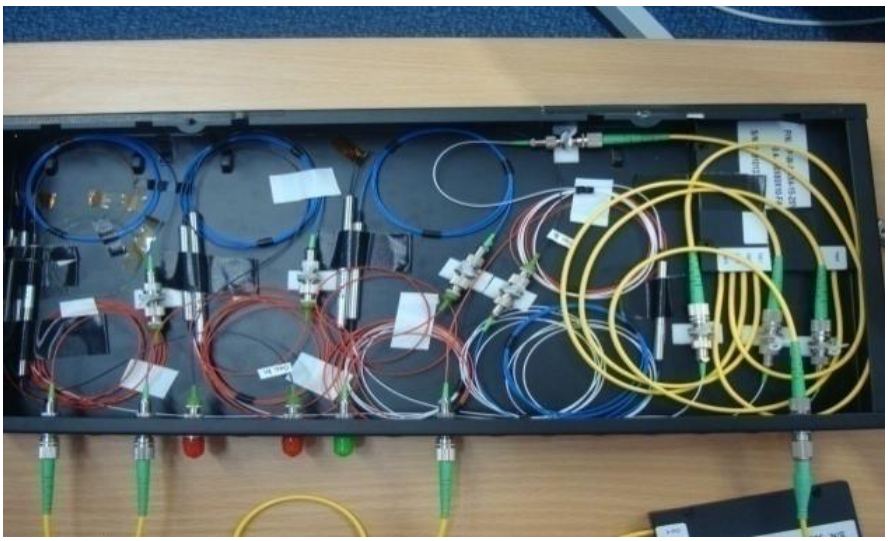

(a)

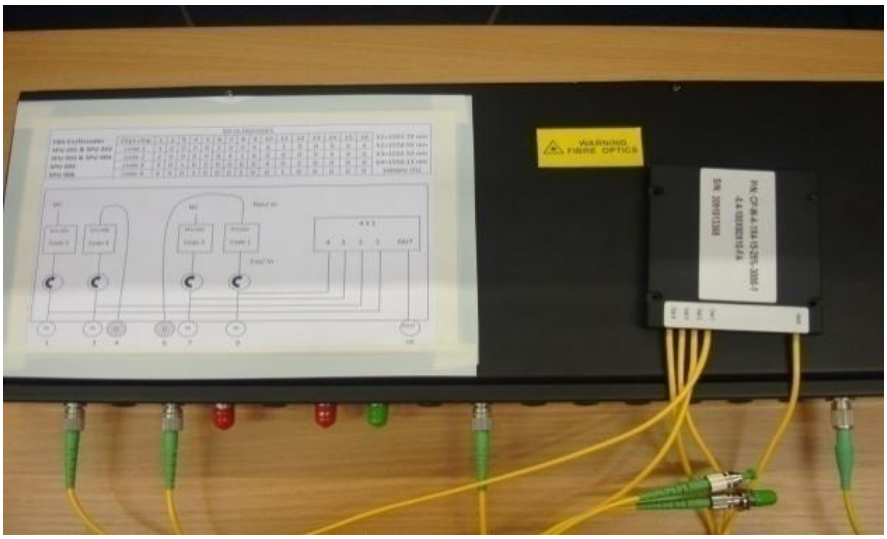

(b)

Fig. 5.4 Assembled OCDMA encoder box where the multiplexer, circulators and fibre optics were laid and wound. (a) Configuration inside the box, and (b) outside view after the box is sealed

The receiving OCDMA terminal consists of the OCDMA user 1 receiver, *Rx 1*, and one OCDMA eavesdropper as depicted in Fig. 5.5.

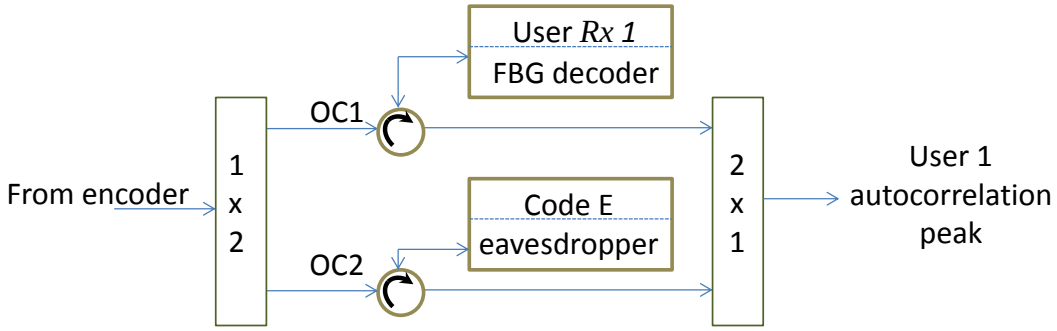

Fig. 5.5 Receiving terminal; OC is optical circulator, with 1×2 and 2×1 power splitter and combiner

5.3 Data Generation

In general, data modulators are used to externally modulate continuous wave (CW) lasers to generate optical digital data to be transmitted through optical fibre [156], [157], [158]. There are two types of external modulators commonly used: electro absorption modulators and electro optic modulators. An electro optic modulator is based on the Mach–Zehnder interferometer (MZI) structure, which uses lithium niobate ($LiNbO_3$) where the refractive index n changes with respect to the voltage V applied across modulator electrodes [159].

$LiNbO_3$ modulators provide the required bandwidth and a means for minimising the effect of the chirp [156], [158]. In analogue systems, linearised external modulators provide very low modulation distortion [156], [160]. Due to such advantages, a $LiNbO_3$ data modulator was also used in this testbed. The schematic diagram of a data modulator is shown in Fig. 5.6. It consists of optical and electrical inputs. A $LiNbO_3$ modulator usually has three inputs. One is used to input the optical signal, one is used as an electrical DC bias, and one is used to input the RF data signal [160].

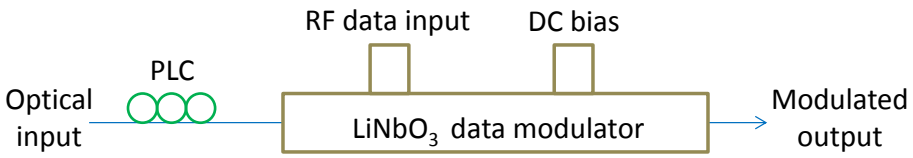

Fig. 5.6 Schematic diagram of data modulator

The optical input port is connected to a laser source. For all applications, the key is to have the optical signal linearly polarised and properly orientated at the modulator input. This can be achieved by using polarisation-maintaining (PM) fibre or by using a polarisation controller over a single-mode (SM) fibre. In commercial systems, this can be done by properly splicing polarisation-maintaining fibre (PMF) from the laser source to the PMF pigtail of the modulator [160]. In this testbed, the polarisation loop controller (PLC) is used to optimise the proper linear polarisation. A PLC is a simple device that flexes standard SMF in a controlled fashion to rotate the optical signal to set the linear polarisation.

The electrical inputs to the modulator consist of the DC bias and RF signal input ports. The DC bias is used to "position the optical signal" in the middle of the steepest part of the response curve [160]. The DC bias may be placed either on the same input port with the RF data signal, via a bias-T, or on a separate electrode (no bias-T required). The choice depends on the modulator type and its application [160]. Figure 5.7 shows the $LiNbO_3$ Mach–Zehnder data modulator in its protective housing. It can be seen that the box is not fully enclosed. The open spaces are to allow air cooling of the 10 Gb/s RF modulator driver (H301 Series, from JDS Uniphase) and for accessing the PLC seen on the left. We used a 10 Gb/s $LiNbO_3$ MZ data modulator from JDS Uniphase (type OC-192 MOD 10024180) [156] is used in this construction.

(a)

(b)

Fig. 5.7 $LiNbO_3$ data modulator: (a) inside the box; (b) view from outside of the box

5.4 Supercontinuum Generation

A number of recent implementations of WH/TS-based coding have been focussed on using multi-wavelength lasers for providing short multi-wavelength pulses. Multi-wavelength sources, using an array of lasers, are limited by the higher complexity in controlling a large number of pulses [92]. System costs rise dramatically if a multi-wavelength source is required at each node [1]. Spectral slicing of a broadband source is an attractive approach to achieving a multi-wavelength source. Various broadband sources have been used: LED, ASE noise from an EDFA [114] and SC generation [115]. Supercontinuum generation, in particular, is very attractive for the generation of coherent broadband pulses.

Supercontinuum generation is an extreme spectral broadening due to nonlinear effects. When a high peak power ultra-short optical pulse propagates through an optical fibre, the FWM process is accompanied by a multitude of other nonlinear effects – such as SPM, XPM, SRS – together with the effects of dispersion [133]. These nonlinear processes occurring simultaneously inside optical fibre can broaden the optical spectrum of the ultrashort pulse so much that it may extend over 100 nm or more, thus generating new frequencies within the pulse spectrum. It turns out that, for a sufficiently intense pulse, the pulse spectrum can become so broad that it extends over a frequency range exceeding 10 THz [96].

Supercontinuum generation attracted considerable attention during the 1990s because of its potential applications [161], [162], [163]. It was initially studied through the propagation of an intense optical pulse in solids and gaseous nonlinear media [161]. In the case of optical fibres, supercontinuum was first observed using multimode fibres [133] and then in SMF [162].

Starting in 1993, supercontinuum generation in SMF was used as a practical tool for obtaining picosecond pulses at multiple wavelengths simultaneously, thus acting as an ideal source for a WDM communication system [164]. Since the SC is generated by the accumulation of frequency chirp due to nonlinear propagation in a normal dispersion fibre [161], [164], [165], no coherent degradation occurs and the relative phase between the adjacent pulses is conserved [166]. By slicing the obtained optical spectrum using optical filters (AWG, FBG, etc.), simultaneous multi-wavelength signals can be generated.

SC generation in optical fibres primarily involves the injection of high-powered short optical pulses into a fibre span with a carefully chosen dispersion and nonlinear profile. The high peak power of the optical pulses results in additional spectral components through a nonlinear mechanism, while the fibre dispersion profile maintains the temporal pulse width throughout the length of fibre. Various demonstrations are summarised in Table 5.2.

Table 5.1 SC generation and the fibre [92]

Type of fibre	Broadening (nm)	Repetition rate	Reference
CW Brillouin/Raman fibre laser (BRFL)	100	–	[167]
Dispersion decreasing fibre (DDF)	150	–	[168]
Dispersion flattening and decreasing fibre (DFDF)	280	–	[169]
Dispersion flattening fibre (DFF)	325	10 GHz	[165]
Dispersion shift fibre (DSF)	420	15 GHz	[170]
Photonic crystal fibre (PCF)	800	–	[171]

A common and efficient method for SC generation in optical filters uses dispersion decreasing fibre (DDF) [168]. The propagation of ultrashort high peak power pulses in optical fibres near the zero dispersion wavelengths results in very large spectral broadening. Pulse spectra extending over as much as 300 nm have been generated using various types of optical fibres [133]. Over 200 nm of optical bandwidth was generated in DDF without serious degradation to the output of optical pulse width [168].

The generation of SC in optical fibres with spectral filtering has been used for multi-wavelength sources for application in WDM/OTDM networks [121], [122] and in WH/TS OCDMA networks [100], [88]. The development of very broad SC entails that the scalability of the system is limited only by the number of channels in the wavelength MUX/DEMUX. Currently, AWG technologies have achieved ports count of up to 80, thus offering 80 wavelengths [92]. As already mentioned, supercontinuum is basically generated by launching ultrashort (ps/fs) laser pulses into the fibre – featuring high nonlinear coefficients.

5.4.1 Implementation of Supercontinuum Generation in Testbed

An optical pulse compressor FP-300 by PriTel, Inc. (OPC) is used to generate the supercontinuum (see Fig. 5.8). The dispersion decreasing fibre (DDF) inside of the generator is ~1000 m long and has a power loss of 1.6 dB. The compressor input is from an Ultrafast Optical Clock generator (PriTel, Inc.), effectively an erbium-doped fibre mode-locked laser pulses, generating 1.9–2.1 ps FWHM pulses at the wavelength 1548.5 nm. At the compressor output, the compressed pulses have 210 fs FWHM and an average power of 132 mW at the repetition rate OC-48, and the spectral width of 3.2 nm around a central wavelength λ_c = 1551 nm.

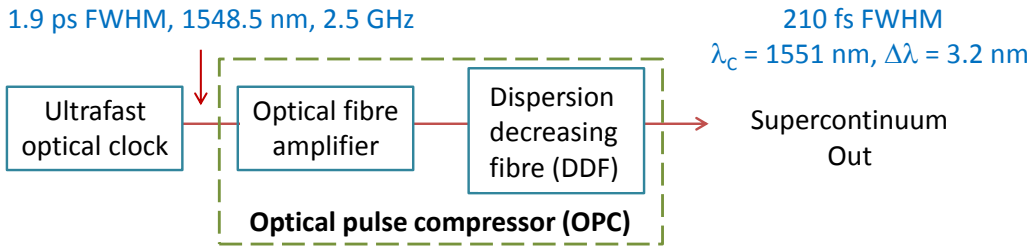

Fig 5.8 Supercontinuum generation

5.5 (4, 53) 2D-WH/TS OCDMA Code Generation Demonstration

OKI fibre Bragg gratings encoders/decoders were used to build the four 2D-WH/TS OCDMA transmitters and two receivers for the testbed as described earlier. Each transmitter produces a different code containing four multicolour optical pulses of ~7.5 ps FWHM by spectral slicing a 3.2-nm-wide optical supercontinuum (OSC) generated as described in Sec. 5.4.1. Related wavelengths are λ_1 = 1551.72 nm, λ_2 = 1550.92 nm, λ_3 = 1552.52 nm, λ_4 = 1550.12 nm on a 100 GHz ITU grid (e.g., 0.8 nm wavelength separation). The OCDMA code length is T = 400 ps and matches the transmission data rate of OC-48 (2.5 Gb/s). Each code has 53 chips that are 7.5 ps wide. Therefore, the code annotation is (4, 53) 2D-WH/TS, where 4 refers to four wavelengths positioned in 53 time chips (see Table 5.1).

Table 5.2 Implementation of four (4, 53) 2D-WH/TS codes used by an OCDMA testbed transmitters

	01	02	03	04	05	06	07	08	09	10	11	12	13	14	15	16	17	18	19	20	21	22	23	24	25	26	27	28	29	30	31	32	33	34	35	36	37	38	39	40	41	42	43	44	45	46	47	48	49	50	51	52	53
C1		λ1																	λ2																	λ3																		λ4	
C2		λ2																				λ4			λ1																					λ3									
C3		λ3							λ1																							λ4								λ2															
C4		λ4										λ3													λ2											λ1																					

The time domain representation of the code 2 is depicted in Fig. 5.9 as seen on a bandwidth-limiting oscilloscope (Agilent 86105B) with 64 GHz optical sampling

head where four wavelengths λ_1 - λ_4 within a complete bit period T = 400 ps could be noted.

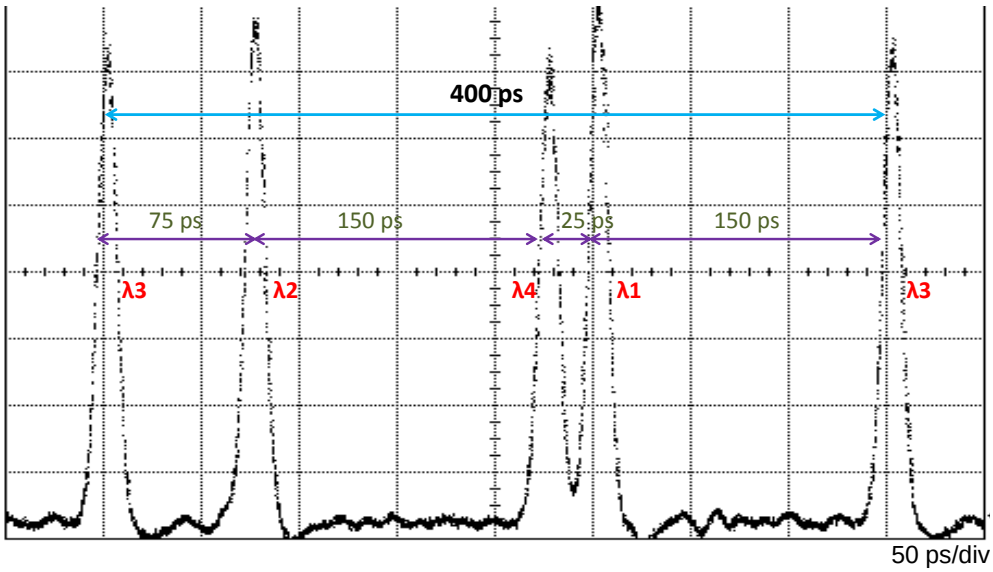

Fig. 5.9 The time domain representation of the code 2

5.6 Summary

In this chapter, my contributions are to design and build OCDMA transmitter and receiver terminals for use in the OCDMA testbed.

Chapter 6: OCDMA Testbed Evaluation

6.1 Investigation of Effects of Residual Chromatic Dispersion on Transmission Channels Due to Short Terminal Relocations

In communications systems, there is often a need to extend the reach of the existing fibre link or to relocate the user's terminal. In events like this, a simple addition of an extra length of fibre would mean also adding "some" amount of dispersion. Therefore, it is necessary to understand how chromatic dispersion accumulates via such fibre link extensions, say by up to a few hundred metres of SMF-28, and how this may affect the overall OCDMA system performance. This residual chromatic dispersion effect is studied in two parts: a short picosecond (ps) laser pulse, and then the 2D-WH/TS OCDMA code based on multicolour picosecond pulses.

6.1.1 Investigation of Residual Dispersion Using a Short Laser Pulse

To investigate the effects of residual dispersion on the transmission system, the setup in Fig. 6.1 was used. This setup is similar to the one in Fig 4.2. Here, the generated 2 ps FWHM laser pulse from an EDF mode-locked laser is amplified and transmitted over a bidirectional dispersion-compensated transmission link between Strathclyde and Glasgow University. On the receiver side, SMF-28 ranged between 0–275 m is added to the original 17 km-long fibre link (see Fig. 6.1).

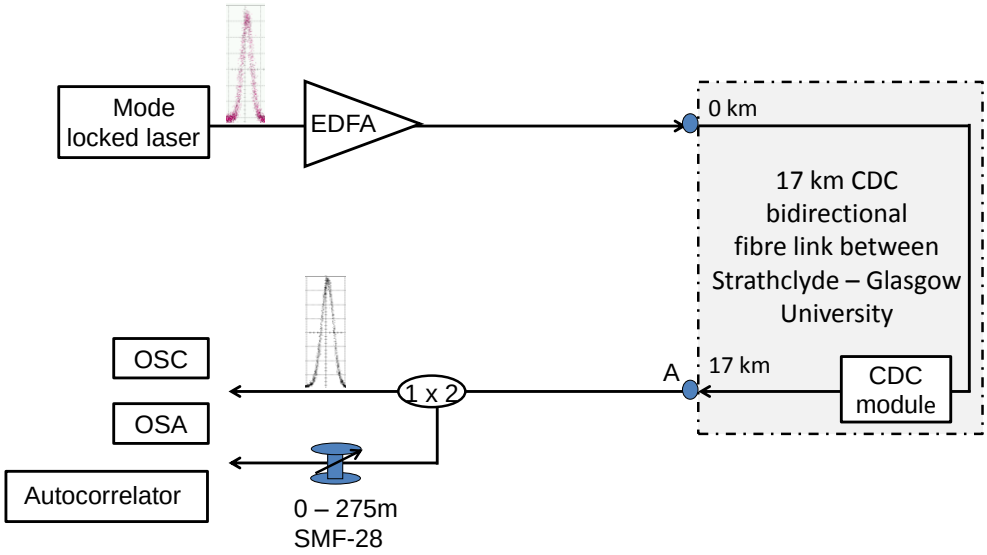

Fig. 6.1 Experimental setup for the effect of residual chromatic dispersion on laser pulse

The pulse width from the MLL, before and after its propagation inside the 17-km-long chromatic-dispersion-compensated fibre link, is monitored using an Agilent 86105B digital communications analyser with a 64 GHz sampling optical head, an optical spectrum analyser (Agilent 86146B), and measured using an optical autocorrelator (Femtochrome).

Figure 6.2 shows the temporal traces of the outgoing, and the received, laser pulse, measured by an optical autocorrelator. The outgoing laser pulse width was 2 ps FWHM, and the received pulse after propagation in the 17-km-long CD-compensated transmission link was 2.2 ps FWHM. By comparing both results, a 0.2 ps pulse broadening was found. This is a 10% mismatch between the outgoing and the received laser pulse width values, thus confirming the calibration results found in Chapter 4.

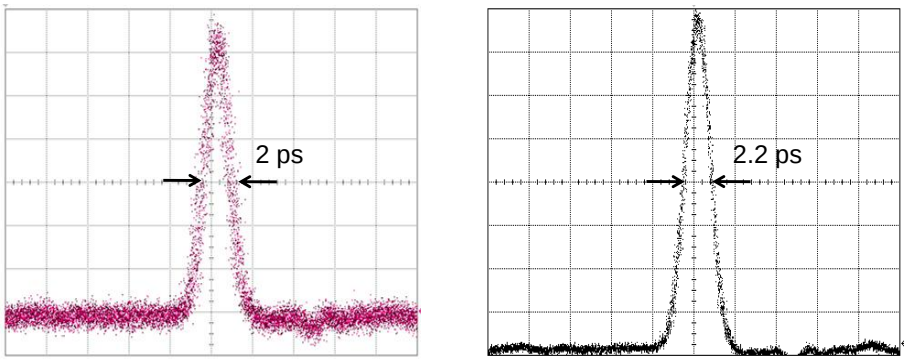

Fig. 6.2 FWHM of laser pulse: (a) before, and (b) after propagation in the 17 km link treated for chromatic dispersion

Now, to investigate how severely a deviation from the link full chromatic dispersion compensation can affect this 2 ps FWHM optical pulse due to terminal relocation, additional experiments were conducted. It should be noted that before different sections of SMF-28 fibre were added to relocate the receiving terminal, the laser pulse width was kept at 2 ps FWHM – as can be seen in Fig. 6.2(a). The resulting pulse broadening can be calculated using Eq. 6.1 (from Chapter 3)

$$\Delta\tau = DL\Delta\lambda \tag{6.1}$$

where D is the dispersion in ps/nm.km, L is the distance, and $\Delta\lambda$ is the spectral width. In this calculation the, dispersion used is 15 ps/nm.km, the distance for added SMF-28 varies from 0.025 km to 0.275 km, and the spectral width is 0.8 nm. Table 6.1 summarises the calculated pulse broadening for different added lengths.

Table 6.1 Data for measured and calculated pulse broadening for different added lengths

		Measured			Calculated		
Total length (km)	Added length (km)	FWHM (ps)	Broadened Pulse (ps)	Ratio	FWHM $\Delta\tau = DL\Delta\lambda$ (ps)	Broadened Pulse (ps)	Ratio
17	0	2.16	0	1	204	0	1
17.025	.025	2.5	0.33	1.15	204.3	0.3	1.15
17.050	.050	2.74	0.57	1.26	204.6	0.6	1.3
17.075	.075	2.95	0.78	1.36	204.9	0.9	1.45
17.200	.200	4.45	2.28	2.05	206.4	2.4	2.2
17.250	.250	5.25	3.08	2.42	207	3	2.5
17.275	.275	5.75	3.55	2.64	207.3	3.3	2.65

The obtained results are summarised in Fig. 6.3. Here, for example, it can be seen that extending the 17-km-long fully CD-compensated link in order to move the terminal by 275 m (by adding 275 m of SMF-28) will lead to 250% pulse broadening ratio. The obtained experimental results are in good agreement with the simulated values (see dotted line in the same figure).

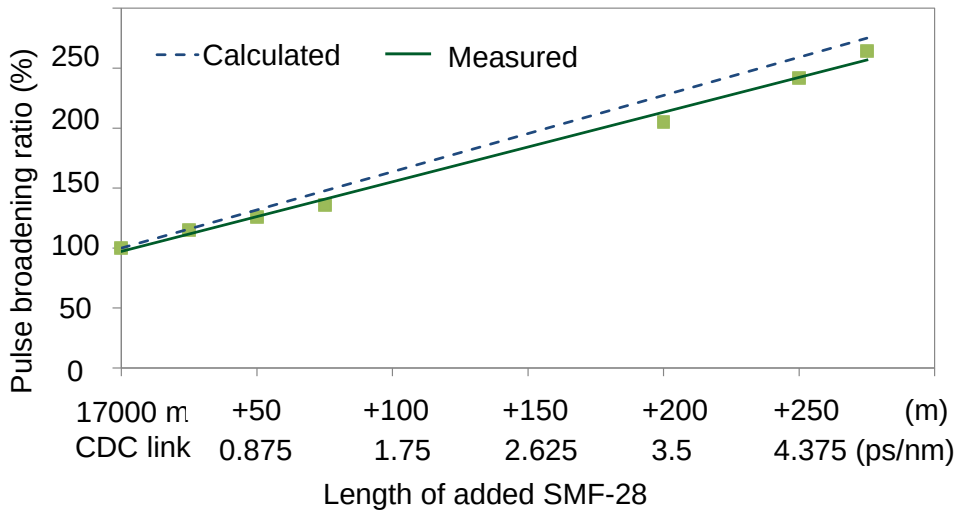

Fig. 6.3 Illustration of relative laser pulse broadening as a result of accumulated chromatic dispersion

6.1.2 Investigation of 2D-WH/TS OCDMA Code under the Influence of Bidirectional Link Residual Dispersion

Similarly, the effect of the fibre link on the propagation of a single 2D-WH/TS OCDMA code, which is based on multi-wavelength picosecond pulses, was investigated. The experimental setup is shown in Fig. 6.4.

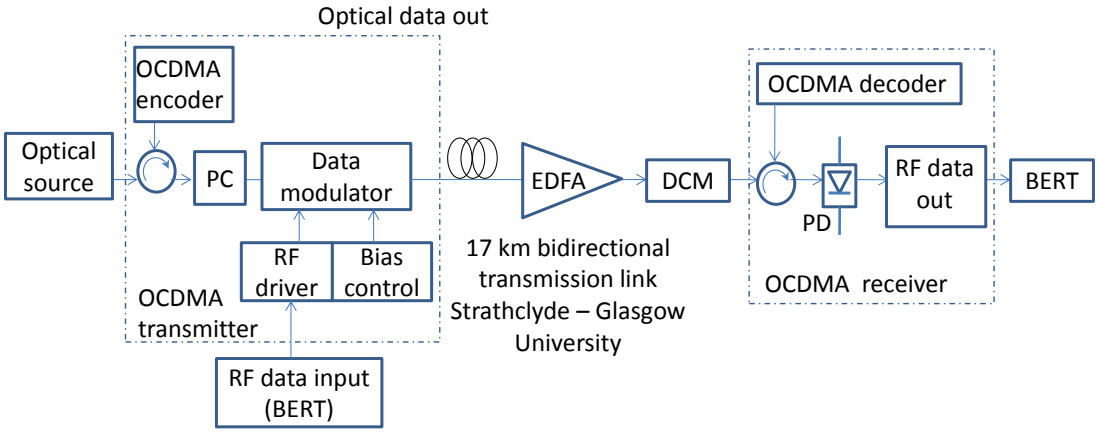

Fig. 6.4 Experimental setup with a lithium niobate data modulator. PLC – polarisation loop controller, RF – radio frequency, DCM – dispersion compensating module, EDFA – erbium-doped fibre amplifier, PD – photodetector, BERT – bit error rate (transmitter and receiver)

The (4, 53)-2D-WH/TS family of OCDMA codes I used in this experiment is represented by four wavelength pulses – λ_1 = 1551.72 nm, λ_2 =1550.92 nm, λ_3 = 1552.52 nm, λ_4= 1550.12 nm – placed accordingly within 53 time chips. The sequence (see Tab. 5.1) is as follows: 1-λ_3, 9-λ_2, 28-λ_4, and 31-λ_1 (see Fig. 6.5). The

numbering indicates the chip's order. The code length was 400 ps and corresponds to the data transmission rate of OC-48 (2.5 Gb/s).

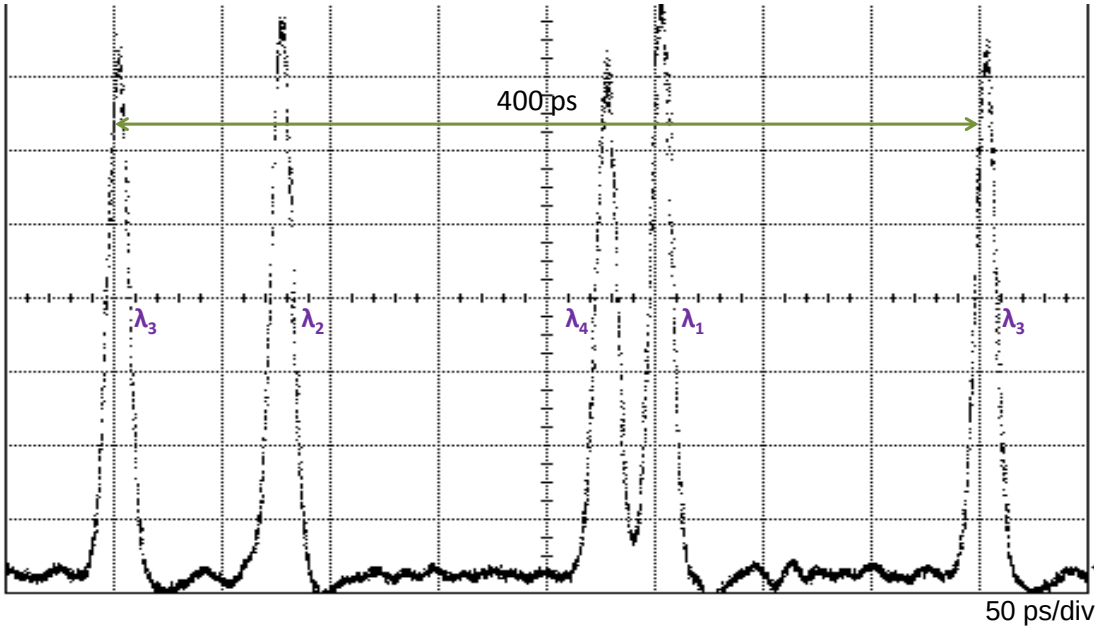

Fig. 6.5 (4, 53) 2D-Wavelength-hopping/time-spreading code (1-λ_3, 9-λ_2, 28-λ_4, and 31-λ_1), as seen on a bandwidth-limited oscilloscope (Agilent 86105B) with a 64 GHz sampling head

The measurement results shown in Fig. 6.6 depict the autocorrelation peak for the back-to-back measurement – Fig. 6.6(a) – and after 17 km of code propagation in the CDC fibre link – Fig. 6.6(b). The respective autocorrelations were obtained by decoding the received signal by the matched OCDMA receiver – as is schematically shown in Fig. 6.4. The observed uneven (asymmetric) autocorrelation shape in Fig. 6.6 (a and b) can be explained by manufacturing imperfections in fabricating the matched OCDMA encoder and decoder pair. From several measurements, the FWHM for the autocorrelation peak is quite consistence for the back-to-back and the OCDMA codes after propagation.

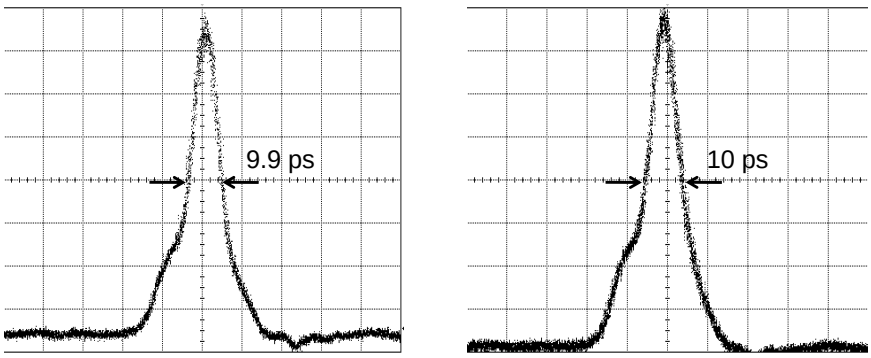

Fig. 6.6 Autocorrelation peaks obtained from (a) back-to-back measurements, and (b) after OCDMA code propagation in the 17 km chromatic dispersion compensated transmission link between University of Strathclyde and Glasgow University

By comparing both autocorrelation peaks side by side, a 0.1 ps mismatch can be seen in their temporal width caused by the residual fibre link chromatic dispersion, which is within ~10% of the back-to-back value. This 10% inaccuracy measured for the autocorrelation peak containing four wavelengths (note the code weight 4 for used OCDMA codes) is the same as the inaccuracy achieved for a single wavelength laser pulse seen in Fig. 6.2. This can be interpreted as showing that the dispersion slope compensation over the range of used wavelengths used by the OCDMA was also achieved.

6.2 Investigation of the Impact of Varying Chromatic Dispersion on OCDMA System Performance in a Multiuser Environment

Not much study has been done in learning how small residual chromatic dispersion extension in a transmission link can affect the performance of an OCDMA system that utilises multi-wavelength picosecond pulses for 2D-WH/TS code creation. The testbed was therefore used to investigate the impact of varying chromatic dispersion on OCDMA system performance in a multiuser environment. The study was carried out using the setup shown in Fig. 6.7. The bit error rate was measured for different receiving terminal locations away from point A (up to point A the link is fully chromatic-dispersion compensated as shown in Sec. 6.1) – specifically, +50 m, +200 m, +250 m and +275 m. An adequate power control was implemented to eliminate the influence of loss associated with the fibre link length increases.

In order to generate four users' data traffic a Mach–Zehnder data modulator, driven at OC-48 by a 2^{31}-1 PRBS from an Agilent N4903A series bit error rate tester was used. Traffic from all OCDMA users was combined and launched via EDFA into the chromatic dispersion-compensated Strathclyde – Glasgow University fibre link. The received OCDMA signal was then decoded using an FBG-based decoder matched to the User 1 encoder. The decoded signal was then sent through an attenuator (Agilent 8157A) to a bit error rate tester with a 10 GHz optical receiver with −18 dB sensitivity (Nortel PP10G) as its front end.

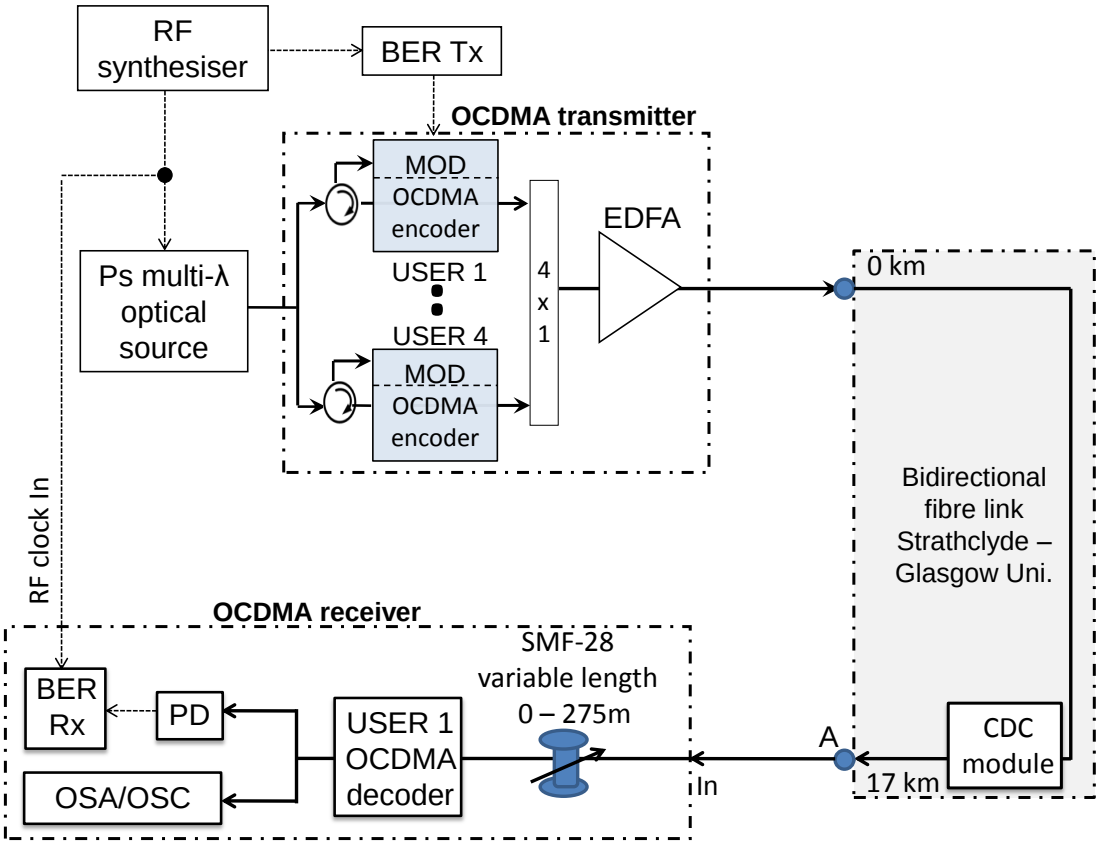

Fig. 6.7 Multi User Chromatic Dispersion Compensation experimental setup

The decoded OCDMA signal was monitored using an oscilloscope, optical autocorrelator, and optical spectrum analyser. Figure 6.8 shows the obtained bit error rate curves when four simultaneous users were broadcasting on the network. No error floor was observed.

The effect of the added CD on the overall User 1 data reception, due to moving his receiving terminal to different locations in relation to point A (where the link is fully compensated), can be seen in Fig. 6.8. The obtained results suggest that to achieve a targeted BER performance of 10^{-9}, moving the terminal by 275 m will result in a 7 dB power penalty if no proper chromatic dispersion accompanies this terminal relocation. On the other hand, moving the terminal just 50 m will lead to only 1 dB of power penalty. It is important to note, again, that these penalties are unrelated to power losses due to the added extra length of SMF-28, since these additional losses were compensated prior to taking BER measurements by EDFA.

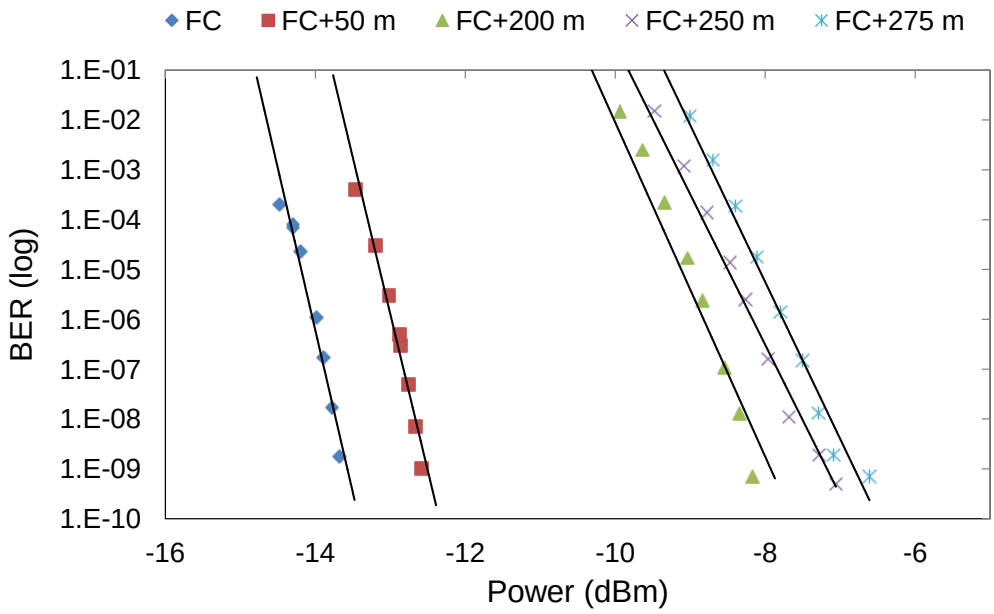

Fig. 6.8 BER system performance measurements for different level of "residual" chromatic dispersion in the transmission link created by adding different lengths of SMF-28 to the 17-km-long fully CD-compensated fibre link. FC – indicates the BER of the system for a fully CD-compensated 17-km-long fibre link between Strathclyde and Glasgow University

The observed performance degradation could be explained by the fact that the introduced chromatic dispersion causes a broadening of multi-wavelength pulses within the OCDMA codes, and also their time skewing. This will impact the autocorrelation peak. It can be seen from Fig. 6.9 that the added chromatic dispersion via terminal relocation introduces broadening and time skewing of the autocorrelation peak. The time skewing misaligns the perfect time overlap of

multiwavelength ps pulses creating the autocorrelation peak, thus lowering and broadening the shape of the autocorrelation peak.

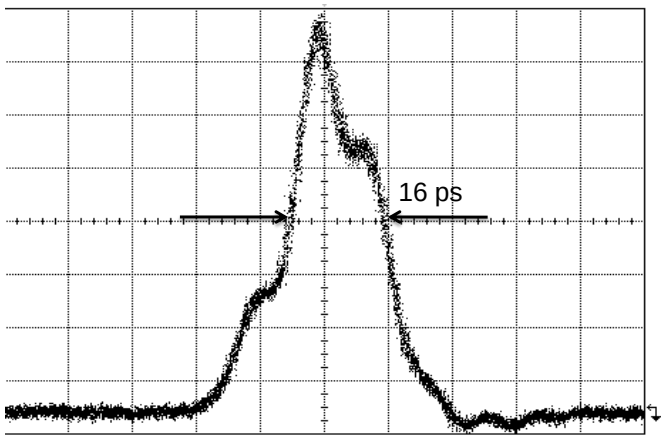

Fig. 6.9 Autocorrelation peak as seen on the oscilloscope after the 17 km OCDMA transmission in the CD-compensated fibre link followed by an extra 200 m SMF-28

In the multiuser environment, cross correlations will also experience chromatic dispersion broadening. From single wavelength measurements, it was estimated that moving the terminal by 275 m resulted in a 275% broadening of pulses, which represents the 2D-WH/TS OCDMA code. Such broadening will considerably increase the multi-access interference and the crosstalk in the multiuser environment. The obtained results suggest that, even if relatively short distance terminal relocations are required, fibre spans should be fully CD compensated to maintain OCDMA system top performance.

6.3 Summary

The main goal of my investigation was to study the effect of laser pulse broadening due to chromatic dispersion after signal transmission over certain distances, observed on two different signals: a short 2 ps FWHM laser pulse and (4, 53) 2D-WH/TS OCDMA code based on multicolour picosecond pulses. Relative laser pulse and autocorrelation broadening as a result of accumulated chromatic dispersion are plotted. For both cases, the broadening is proportional to the travel distance and residual chromatic dispersion.

Next, the testbed is tested on the impact of varying chromatic dispersion on OCDMA system performance in a multiuser environment. In this environment, the received signal consists of autocorrelation peak generated from the desired code and the cross-correlation peak (MAI) generated from other users. The plotted graph shows the effect of the added chromatic dispersion on the overall User 1 data reception due to moving it's receiving terminal to different locations relative to point A (where the link is fully compensated). The obtained results also suggest that to achieve a targeted BER performance of 10^{-9}, moving the terminal by 275 m will result in a 7 dB power penalty if no chromatic dispersion accompanies this terminal relocation. On the other hand, moving the terminal just 50 m will lead to only 1 dB of power penalty. It is important to note that these penalties are unrelated to power losses due to the added extra length of SMF-28, since these additional losses were compensated prior to taking BER measurements. The above experiments were implemented at OC-48 (data rate of 2.5 Gb/s). Investigations of the 2D-WH/TS OCDMA system based on multicolour ps pulses under similar conditions have never been reported before.

Chapter 7: Synchronisation and AOCR

7.1 Introduction

Transmitting data at increased data rates over long transmission distances will incur timing jitter. The effect of timing jitter can be reduced by proper synchronisation. All- optical clock recovery from the received data is the preferred method for establishing data synchronisation at the receiver side.

Implementations of a variety of clock extraction techniques [172] for a receiver synchronisation were predominantly developed for wavelength division multiplexed (WDM) [173], [174] and optical time division multiplexed (OTDM) [175], [176], [177] systems. However, their application in OCDMA is very limited or even impossible. Clock recovery techniques for OCDMA systems were reported [178], [179]; however, these approaches were not implemented all-optically. The clock recovery approach for suppressing the effect of timing jitter in an OCDMA signal was demonstrated by using a nonlinear optical loop mirror (NOLM) or terahertz optical asymmetric multiplexer (TOAD) [33], [57]. However, realisations of a suitable all-optical clock extraction circuit, which will recover synchronisation signal from the incoming OCDMA data stream and can produce a local optical clock without any intermediate electronic stage, is needed.

Since the early 1990s, researchers have focussed on applications like optical wavelength conversion, optical header recognition, optical sampling [180], optical bit rate conversion and optical packet buffering [181], [182], [183], [184]. Some of these all-optical signal processing applications also required an optical clock that is extracted from the signal to be processed. All-optical clock recovery was first demonstrated in 1991 [185] at a bit rate of 5 Gb/s using a self-pulsating laser diode. In 1993, a 40 Gb/s all-optical clock extraction was also demonstrated [186]. Today, clock recovery circuits based on self-pulsating laser diodes [187], as well as all fibre devices [188], have been demonstrated for both the 1330 nm and 1550 nm telecommunications windows [189] for application in WDM, TDM or even OCDMA.

7.2 All-Optical Clock Recovery Technique for Receiver Synchronisation

Realisation of suitable all-optical clock extraction circuits, which can recover timing signals from an incoming OCDMA data stream and produce an optical clock without an intermediate electronic stage, is needed. In principle, recovering an optical clock from incoming OCDMA data means extracting a periodic signal with a period reciprocal of the data bit rate, while free of information carried by data and without phase noise [1]. A high-quality jitter-free clock is not always available at the receiver side. Therefore, my investigation aimed to see if an optical clock can be recovered all-optically from the OCDMA signal by an OCDMA receiver with an incorporated suitable all-optical clock recovery circuit.

Figure 7.1 shows an optical clock recovery circuit based on [173], which I adopted and built from commercially available components. The clock recovery circuit uses a semiconductor optical amplifier (SOA) and is based on a fibre ring laser.

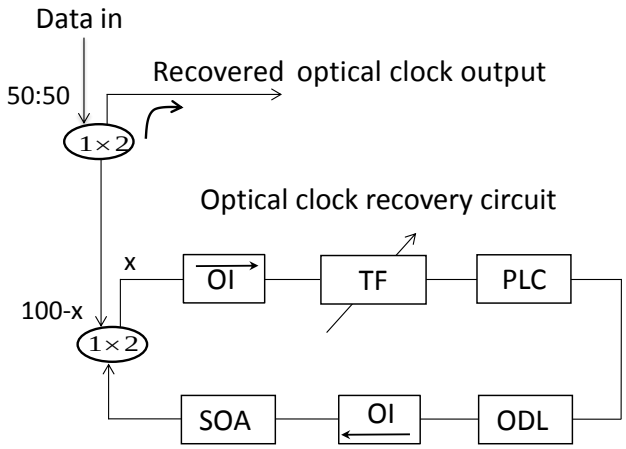

Fig. 7.1 Schematic diagram of the fibre optical clock recovery circuit. ODL – optical delay line, PLC – polarisation loop controller, OI – optical isolator, TF – optical tuneable filter, SOA – semiconductor optical amplifier, 1×2 power splitter

In my implementation for use with 2D-WH/TS codes based on multicolour ps pulses, the operation of the all-optical clock recovery (AOCR) circuit relies on fast gain saturation of the SOA by the incoming data (decoded user autocorrelation), resulting in the cavity modulation leading to fibre ring-laser locking. The cavity of the optical clock recovery circuit (see Fig. 7.1) was constructed from fibre pigtailed devices.

The incoming data is introduced into the loop by a 50:50 optical fibre coupler, and the recovered optical clock signal is extracted out of the loop by a 2×1 optical power coupler with a (100−x)**:** x coupling ratio.

A rotating optical tuneable filter (TF) based TFF Fabry Perot was used for wavelength selection of the recovered optical clock, and a variable optical delay line (ODL) was used to adjust the laser cavity length of the AOCR to match the incoming data at rate. When the ODL is properly adjusted so that the repetition rate of the input data is equal to an integer multiple of the fundamental frequency of the fibre ring cavity (the AOCR circuit is properly synchronised with the input data), the cavity will harmonically lock and the optical clock signal will be generated.

The condition for the resonance in a ring resonator is that the round trip distance, $2d$, is equal to an integer number of wavelengths λ. The round trip cavity length at the resonance can be calculated using Eq. 7.1 as

$$2d = N\lambda \tag{7.1}$$

where d is the cavity length, N is an integer and λ is the signal wavelength.

7.3 All-Optical Clock Recovery (AOCR) from an Incoming OCDMA Signal

An all-optical clock is necessary for the receiver synchronisation, especially if the OCDMA receiver will use an all-optical time gate for all-optical post processing of the received data (for example to remove MAI). It is therefore essential to recover a synchronisation signal (optical clock) from the incoming optical OCDMA data in order to eliminate the effect of a timing jitter on the data detecting system.

7.4 Experimental Setup

Figure 7.2 is a schematic diagram of the developed OCDMA receiver with the built-in all-optical clock recovery demonstrated in the previous section [29]. First, the incoming OCDMA traffic is decoded by an OCDMA decoder to produce the autocorrelation peak, which is then split two ways. One is used for OCDMA data detection (see Fig. 7.2), while the other is sent into the AOCR circuit described in

Fig. 7.1 for all-optical clock generation. The recovered optical clock is extracted out of the AOCR by a 2×1 optical fibre coupler with the power splitting ratio (100−x): x. Two different coupling configurations (with x = 10 and x = 20) were tested to look for optimised performance of the AOCR. Better results were obtained using x = 10. A 5 nm tuneable optical filter inside the loop was used for the wavelength selection for the recovered optical clock, and a variable optical delay line (ODL) was used for adjusting the cavity length of the AOCR circuit for precise matching of the data rate (OC-48) of the incoming signal.

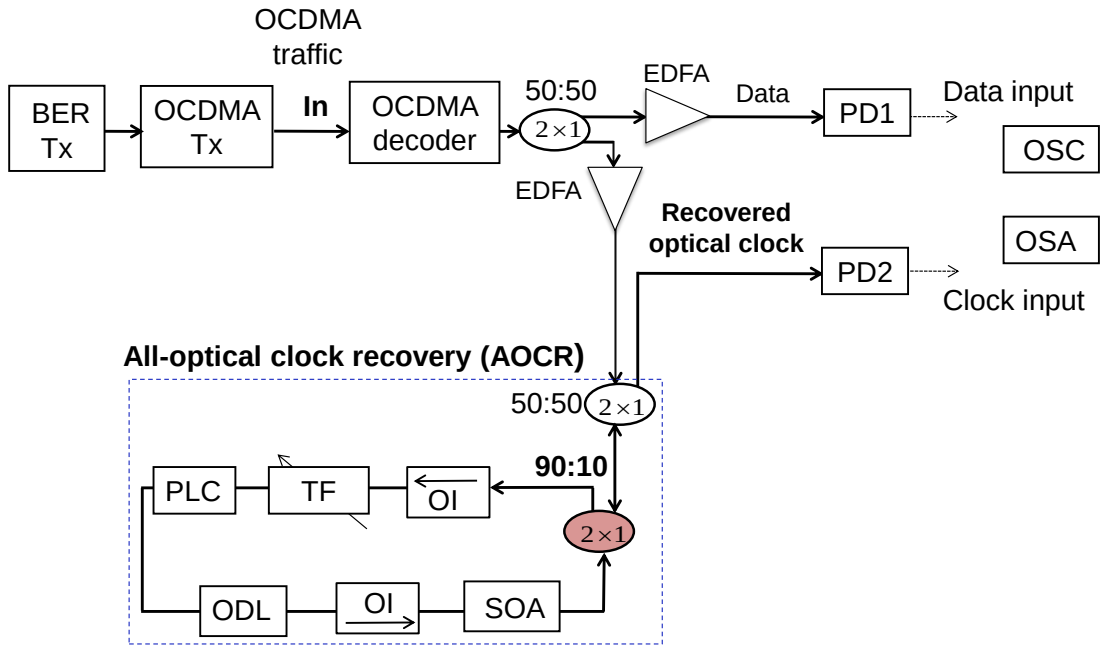

Fig. 7.2 OCDMA receiver with built-in all-optical clock recovery

When the ODL is properly adjusted, so that the repetition rate of the OCDMA data is equal to integer multiples of the fundamental frequency of the fibre ring cavity, the AOCR circuit becomes synchronised to the input signal. The cavity becomes harmonically locked and the optical clock signal is generated. Two optical isolators inside the loop maintain the direction of the signal circulation. The all-optically generated clock by the AOCR was then evaluated by the BER tester for its stability.

7.4.1 Obtained Results and discussion

Two different OCDMA data patterns, 2^7-1 PRBS and data sequence "1010", were tested respectively. The recovered clock from both data patterns was then compared. An example of the input data pattern, and all-optically recovered clock generated from the received OCDMA data, is shown in Fig. 7.3 (as seen by a bandwidth-limited oscilloscope with a 64 GHz optical sampling head).

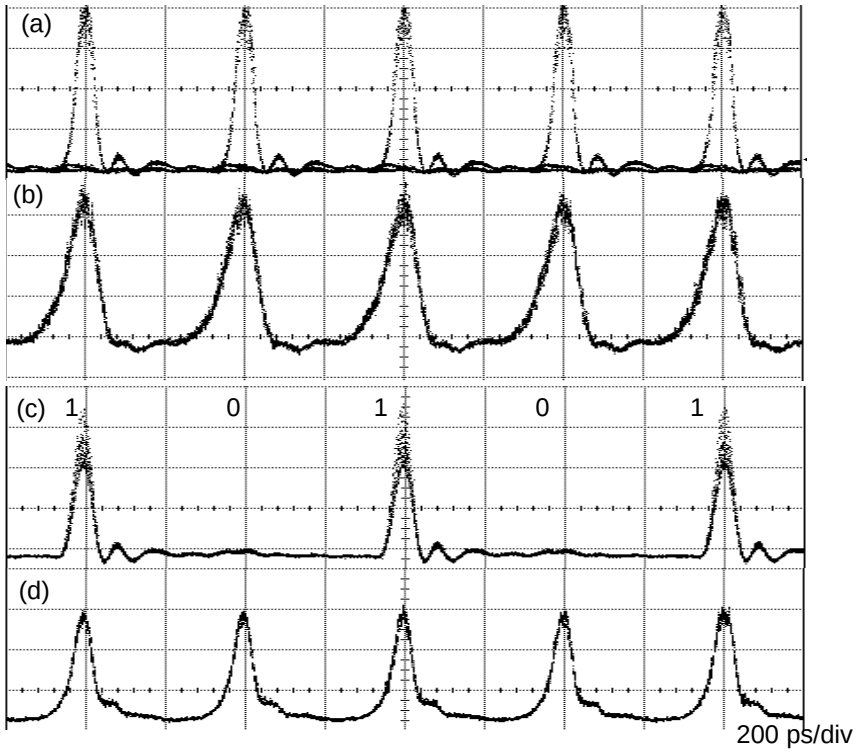

Fig. 7.3 Experimental results

(a) Eye diagram of the decoded incoming 2^7-1 PRBS OCDMA data (autocorrelation)

(b) All-optically recovered clock from the received OCDMA data for 2^7-1 PRBS OCDMA data

(c) Decoded data pattern "1010" (autocorrelation)

(d) All-optically recovered clock from the received OCDMA data for decoded data pattern "1010"

The received signal in Fig. 7.3 monitored by the oscilloscope was also viewed by an optical spectrum analyser (See Fig. 7.4). Two parts of the signal were noted between 1550 nm and 1560 nm – as depicted in Fig. 7.4. The first part is the optical spectrum of the 2D-WH/TS OCDMA code, and the second part is the all-optically recovered clock at λ_{AOCR} = 1558 nm.

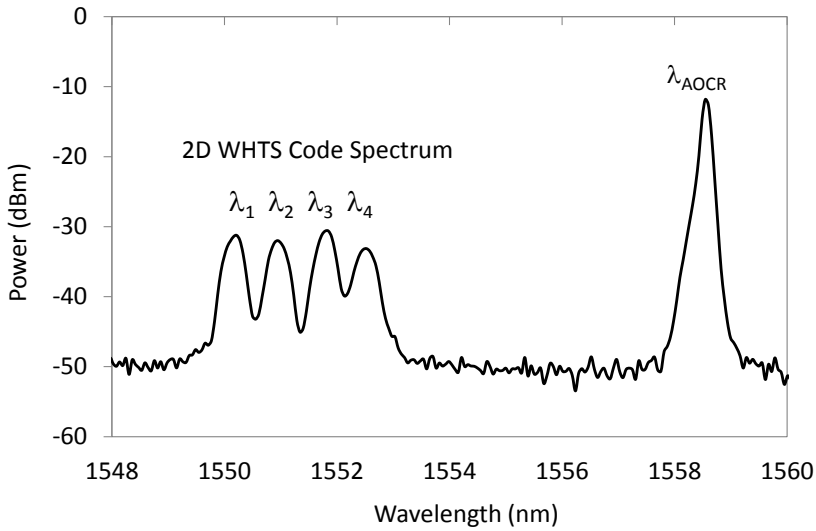

Fig. 7.4 Recorded optical spectrum of 2D-WH/TS OCDMA code; λ_{AOCR} belongs to the all-optically recovered clock

7.4.2 Investigation of AOCR in the Testbed

An OCDMA receiver with built-in AOCR was then tested in our field-based optical testbed. The setup in Fig. 7.5 consists of a 4-user OCDMA transmitter, a 17-km-long bidirectional fibre optic link and an OCDMA receiver with built-in AOCR. The experiment was implemented by using 2D-WH/TS OCDMA codes. These were based on four wavelengths – λ_1 = 1551.72 nm, λ_2 = 1550.92 nm, λ_3 = 1552.52 nm, λ_4 = 1550.12 nm – which were placed by OCDMA encoders (based on fibre FBG) within 53 time chips, each having a duration of ~7.5 ps, thus creating the (4,53)-2D-WH/TS family of codes. The system was running at OC-48 and used a 2^7-1 PRBS data pattern generated by an Agilent N4903A BER Tester.

The generated OCDMA traffic was amplified using EDFA and launched into the 17 km bidirectional fibre optic link with chromatic dispersion compensation.

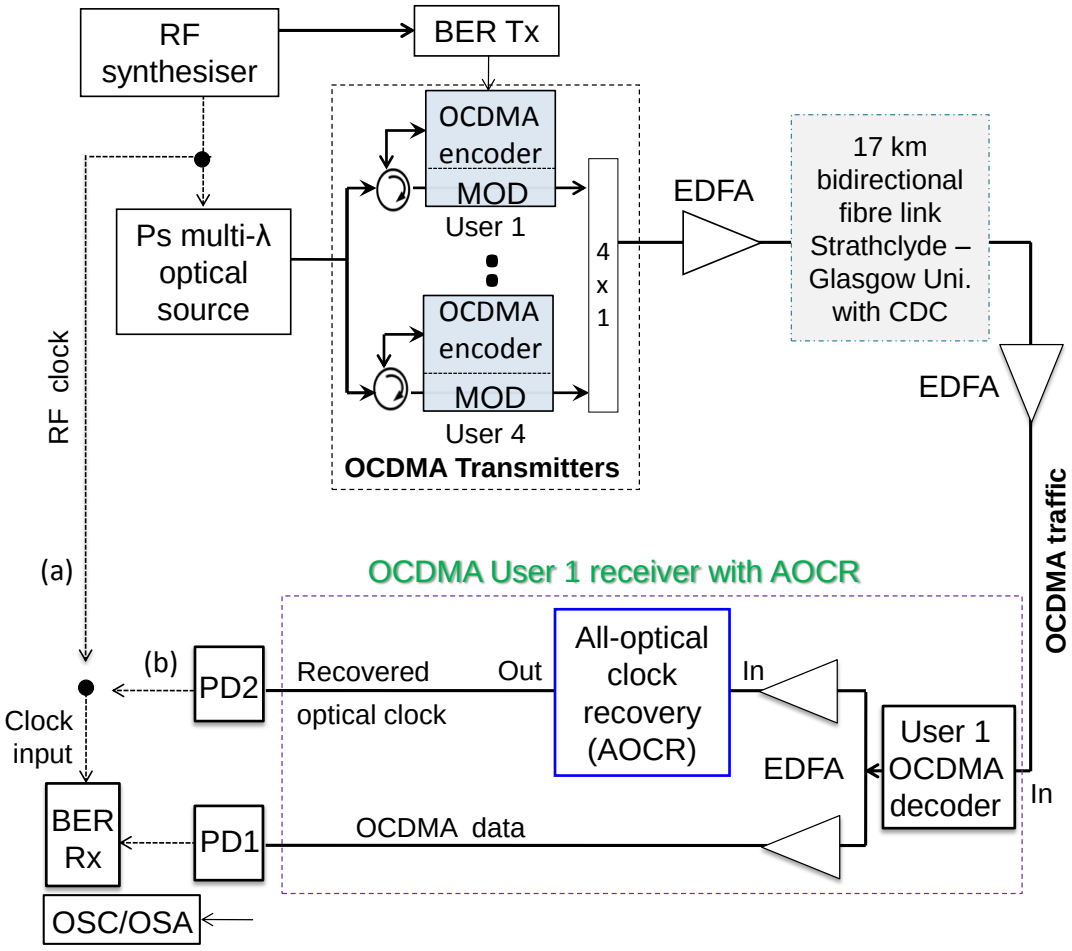

Fig. 7.5 Field-based multiuser OCDMA testbed. (a) BER Rx is synchronised locally from an RF synthesiser, and (b) BER Rx is synchronised by the all-optically recovered clock generated by the OCDMA receiver with built-in all-optical clock recovery. BER Tx is a bit error rate transmitter, BER Rx – bit error rate receiver, MOD – data modulator, PD – photodiode, OSC – oscilloscope, OSA – spectrum analyser, CDC – chromatic dispersion compensation, OC – optical circulator, MOD – $LiNbO_3$ data modulator

On the receiver side, the recovered signal was preamplified and then decoded by the User 1 OCDMA decoder. Such decoded data is then split into two: one arm is sent to an 11 GHz Nortel PP10G optical photodiode (PD1 in Fig. 7.5), while the other arm is sent to the AOCR circuit to produce the optical clock signal. The generated clock and decoded OCDMA data are then sent to the bit error rate tester receiver (BER Rx) – as shown in Fig. 7.5.

As indicated, the received OCDMA data and recovered optical clock were also monitored using an Agilent 86105B oscilloscope and Agilent 86146B optical

spectrum analyser. To investigate how the all-optical clock recovery improved the OCDMA system performance, the evaluation was performed by taking BER measurements by two different ways of BER Rx synchronisation (see Fig. 7.5): first, using the RF local clock (2.5 GHz sinusoidal wave) generated by the RF synthesiser (Agilent E4432B) – as depicted in Fig. 7.5(a) – and then as shown in Fig. 7.5(b) using the all-optically recovered clock generated by the receiver under the test from the received OCDMA data. An optical spectrum analyser and oscilloscope were also used to monitor the wavelength spectrum and eye diagram as indicated in Fig. 7.5.

Figure 7.6 shows two separate BER curves for the received 2^7-1 PRBS OCDMA data named (a) and (b). The (a)-BER plot represented the system with synchronisation using the all-optically recovered clock from received OCDMA data, and the (b)-BER curve represented synchronisation using the direct clock from the RF synthesiser. As demonstrated in Fig. 7.6, a very significant ~7.5 dB power budget improvement was noted when the all-optically recovered clock was used for the BER Rx synchronisation. This improvement results from a fact that the all-optically recovered clock, when used to synchronise the receiver, "follows" the OCDMA signal time jitter and drags it to follow the jitter, which in turn eliminates the jitter and thus improves the BER.

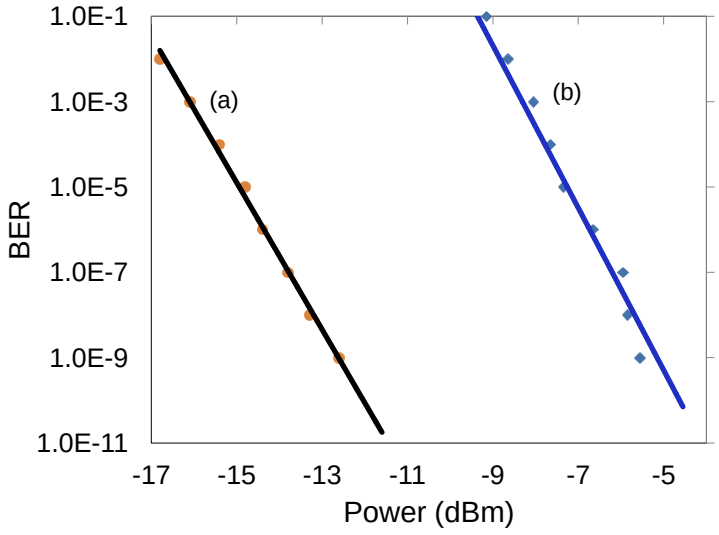

Fig. 7.6 Measured BER for received 2^7-1 PRBS data.
(a) Synchronisation done by using the all-optically recovered clock from the received OCDMA data
(b) Synchronisation done directly by the clock from the RF synthesiser

The related eye diagrams for the received data are depicted in Fig. 7.7. The first eye diagram (a) was obtained when the all-optically recovered clock was used to synchronise the BER Rx – see Fig. 7.3(b) – the other eye diagram (b) is obtained when the BER Rx was synchronised locally by the clock from the RF Synthesiser – see Fig. 7.3(a). Using the all-optically recovered clock for the BER Rx synchronisation resulted in a wider eye opening: 101.1 ps width and 989 mV height – compared to 57.5 ps width and 860 mV height when using the local clock from the RF synthesiser.

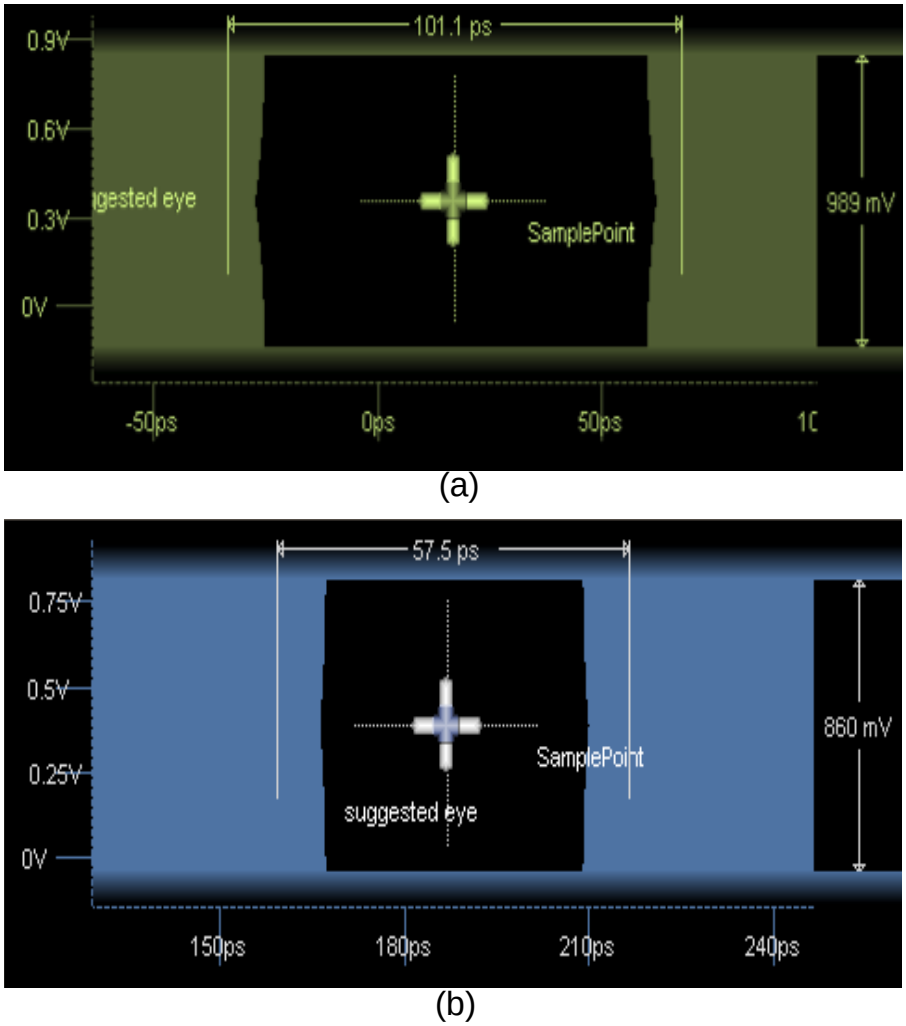

Fig. 7.7 Eye diagram for received 2^7-1 PRBS data.

(a) Synchronisation done by using the all-optically recovered clock from the received OCDMA data

(b) Synchronisation done directly by the clock from the RF synthesiser

7.5 Summary

For the first time, an optical receiver with a built-in and robust all-optical clock recovery for use in incoherent OCDMA was proposed and successfully demonstrated in the field trials. The receiver was evaluated under realistic out-of-laboratory conditions at an OC-48 data rate to process 2D-WH/TS OCDMA codes based on multi-wavelength picosecond pulses. Evaluation started with the data and clock signal observation. Different input patterns of '1010' and 2^7-1 PRBS OCDMA data were tested on the testbed. The recovered clock pattern remains the same no matter what the incoming data pattern is. It shows that the proposed all-optical clock recovery circuit is suitable for OCDMA data applications.

In ensuring reliable results, the optical spectrum was also monitored. The all-optically recovery clock wavelength was ~1558.7 nm, and can be changed by changing the all-optical clock recovery cavity length via the delay line adjustment.

Error-free operation up to 10^{-11} (no error floor) was measured when using the recovered clock generated from incoming OCDMA data with a significant power budget improvement of ~7.5 dB. A bigger and wider eye opening was also observed when using the all-optically recovered clock from the received data versus that when using a clock generated locally by the RF synthesiser.

Chapter 8: All-Optical Time Gating

8.1 Introduction

OCDMA is a multiple-access technique. Since the 2D-WH/TS OCDMA receiver receives signals from all of the users on the network, the decoder must discriminate between intended and interfering data streams by correlating the received signal with the appropriate code matrix. The OCDMA decoder thus undoes the time spreading for the appropriate code sequence and aligns (stacks) its wavelength pulses in time (see Fig 4.6). When the matched code sequence is received, the output of the decoder consists of a *w* pulses that are aligned on top of each other and this is known as the autocorrelation peak (recall - *w* is the code weight). The unmatched code sequences at the decoder are further spread over the bit period, resulting in lower intensity MAI. The MAI is a result of a non-zero cross correlation among codes used by simultaneous users [15].

The use of 2D-WH/TS families of codes has been widely researched for use in different OCDMA applications [50] because this coding approach has several advantages including reduced cross correlation, increased cardinality and nonexistence of autocorrelation side lobes [54]. There has also been wide study of the family of prime codes [1], [54] employing multi-wavelength short pulses for 2D-WH/TS codes generation.

MAI increases with the growing number of simultaneous users, resulting in deterioration in the bit error rate (BER) and system performance [15], [89]. Eventually, upper limit for the maximum number of simultaneous users at any given BER will be reached – a property known as ‘soft blocking’. Analyses have shown that MAI is still the dominant effect, even when an optical beat noise among optical pulses of the same wavelength from different users is taken into account [190]. Research efforts to reduce MAI in OCDMA systems include development of novel coding schemes as well as hardware techniques that either help to reduce MAI or provide improved performance in the presence of MAI [178].

Several techniques have been proposed for MAI reduction for use in OCDMA systems. Some examples are: "optical time gating" and "optical thresholding" of the recovered autocorrelation peak. These techniques have the advantage of being compatible with a wider family of codes and are also suitable for ultrahigh data rates [1]. Another method for suppressing MAI in the OCDMA system using 2D-WH/TS OCDMA codes generated using fibre Bragg grating encoders was demonstrated [191]. However, in general, when "cleaning" the autocorrelation, it should be kept in mind that approaches used for reduction of MAI in the time domain have their limitations such as a finite extinction ratio of sampling gates and a crosstalk produced by MAI pulses in adjacent chips to the autocorrelation peak [87]. In the wavelength domain, crosstalk from adjacent wavelength channels can also lead to spreading of the energy over the bit period in the time domain. The all-optical thresholder was demonstrated to select and pass the autocorrelation signal as the highest intensity peak while rejecting the MAI as the lower intensity peaks [1].

I have concentrated part of my research on the topics related to time gating as the means for removing the MAI noise.

8.2 The Concept of Time Gating

The time gate opens the "time window" for the duration of $\Delta\tau$ at the bit rate $1/T$ (see Fig 8.1) at the moment when the autocorrelation peak passes. The Fourier spectrum of the time gate has discrete frequency components with the frequency interval of $1/T$ and the bandwidth of $1/\Delta\tau$. It samples only the data-bearing fraction of each bit, thereby rejecting the side lobes of autocorrelation and the interference codes that fall outside the gate interval. This operation is somewhat equivalent to narrow-bandpass filtering in the wireless CDMA [39]. Placing the optical time gate before the photodetector has a substantial advantage because the requirement for the detector bandwidth is significantly related to the bit rate of $1/T$. Autocorrelation detection without the time gate would require the detector bandwidth of chip rate $1/\Delta\tau$ [33].

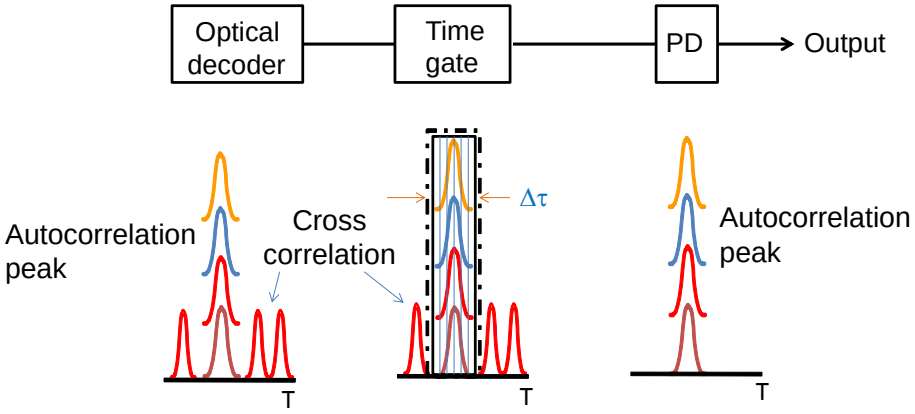

Fig. 8.1 Concept of OCDM autocorrelation filtering using a picosecond time gate [169]

Optical time gating to suppress MAI in OCDMA has been implemented and reported [44], [88], [192], [193]. The optical time gate implementation improved the obtained BER and the system power budget. Figure 8.2 shows the reported BER curves for the OCDMA system equipped with the time gate to filter out the MAI [44], [43], [194]. Comparison of both sets of BER measurements clearly shows the left-shift of the BER curve corresponding to a ~2 dB power budget improvement after applying the autocorrelation filtering time gating before the photodetection.

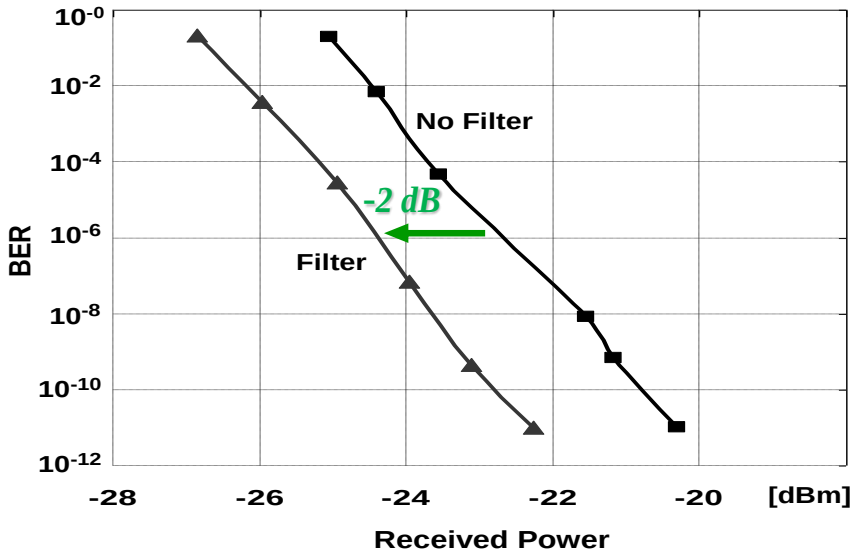

Fig. 8.2 BER measurements with and without optical time filtering to suppress MAI [43]

Examples of time gating methods in Table 8.1, based on the FBG sampler, and TOAD [193], have been shown.

Table 8.1 The summary of optical time gating/filtering using different methods

Gating Method	No. of simultaneous users in the testbed	Gating windows	Improved power budget
Sampler FBG	4	12–14 ps	~2 dB
TOAD [44]	3	2 ps	~2 dB
TOAD [88]	4	2 ps	~0.5 dB

The gate width selection is critical in achieving an optimised performance. The effectiveness of the time filtering is reduced if the gate width is larger than the autocorrelation peak [44]. Increasing the number of simultaneous users creates more cross correlation, thus generating more MAI. Under this circumstance, the possibility of MAI overlapping with the autocorrelation peak is higher, especially if the filtering window is larger in its width – resulting in overall system performance degradation.

The next step is to investigate the effectiveness of 'time filtering' as a way of boosting the number of simultaneous users in a case when the OCDMA system uses carrier-hopping prime codes. Carrier-hopping prime codes [15], [195] were proposed to increase OCDMA efficiency. System performance using 2D-WH/TS codes can be evaluated by calculating the relationship between the probability of error P_e and the number of simultaneous users K [19].

$$\boldsymbol{P_e = \frac{1}{2}\sum_{i=0}^{Th}(-1)^i\binom{w}{i}\left(1-\frac{iq}{w}\right)^{K-1}} \tag{8.2}$$

parameter q in Eq. 8.2 is given [18]:

$$q = w^2(2LNx)^{-1} \tag{8.3}$$

where Th denotes the decision threshold of the receiver and K the total number of simultaneous users in the system (for optimal system operation, Th is usually set to be equal to a code weight w). L is number of wavelengths and N is number of chips.

The parameter *x* is equal to a chip width divided by the bandwidth of the time gating window used by the OCDMA receiver.

As Eq. 8.2 indicates, the error probability improves with an increasing number of wavelengths *L* and/or with the increasing number of chips *N*. Because of the code properties, the carrier-hopping prime code – through the adjustment of the number of wavelengths, or the number of chips, or both – can deliver the targeted BER for the targeted number of simultaneous users *K*, thus providing flexibility and, at the same time, very robust system performance.

Using Eq. 8.2 and Eq. 8.3 [19], [196], a simulation was used to see the relationship between chip size and time gate size, as well as time size and the number of simultaneous users versus the probability of error. The simulated curve for the probability of error, as the number of simultaneous users increases at various time gate sizes, is depicted in Fig. 8.3. Note, that at the same error floor, the narrower time-gating window accommodates more simultaneous users as there is less cross correlation to overlap (less MAI).

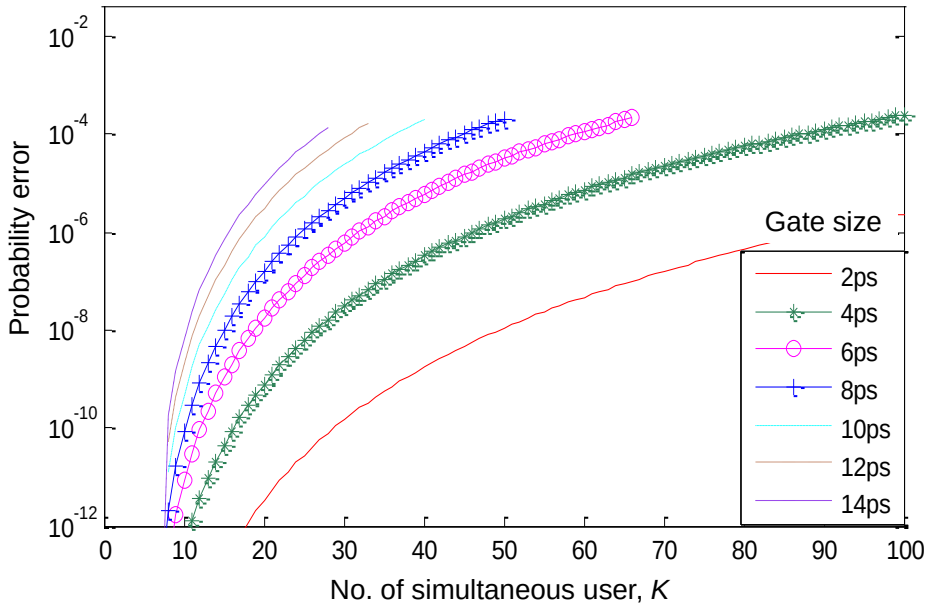

Fig. 8.3 Probability error versus number of simultaneous users for different time-gating windows

Figure 8.4 shows the simulation result when the systems adopt or withdraw time gating in order to control MAI. There is a significant effect when sampling using time-gating is implemented. At the same error floor – for example, at 10^{-9} using 8 ps sampling time gate – the number of simultaneous users can be increased by up to 13 (from 7 to 20).

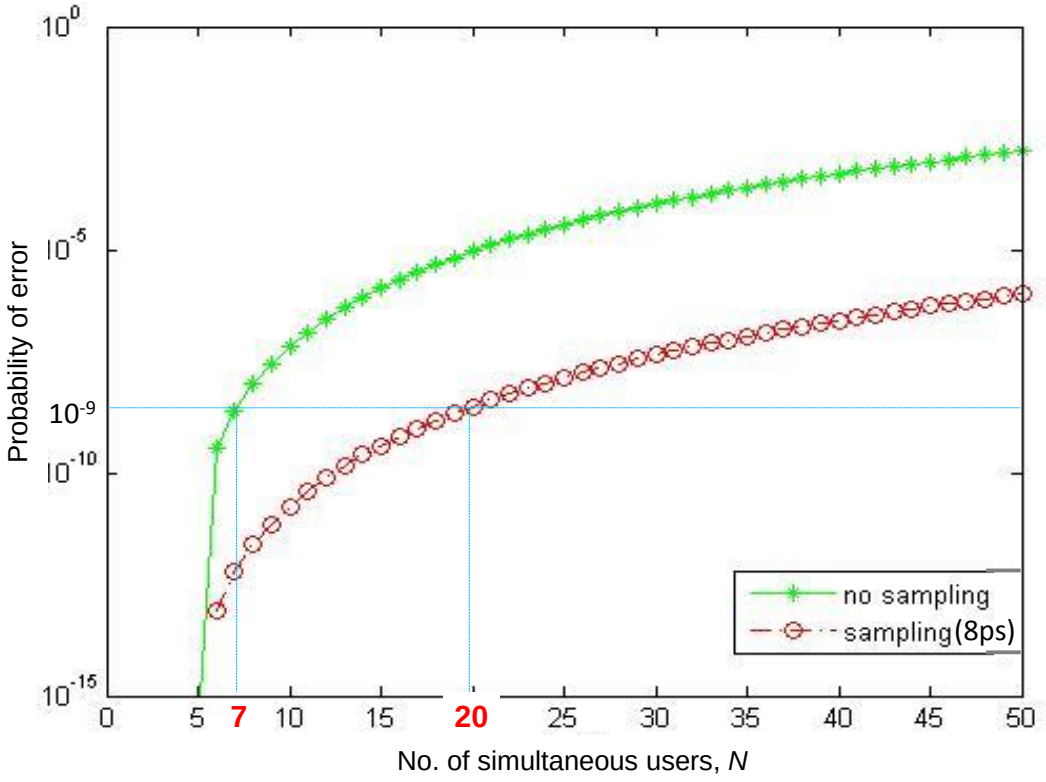

Fig. 8.4 Probability of error versus number of simultaneous users with and without 8 ps sampling time-gating

8.3 SOA-Based MZI Switch as an All-Optical Time Gate (TG)

The implementation of an all-optical picosecond time gate requires an optical clock to open and close the switching window of the time gate. Research efforts in photonic integration have led to the development of high-speed SOA-based all-optical switching devices [197], [198] with a good potential for the variety of signal processing applications including time gating [199], [200]. The semiconductor optical-amplifier-based Mach–Zehnder interferometer (SOA-MZI) is an integrated all-optical device (see Fig. 8.5) which can perform ultrafast all-optical switching applications [201]. Conceptually, the device operation is well known and quite

straightforward. The switching is achieved all-optically by inducing differential phase shifts to SOAs, each located in one arm of the MZ interferometer [197]. The carrier dynamics enable this switch to be suitable for all-optical signal processing at ultrahigh speeds [202].

Figure 8.5 is a conceptual schematic diagram of the integrated SOA-MZI switch used in this experiment (40G-2R2-ORP from CIP Photonics, Inc). In order to create the desired switching window to match the autocorrelation peak width of 8 ps, a differential delay is needed between both SOA-MZI control signals. This was set by using an optical delay line (ODL2) at the clock input port. At the switch output, an optical low pass filter, F, is deployed to block the clock and pass the received OCDMA data cleared of MAI before entering a photodetector, PD (Nortel 10 Gb/s NRZ receiver with −18 dBm sensitivity) (see Figures 8.6 and 8.7).

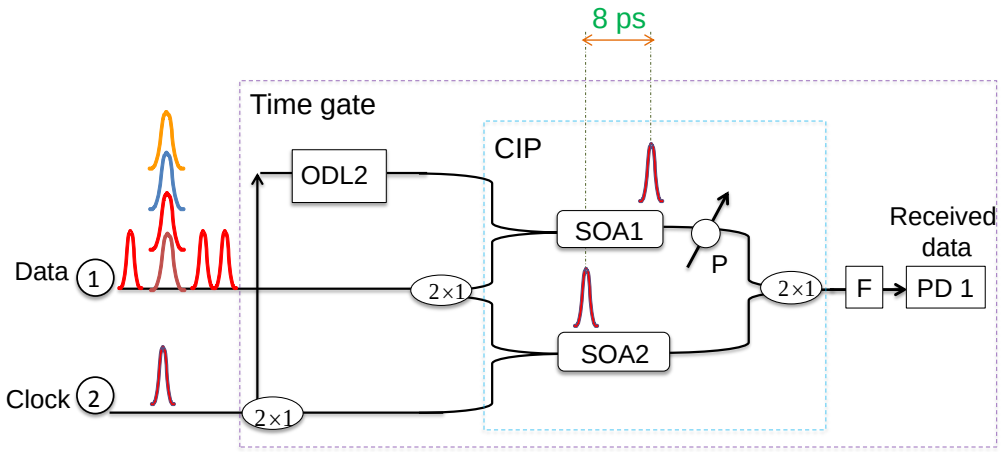

Fig. 8.5 SOA-MZI all-optical switch. SOA1 and SOA2 are semiconductor optical amplifiers, ODL – optical delay line, F – low pass filter, P – phase adjustment heating element

To implement the optical time-gating technique, an optical clock is needed to precisely control (synchronise) the position of the switching window of the time gate to allow the user-decoded OCDMA data – referred to as autocorrelation peak – to pass, while blocking the MAI – cross-correlations – that falls outside of it (see Fig. 8.1). A "dynamic" synchronisation of this time gate is needed if timing jitter is present, and in this case a clock recovery from the incoming data is the only possibility [1], [172], [173]. To implement all-optical gating in ultrahigh-speed

OCDMA networks transmitting over long distance transmissions therefore requires a self-clocked time gate. The next section demonstrates my approach for obtaining a synchronization signal using all-optical clock recovery from the incoming OCDMA data for all-optical time gate synchronization.

8.4 Self-Clocked All-Optical Time Gate for MAI Removal/ Filtering

Figure 8.6 shows the MAI removal by the time-gate controlled via local clock distribution from the RF synthesiser. However this cannot be implemented over transmission link with the timing jitter.

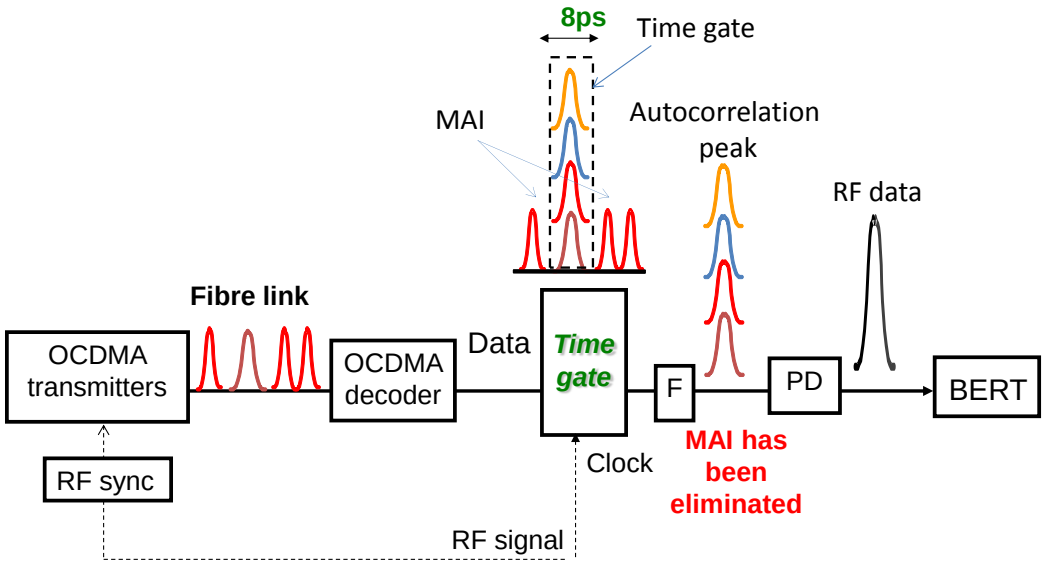

Fig. 8.6 Concept of time-gate synchronisation implemented in the laboratory using local clock distribution from the RF synthesiser.

In contrast, the concept of the time-gate using on all-optical self-clocking is depicted in Fig. 8.7. This gate could be based either on the SOA-MZI all-optical switch shown in Fig. 8.5 or could be by the one reported in [206].

In the approach shown in Fig 8.7 the User 1 OCDMA decoder first decodes the OCDMA traffic generated by OCDMA transmitters, which was sent through the bidirectional fibre link. The outcome is an autocorrelation peak (User 1 OCDMA data) and the cross correlation (MAI). The signal is then divided into two – both amplified by using EDFAs. The signal of the upper branch is sampled by the all-

optical time gate in order to filter out the MAI [44], [203] while the signal from the lower branch is used for the time-gate self-synchronisation. Here, an optical delay line (ODL1) sets proper timing between the gating window generated by the time gate and the incoming autocorrelation peak to achieve effective MAI filtering. The signal in the lower branch is used to obtain an optical clock which will control the time-gate operation. A band-pass filter (BPF) is used after the EDFA to pass the autocorrelation peak and remove the ASE.

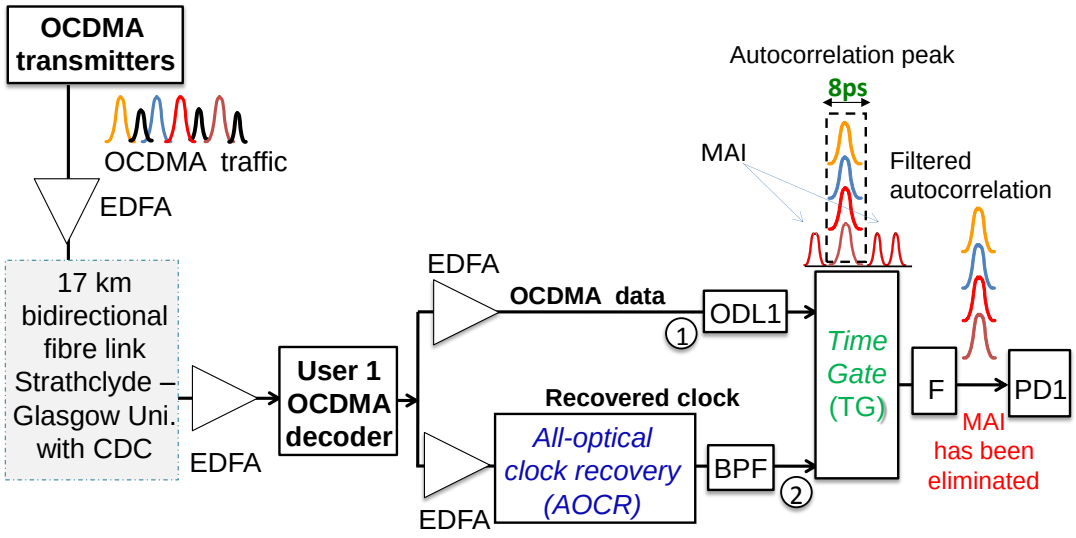

Fig. 8.7 The concept of OCDMA optical time gating with the need for AOCR for synchronisation and to open the switching window for MAI elimination where ODL1 is an optical delay line, BPF – optical bandpass filter, PD – photodetector, F – low pass filter, CDC – chromatic dispersion compensation with picosecond accuracy

8.5 Experimental Result

For the first time, experiments were conducted to test developed AOCR for its "ability" to drive an SOA-MZI all-optical time gate. As shown in Fig. 8.7, the all-optically recovered clock by AOCR was used as the control signal for the SOA-MZI all-optical time gate. The experimental results showing the MAI free autocorrelation after the time filtering by the time gate, as seen by a bandwidth-limited oscilloscope with a 64 GHz optical sampling head (Agilent 86105B), can be seen in Fig. 8.8. It shows a clean, wide-open eye diagram of the recovered autocorrelation (User 1 OCDMA data).

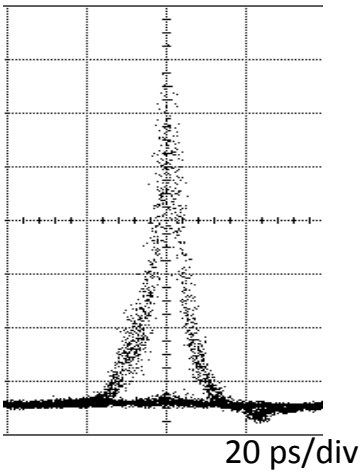

Fig. 8.8 Autocorrelation (received User 1 data) after the time filtering by a 2×2 SOA-based MZI switch used as an all-optical time gate as seen by a bandwidth-limited oscilloscope with a 20 GHz optical sampling head

8.6 Summary

Synchronisation and timing jitter are serious issues that arise when digital data are transmitted over long distances at high data rates. The results from my investigation in Chapter 7 were applied here to address these issues. An incoherent OCDMA receiver with incorporated all-optical clock recovery for self-synchronisation of a time gate for the multi-access interference (MAI) suppression, and minimising the effect of data time jitter in an incoherent OCDMA system, was successfully developed and demonstrated [65], [66], [204]. The solution was implemented and tested in a multiuser environment in an out-of-laboratory OCDMA testbed with a 2D-WH/TS coding scheme and at an OC-48 (2.5 Gb/s) data rate. The developed self-clocked all-optical time gate uses an SOA-based fibre ring-laser for optical clock recovery. Optical clock recovered all-optically from the received OCDMA traffic controls time gate's switching window for cleaning the autocorrelation peak from the surrounding MAI and timing jitter.

Apart from the all-optical clock recovery time-gate application, my contribution in this chapter is to run the analytical simulation for the probability of error versus the number of simultaneous users and time-gating windows sizes to filter out MAI.

Chapter 9: Testbed Application

9.1 Introduction

Our research group has a good relationship with the industry. The collaboration is established between our group and companies such as OSAKI and OKI from Japan. The industries provide the components or equipment to be tested and analysed. The results are then fed back to improve their performance.

In this research, 2D-WH/TS OCDMA coders from OKI were tested in our testbed. Similarly, for OSAKI, 10 GHz and 40 GHz tuneable dispersion compensators (TDC) were tested. In this chapter, the chromatic dispersion compensation using OSAKI tuneable compensators of 10 Gb/s and 40 Gb/s is investigated.

9.2 Tuneable Dispersion Compensator (TDC)

The attainment of an optical communication link is fundamentally determined by its loss and chromatic dispersion. Generally, the loss can be compensated by using an optical amplifier. With continuously increasing transmission data rates, dispersion becomes prominent and must be controlled/ eliminated, as the dispersion limitation varies inversely to square of the data rate [205], [206], [207]. Various methods were developed to compensate for the chromatic dispersion. Dispersion compensating fibre (DCF) is the most common form of dispersion management used in optical communication systems due to its wide operating bandwidth. Unfortunately, a given DCF block only has a compensation ability for a fixed length of fibre [206].

To overcome the static limitation in DCFs, a tuneable dispersion compensator (TDC) that can provide a dynamic range of compensation is needed. Dynamic dispersion compensation control is needed to offset dispersion variations due to environmental changes or variations in manufacturer network-link designs due to changes in transmission fibre span [208]. In high bit rate optical transmission systems, such as 40 Gb/s, TDC is needed in order to compensate for the chromatic dispersion fluctuations due to temperature changes or power variations [209].

At lower bit rates (10 Gb/s and below), tuneable dispersion is usually required for static trimming of the system to compensate for dispersion slope mismatch, or system reconfiguration. The need for tuneable optical dispersion compensation at 10 Gb/s is diminished. Today, TDC is primarily geared towards incoherent 40 Gb/s systems, where the cost per bandwidth is more favourable, the dispersion range is more easily realised and electronic equalisers are less practical [210].

TDC must provide positive and negative dispersion, polarisation independence, and a large tuning range [211]. Tuneable dispersion has been implemented in various platforms including fibre grating, planar waveguides, thin-film etalons, and bulk optic technologies. Most common TDC technologies exploit the frequency-dependent phase response of an optical filter. Examples include planar waveguide-based devices (such as ring resonators [212]), waveguide grating [213], [214], [215], free-space devices (such as tuneable etalons [216] and virtually imaged phased arrays (VIPA) [217]), and chirped fibre Bragg gratings (CFBG) [218] . While such devices offer an attractive means to manage dispersion variations on an optical link, they do not possess the versatility, bandwidth, bit-rate or bit-format transparency, and low loss characteristics of their widely deployed static counterparts.

9.3 OSAKI MZI-Based 10 Gb/s and 40 Gb/s TDC

Our collaborator, OSAKI, also contributed to this technology by developing MZI-based tuneable optical dispersion-compensating (TDC) modules for 10 Gb/s and 40 Gb/s WDM optical systems. They can introduce either positive or negative dispersion to balance or offset the dispersion in the transmission fibre. The proprietary TDC module is based on planar lightwave circuit (PLC) technology and can address multiple-channel or single-channel dispersion compensation in WDM system. OSAKI MZI-typed TDC modules are pigtailed with standard single-mode fibre, and controlled via an analogue RS-232 interface [219].

The used proprietary PLC technology provides a large dispersion tuning range, (ms) tuning speed, colourless operation, high reliability and is compact in size. The applications include long haul or ultra-long haul, METRO DWDM, submarine

optical transmission system, and pre and post compensation. The key features for 10 Gb/s and 40 Gb/s TDC modules are summarised in Table 9.1.

The OSAKI TDC module requires electronic control. The electronic board provides an analogue voltage that is proportional to the amount of dispersion needed, and two resistive heaters set the amount of dispersion compensation. A third heater is used to control the temperature of the entire chip. To achieve the full dispersion range, covering from positive to negative dispersion values, both heaters need to be operated separately [220].

Table 9.1 Optical operating specification for 10 Gb/s and 40 Gb/s OSAKI TDC [219]

Parameter	10 Gb/s	40 Gb/s	Unit
Dispersion tuning range (CD)	−2100 to 2100	−220 to 220	ps/nm
Turning speed (T)	10		ms
Tuning resolution	20	10	Ps/nm
Centre wavelength	C-band		nm
Channel spacing	100	100	GHz
Number of channel	Up to 80		
Insertion loss (IL)	≤ 8.5	≤ 8.0	dB
3 dB Transmission bandwidth	Typical infinite	Typical infinite	GHz
Dispersion bandwidth for GDR	≥ 16	≥50	GHz
Group delay ripple (GDR)	≤± 28	≤± 12	ps
Set point temperature (TEC)	65 to 95		°C
Polarisation mode dispersion (PMD)	≤ 5.0	≤ 1.0	ps
Polarisation-dependent loss (PDL)	≤ 0.3		dB

9.4 Evaluation of OSAKI TDC

The experimental setup used to evaluate chromatic dispersion compensation using the TDC technique on the Strathclyde–Glasgow University testbed is depicted in Fig. 9.1. This setup is similar to the setup in Chapter 6. The only difference is that the dispersion compensation technique used to compensate for the chromatic dispersion is now based on the OSAKI TDC, not the DCF module.

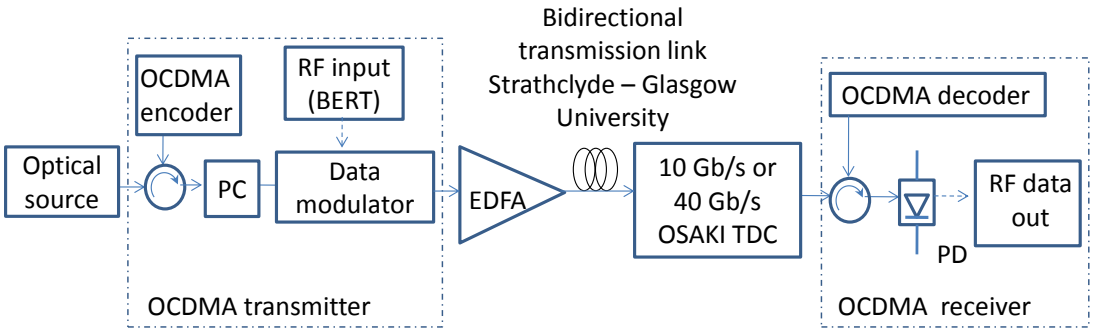

Fig. 9.1 Experimental setup of chromatic dispersion compensation using OSAKI TDC

In the evaluation, the transmitter generates 2D-WH/TS OCDMA codes based on multicolour ps pulses at OC-48. The return signal is then post compensated using either DCF or a 10 Gb/s or 40 Gb/s TDC. The compensated signal is then decoded using an OCDMA decoder, and the decoded output is monitored (see Fig. 9.2) by a bandwidth-limited oscilloscope with an optical sampling head of 64 GHz (Agilent 86105B), and by an optical spectrum analyser. Figure 9.2 shows the data achieved when DCF module described in earlier Chapters was used, and this served as the benchmark to which the results using TDC will be compared.

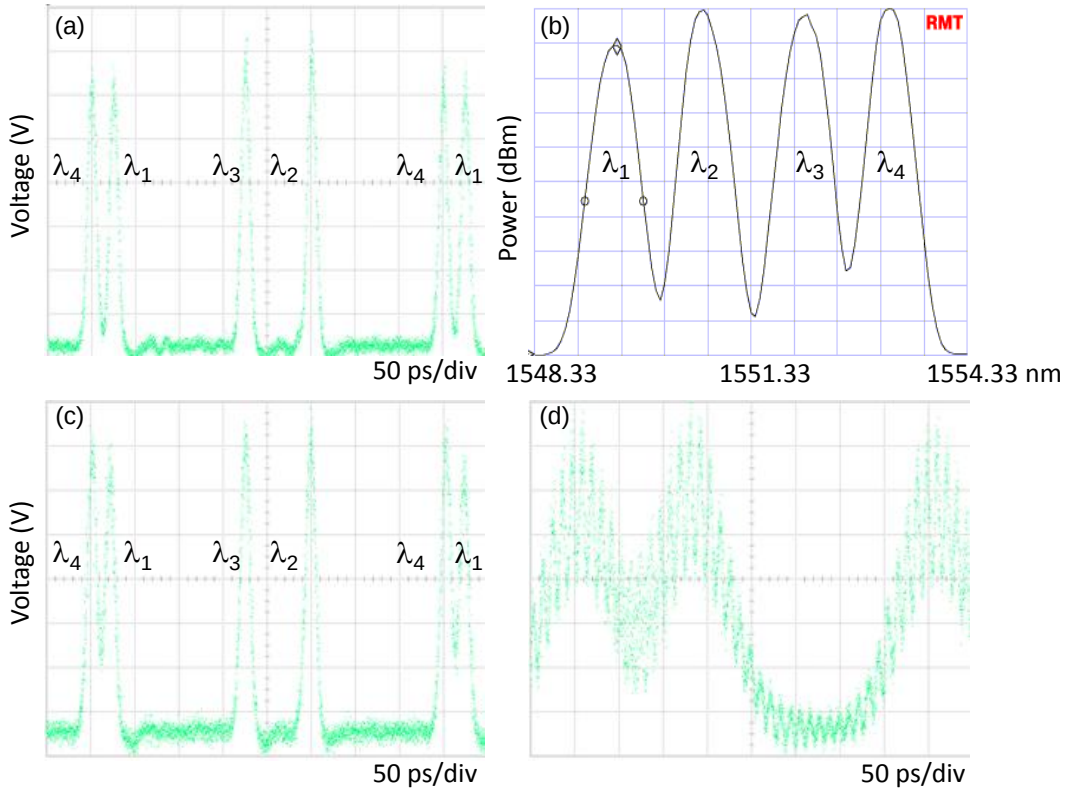

Fig. 9.2 (a) OCDMA code direct from the encoder, (b) corresponding optical spectrum for OCDMA code, (c) same as (a) after 17 km propagation after chromatic dispersion compensation using DCF, and (d) distorted OCDMA code without proper dispersion compensation. The oscilloscope reading was taken at 50 ps/div.

9.5 Evaluation of Dispersion Compensation by OSAKI TDC Module

The experiment started with the 10 Gb/s TDC module. For the 10 Gb/s TDC module, the tuning range varies from −2100 to +2100 ps/nm. First, Fig. 9.3(a) shows the OCDMA code, after being sent through the 17 km testbed while being compensated for chromatic dispersion by DCF, and its optical spectrum. Figure 9.3(b) shows the same OCDMA code and the optical spectrum when “compensated” using the OSAKI 10 Gb/s TDC module at the 0 ps/nm control setting. When the control setting is set to 0 ps/nm, it means that no dispersion compensation is applied to the signal.

Then, the dispersion has been changed from a negative to positive value in an attempt to find the signal that best matches the OCDMA code compensated by DCF in Fig. 9.3(a). The output signal is observed, and the “best/closest-match" compensation was achieved for a control setting of −550 ps/nm – as shown in Fig.

9.3(c). All was monitored using an oscilloscope with a 64 GHz sampling head (Agilent 86105B), and the readings were taken at 50 ps/div.

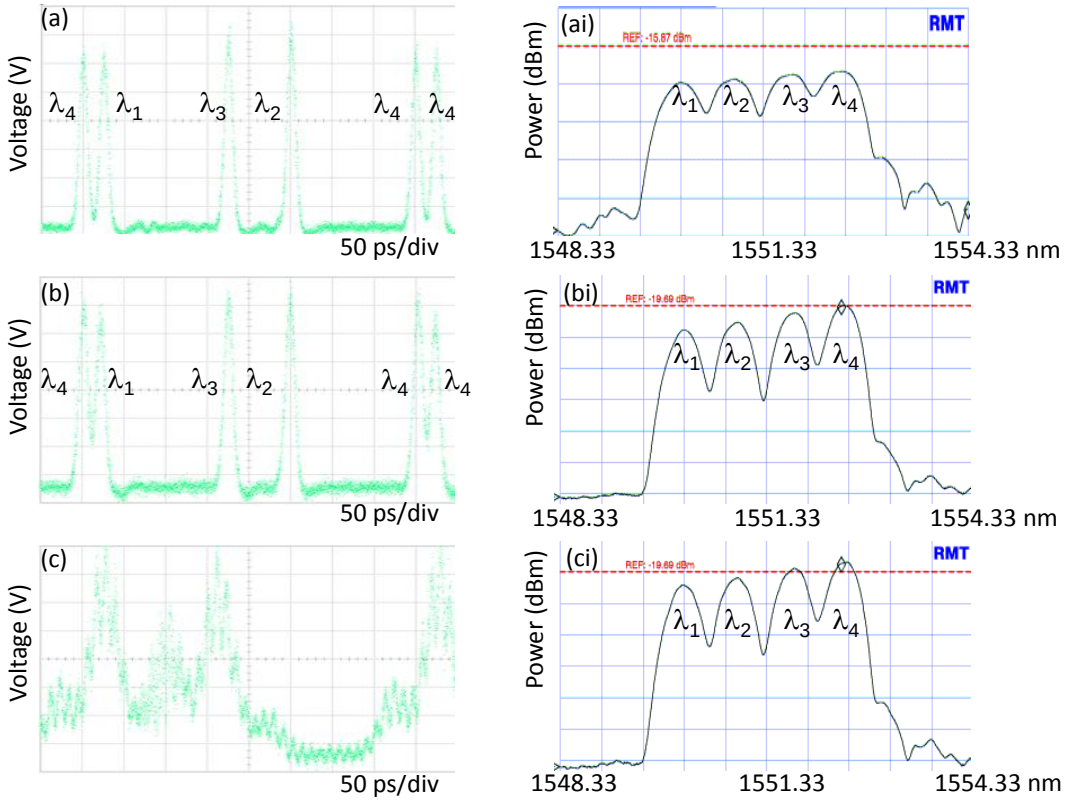

Fig. 9.3 OCDMA code and its corresponding optical spectrum after travelling 17 km in SMF-28 using (a) DCF, (b) at the control setting of 0 ps/nm, (c) at the control setting of −550 ps/nm using the OSAKI 10 Gb/s TDC – as seen by an oscilloscope with a sampling head of 64 GHz (Agilent 86105B)

The OCDMA codes were also verified using an optical spectrum analyser before and after travelling through the 17-km-long testbed – see Fig. 9.3(ai) and Fig. 9.3 (bi–ci) for a tuneable dispersion control setting of 0 ps/nm and −550 ps/nm, respectively. Four expected code wavelengths are observed within 1550 nm to 1553 nm – as should be. However, even the best matched signal I found (at a dispersion control setting of −550 ps/nm) is far from the CD compensation achieved when using DCF.

Figure 9.4 is an illustration of CD code distortion for various settings of the OSAKI 10 Gb/s TDC.

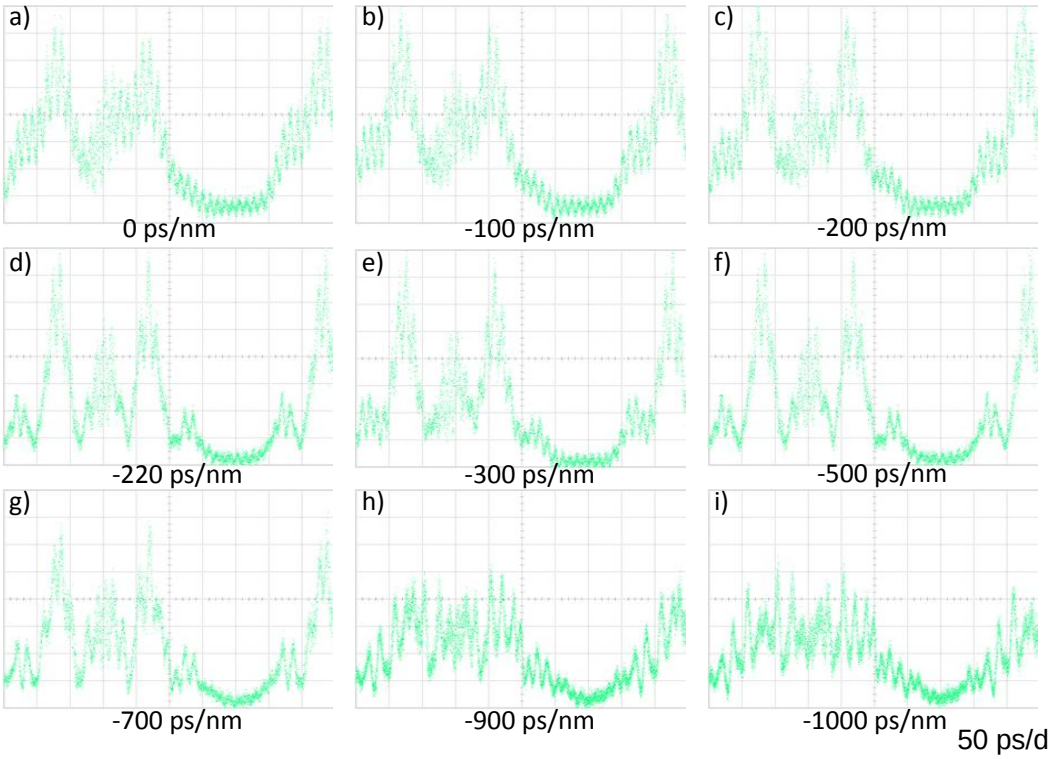

Fig. 9.4 OCDMA signal compensated using the OSAKI 10 Gb/s TDC at various dispersion control settings: (a) 0 ps/nm (b) −100 ps/nm (c) −200 ps/nm (d) −220 ps/nm (e) −300 ps/nm (f) −500 ps/nm (g) −700 ps/nm (h) −900 ps/nm and (i) −1000 ps/nm

The experiment is then repeated, but with the OSAKI 40 Gb/s TDC. The tuning range for this device is within −220 to 220 ps/nm. The summarised results are depicted in Fig. 9.5. Similar to the OSAKI 10 Gb/s TDC, both, OCDMA code and its corresponding optical spectrum were compared to the compensation results by DCF and shown in Fig. 9.5(a) and Fig. 9.5(ai).

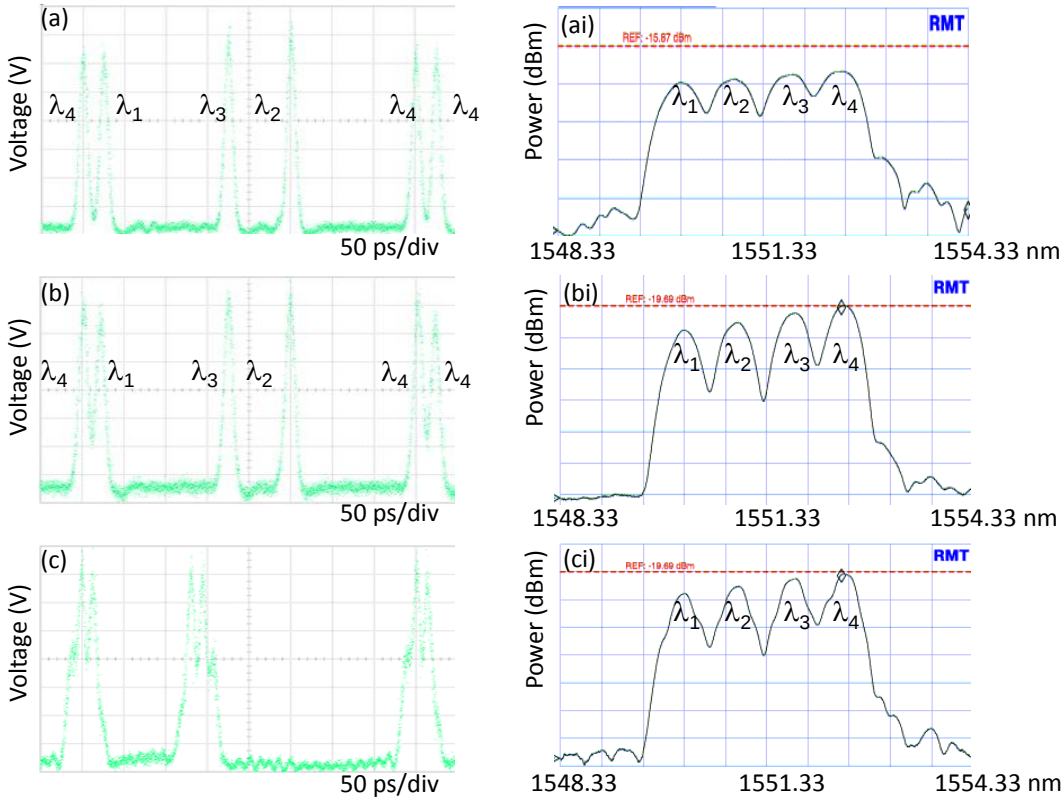

Fig. 9.5 OCDMA code and its corresponding optical spectrum after travelling 17 km in SMF-28 using: (a) DCF and the OSAKI 40 Gb/s TDC, (b) output signal at the control setting of 0 ps/nm, (c) the best matching signal achieved at the control setting of −220 ps/nm

Figure 9.5(b) shows the OCDMA code and its optical spectrum being compensated using the OSAKI 40 Gb/s TDC module at a 0 ps/nm control setting. Figure 9.5(c) shows the code after travelling 17 km in SMF-28 at the minimum TDC control setting of −220 ps/nm (this control setting was the "best-match"). The corresponding optical spectrum is depicted in Fig. 9.5(bi) and Fig. 9.5(ci). It can be seen that even the 40 Gb/s TDC module is not able to compensate for chromatic dispersion of OCDMA code which is based on ps multicolour pulses.

Figure 9.6 illustrates the OCDMA code – indicating for a negative setting from 0 ps/nm to −220 ps/nm.

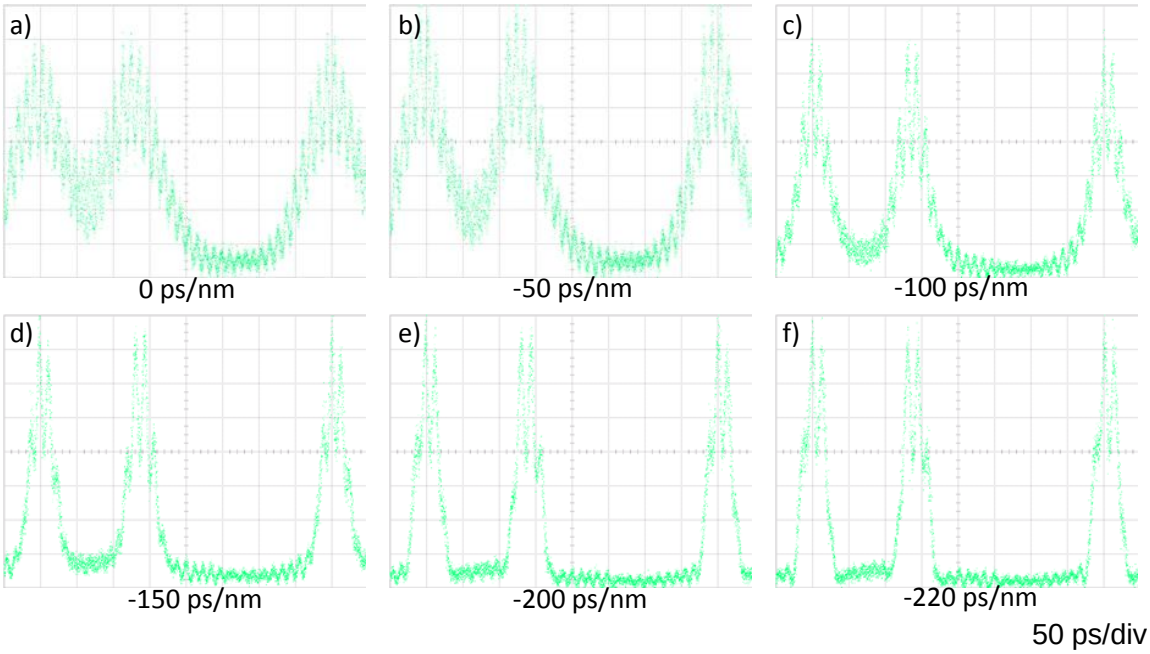

Fig. 9.6 OCDMA signal compensated using the OSAKI 40 Gb/s TDC at various dispersion control settings: (a) 0 ps/nm (b) −50 ps/nm (c) −100 ps/nm (d) −150 ps/nm (e) −200 ps/nm (f) −220 ps/nm

Figure 9.7 illustrates results obtained for positive dispersion between 6.7 ps/nm and 8.2 ps/nm.

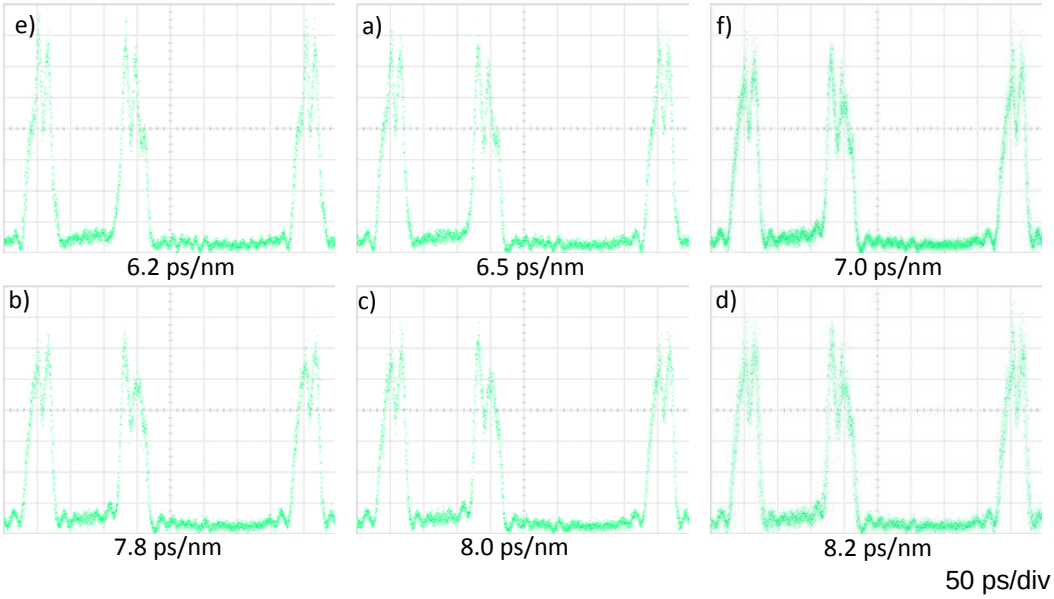

Fig. 9.7 OCDMA signal compensated using the OSAKI 40 Gb/s TDC at various positive dispersion settings: (a) 6.2 ps/nm (b) 6.5 ps/nm (c) 7.0 ps/nm (d) 7.8 ps/nm (e) 8.0 ps/nm (f) 8.2 ps/nm

9.6 Summary

Based on my research I found that neither the 10 Gb/s TDC nor 40 Gb/s TDC have enough spectral bandwidth to support the OCDMA transmission based on multicolour picosecond pulses. Discussions with OSAKI confirmed that their devices are not yet being designed to support narrow multicolour ps pulses even if used for data transmissions as low as OC-48 (~2.5 GHz) data rates.

My contributions in this chapter include the design and implementation of the experimental setup for testing and investigation of the OSAKI 10 Gb/s and 40 Gb/s TDCs in application with multicolour ps optical pulses.

Chapter 10: Conclusion and Future work

10.1 Conclusion

As the demand for broadband services continues to grow, it becomes necessary for service providers to keep increasing the capacity of their optical data networks. While this is certainly the case for backbone networks, current access networks (still predominantly "copper" based) are limited in terms of "speed-transmission distance" product they can achieve. Optical networks are therefore required to move closer to the end user. The success of CDMA in cellular networks has resulted in great amount of interest and subsequent research has translated the RF multiplexing technique from radio frequency domain to optical networks. Optical CDMA offers a number of inherent advantages which will particularly benefit optical access networks mainly by better cost efficiency, high degree of flexibility, scalability and reconfigurability. These advantages made OCDMA a suitable player in accessing networks.

Despite the fact that OCDMA systems have been investigated worldwide, field trials and out-of-the laboratory experimental demonstrations are still limited. My goal was to make a significant contribution to this area. My research motivation was also to investigate the implementation and application of optical and all-optical switching to improve incoherent OCDMA system performance in field trials. To do that I have first designed, built and then investigated chromatic dispersion of the fibre optic testbed I have built between CIDCOM laboratory in University of Strathclyde and the University of Glasgow.

Different technologies for implementing 2D-WH/TS OCDMA codes were investigated in Chapter 2. WH/TS code approaches provide many promising features for next-generation access networks. These include asynchronous access and support for multiple traffic types that either require different bit rates or quality of service. The soft limit governing the number of simultaneous OCDMA network users offers graceful degradation of performance, while allowing the network size to grow. It is arguable if 2D-WH/TS code-based systems shown in Chapter 2 will provide a higher utilisation in access networks.

Chromatic dispersion has been discussed in Chapter 3 as the significant impairment factor, which affects the 2D-WH/TS incoherent OCDMA code with multicolour picosecond pulses. Then, Chapters 4–6 relate to fibre optic testbed investigations of chromatic dispersion compensation implementation, including the effect of residual chromatic dispersion and data transmission. Chromatic dispersion strongly affects incoherent OCDMA systems. This effect becomes more severe if narrow picosecond pulses are used for OCDMA code generation. Fundamental experiments were conducted to study these effects using Strathclyde–Glasgow University testbed. Different pulse sources (mode locked fibre laser and OCDMA encoder) were used to study these effects. The effect of chromatic dispersion on pulse broadening, autocorrelation peak power reduction broadening and time skewing were investigated.

The contribution in Chapter 5 is in the preparation and building of components and equipment to enable building advanced systems before testing using the testbed. OCDMA encoder/decoder transmitter and receiver terminals were designed and developed. In addition, $LiNbO_3$ data modulator, 10 GHz photodetector (PD) for optical to electrical (O/E) signal conversion and picosecond optical sampler were also built.

The experimental setup to investigate the effect of residual dispersion on picosecond laser pulses and 2D-WH/TS OCDMA codes in a single and multiuser environment including results and analysis is presented in Chapter 6. With the aid of Femtochrome autocorrelator, I have determined for the laser pulse the pulse broadening for various deviations from full chromatic dispersion. However, for the OCDMA code, where the autocorrelation peak consists of the stack of four wavelengths, pulse broadening due to residual dispersion was determined by comparing it back to back with the received peak. Roughly, 10% pulse broadening was measured due to residual chromatic dispersion. Comparing BER with multiuser OCDMA environment it was found that even small deviation from the full chromatic dispersion compensation affects the power budget. For example, the addition of 200 m of SMF-28 to fully compensated link will degrade 6 dB in the system power

budget. This means that small deviation has a great impact on the system performance as shown in my publication **[64]**.

The performance of 2D-WH/TS OCDMA codes based on multiwavelength picosecond pulses under the influence of environmental temperature changes have also been analysed for 2D-WH/TS codes after propagating in a fully dispersion-compensated fibre link **[20]**. It has been shown that temperature changes would adversely affect these codes. Because of the dynamic nature of the temperature changes, tunable compensation schemes are needed but their implementation may involve additional cost and complexity.

Other related issues affecting OCDMA systems I have studied were receiver synchronisation, time jitter and MAI. They all impact the 2D-WH/TS incoherent OCDMA code with multicolour picosecond pulses as described in Chapters 7 and 8. A method for suppressing MAI in OCDMA systems using 2D-WH/TS OCDMA codes generated using fibre Bragg grating encoders is analysed in [191]. The novel method resulted in a 1.5 dB power budget improvement. The calculations imply that using a time gate can increase the number of simultaneous users from 7 up to 20 if compare the system without time gate.

An incoherent OCDMA receiver with built-in all-optical clock recovery has been developed and successfully demonstrated in Chapter 7. OCDMA receiver with built-in AOCR was tested in field-based optical testbed using 2D-WH/TS OCDMA codes with four users over 17-km-long bidirectional fibre optical link. The all optically recovered clock was then successfully used for self-synchronisation of the picosecond SOA-based MZI optical switch used as the time gate for the suppression of MAI. I have developed and successfully demonstrated an incoherent OCDMA receiver with built-in all-optical clock recovery **[65]**. The recovered all-optical clock was then successfully used for self-synchronisation of the picosecond SOA-based MZI all-optical switch as the time gate for MAI suppression **[66]**.

The receiver with built-in all-optical clock recovery was tested by taking the BER when received data was synchronised with the all-optically recovered clock from the incoming OCDMA traffic and when an RF synthesiser was used with the generated clock. Improvement of ~7.5 dB was observed with the all-optical clock recovery approach.

The testbed was also used to test the devices from OSAKI. I have designed and implemented an experimental setup for testing and investigating OSAKI 10 Gb/s and 40 Gb/s TDC in application with short optical pulses. However, the 10 Gb/s or 40 Gb/s OSAKI devices do not have enough bandwidth to support the OCDMA transmission based on multicolour picosecond pulses. The result was sent to OSAKI.

To the best of my knowledge there are no published reports on high-precision (sub-picosecond) dispersion compensation for out-of-laboratory fibre optic transmission link for OCDMA system applications. The performance of 2D-WH/TS incoherent OCDMA codes has also not been analysed and demonstrated in out-of-laboratory environment and under the influence of physical impairment during transmission over longer distances. Developed incoherent OCDMA receiver with built-in all-optical clock recovery has been successfully demonstrated and for the first time used for the self-synchronisation of a picosecond SOA-based MZI all-optical switch as the time gate. Finally, from all the obtained results and finding, it is hoped that the work in this thesis will contribute to the development of future optical access networks.

10.2 Future Work

The impact of 2D-WH/TS codes used by the incoherent OCDMA system in field trials was demonstrated and analysed. Additional research is needed to further enhance and improve the overall system performance. Tuneable dispersion compensators are needed for high-accuracy chromatic dispersion compensation. These compensators will help stabilise the effect of temperature fluctuations thus eliminating the changing residual dispersion. Another improvement suggested is to design and develop a more compact integrated clock recovery circuit with advanced time-gating capabilities for receiver synchronisation.

References

[1] P. R. Prucnal, *Optical Code Division Multiple Access : Fundamentals and Applications*, 1st ed. Boca Raton: Taylor & Francis, 2006, p. 377.

[2] G. Kramer and G. Pesavento, “Ethernet Passive Optical Network (EPON): building a next generation optical access network,” *IEEE Communications Magazine*, pp. 66–73, 2002.

[3] M. Medard and S. Lumetta, “Architectural Issues for Robust Optical Access,” *IEEE Communications Magazine*, no. July, pp. 116–122, 2001.

[4] T. O. Ramjee Prasad, “An overview of CDMA evolution towards wideband CDMA,” *IEEE Communications SURVEYS*, vol. 57, no. 1, pp. 223–223, 2000.

[5] D. D. Sampson, G. J. Pendock, and R. A. Griffin, “Photonic Code-Division Multiple-Acess Communications,” *Fiber Integr. Opt.*, vol. 16, pp. 129–157, 1997.

[6] K. Kitayama, X. Wang, and N. Wada, “OCDMA Over WDM PON — Solution Path to Gigabit-Symmetric FTTH,” *J. Eur. Opt. Soc. Rapid Publ.*, vol. 24, no. 4, pp. 1654–1662, 2006.

[7] L. G. Kazovsky, W.-T. Shaw, D. Gutierrez, N. Cheng, and S.-W. Wong, “Next-Generation Optical Access Networks,” *J. Light. Technol.*, vol. 25, no. 11, pp. 3428–3442, Nov. 2007.

[8] P. R. Prucnal, M. A. Santoro, and T. R. Fan, “Spread spectrum fiber-optic local area network using optical processing,” *J. Light. Technol.*, vol. 4, no. 5, pp. 547–554, 1986.

[9] A. M. Weiner, J. P. Heritage, and J. A. Salehi, “Encoding and decoding of femtosecond pulses.,” *Opt. Lett.*, vol. 13, no. 4, pp. 300–2, Apr. 1988.

[10] J. A. Salehi, “Code Division Multiple-Access Techniques in Optical fiber networks- Part 1: Fundamental principles,” *IEEE Trans. Commun.*, vol. 37, no. 8, pp. 824–833, 1989.

[11] J. A. Salehi and C. A. Brackett, “Code Division Multiple-Access Techniques in Optical Fibre Networks - Part II: Systems Performance Analysis,” *IEEE Trans. Commun.*, vol. 37, no. 8, pp. 834–842, 1989.

[12] R. Fan, K. Chung, J. A. Salehi, and V. K. Wei, “Optical Orthogonal Codes : Design , Analysis and Applications,” *IEEE Trans. Inf. Theory*, vol. 35, no. 3, pp. 595–604, 1989.

[13] W. C. Kwong, P. A. Perrier, and P. R. Prucnal, “Performance Comparison of Asynchronous and Synchronous Code Division Multiple Access Techniques

for Fibre-Optic Local Area Networks," *IEEE Trans. Commun.*, vol. 39, no. 11, pp. 1625–1634, 1991.

[14] G.-C. Yang and W. C. Kwong, "Performance analysis of optical CDMA with prime codes," *Electron. Lett.*, vol. 31, no. 7, pp. 569–570, 1995.

[15] L. Tancevski and I. Andonovic, "Wavelength hopping/time spreading code division multiple access systems," *Electron. Lett.*, vol. 30, no. 17, pp. 1388–1390, 1994.

[16] E. Park, A. J. Mendez, and E. M. Garmire, "Temporal/spatial optical CDMA networks-design, demonstration, and comparison with temporal networks," *IEEE Photonics Technol. Lett.*, vol. 4, no. 10, pp. 1160–1162, Oct. 1992.

[17] L. Tancevski and I. Andonovic, "Hybrid wavelength hopping/time spreading schemes for use in massive optical networks with increased security," *J. Light. Technol.*, vol. 14, no. 12, pp. 2636–2647, 1996.

[18] L. Tancevski, I. Andonovic, M. Tur, and J. Budin, "Hybrid wavelength hopping / time spreading code division multilple access systems," *Optoelectron. IEE Proc.*, vol. 143, no. 3, pp. 161–166, 1996.

[19] G.-C. Yang and W. C. Kwong, *Prime Codes with Applications to CDMA Optical and Wireless Networks*. Norwood, MA: Artech House, 2002.

[20] T. B. Osadola, S. K. Idris, I. Glesk, and W. C. Kwong, "Effect of Variations in Environmental Temperature on 2D-WH/TS OCDMA Code Performance," *J. Opt. Commun. Netw.*, vol. 5, no. 1, p. 68, Dec. 2012.

[21] B. Aazhang and H. V. Poor, "Performance of DSISSMA Communications in Impulsive Channels - Part II: Hard-Limiting Correlation Receivers," *IEEE Trans. Commun.*, vol. 36, no. 1, pp. 88–97, 1988.

[22] J. A. Salehi, A. M. Weiner, and J. P. Heritage, "Coherent ultrashort light pulse code-division multiple access communication systems," *J. Light. Technol.*, vol. 8, no. 3, pp. 478–491, Mar. 1990.

[23] X. S. Yao, J. Feinberg, R. Logan, and L. Maleki, "Limitations on Peak Pulse Power , Pulse Width , and Coding Mask Misalignment in a Fiber-optic Code-Division Multiple-Access System," *J. Light. Technol.*, vol. 11, no. 5/6, pp. 836–846, 1993.

[24] K. Kravtsov and P. R. Prucnal, "Ultrashort Optical Pulse Detection for High-Speed Asynchronous Optical CDMA Networks," *J. Light. Technol.*, vol. 27, no. 18, pp. 4069–4075, Sep. 2009.

[25] Y.-K. Huang, B. Wu, I. Glesk, K. Kravtsov, E. E. Narimanov, and P. R. Prucnal, "Achieving physical layer security / privacy with self-wrapped

OCDM transmission," in *Proc. Military Commun. Conf., Orlando, FL, Oct.*, 2007, pp. 1–5.

[26] T. B. Osadola, S. K. Idris, I. Glesk, K. Sasaki, and G. C. Gupta, "In Situ Method for Power Re-Equalization of Wavelength Pulses Inside of OCDMA Codes," *IEEE J. Quantum Electron.*, vol. 47, no. 8, pp. 1053–1058, 2011.

[27] S. Goldberg and P. R. Prucnal, "On the Teletraffic Capacity of Optical CDMA," *IEEE Trans. Commun.*, vol. 55, no. 7, pp. 1334–1343, Jul. 2007.

[28] J. P. Heritage and A. M. Weiner, "Advances in Spectral Optical Code-Division Multiple-Access Communications," *J. Sel. Top. Quantum Electron.*, vol. 13, no. 5, pp. 1351–1369, 2007.

[29] V. Baby, C. Bres, L. Xu, I. Glesk, and P. R. Prucnal, "Demonstration of differentiated service provisioning with 4-node 253 Gchip/s fast frequency-hopping time-spreading OCDMA," *Electron. Lett.*, vol. 40, no. 12, pp. 4–5, 2004.

[30] V. Baby, I. Glesk, R. J. Runser, R. Fischer, Y. Huang, C. Bres, W. C. Kwong, T. H. Curtis, and P. R. Prucnal, "Experimental Demonstration and Scalability Analysis of a Four-Node 102-Gchip/s Fast Frequency-Hopping Time-Spreading Optical CDMA Network," *IEEE Photonics Technol. Lett.*, vol. 17, no. 1, pp. 253–255, 2005.

[31] R. Adams and L. R. Chen, "Effect of encoder-decoder mismatch due to wavelength and time misalignments on the performance of two-dimensional wavelength-time optical code-division multiple access systems.," *Appl. Opt.*, vol. 44, no. 20, pp. 4368–4374, Jul. 2005.

[32] R. M. H. Yim, L. R. Chen, and J. Bajcsy, "Design and Performance of 2-D Codes for Wavelength-Time Optical CDMA," *IEEE Photonic Technol. Lett.*, vol. 14, no. 5, pp. 714–716, 2002.

[33] J. P. Sokoloff, P. R. Prucnal, I. Glesk, and M. Kane, "A terahertz optical asymmetric demultiplexer (TOAD)," *IEEE Photonics Technol. Lett.*, vol. 5, no. 7, pp. 787–790, Jul. 1993.

[34] W. C. Kwong and P. R. Prucnal, "Ultrafast all-optical code-division multiple-access (CDMA) fiber-optic networks," *Comput. Networks ISDN Syst.*, vol. 26, no. 6–8, pp. 1063–1086, Mar. 1994.

[35] I. Glesk and P. Prucnal, "Ultrafast operations in all-optical devices for communications networks," *SPIE*, pp. 2–3, 2008.

[36] I. Glesk, P. J. Bock, P. Cheben, J. H. Schmid, J. Lapointe, and S. Janz, "All-optical switching using nonlinear subwavelength Mach-Zehnder on silicon.," *Opt. Express*, vol. 19, no. 15, pp. 14031–9, Jul. 2011.

[37] A. J. Mendez, R. M. Gagliardi, H. X. C. Feng, J. P. Heritage, and J. Morookian, “Strategies for Realizing Optical CDMA for dense, high-speed, long span, optical networkApplications,” *J. Light. Technol.*, vol. 18, no. 12, pp. 1685–1696, 2000.

[38] A. J. Mendez, V. J. Hernandez, R. M. Gagliardi, S. W. Braun, C. V Bennett, and W. J. Lennon, “A WDM / Optical-CDMA (WDM / O-CDMA) Concept for Avionics Integration,” in *IEEE Conference on Avionics Fiber-Optics and Photonics, 2005.*, 2005, vol. 22, pp. 62–63.

[39] K. Kitayama, H. Sotobayashi, and N. Wada, “Optical Code Division Multiplexing (OCDM) and its applications to photonic networks,” *IEICE Trans. Fundam. Electron. Commun. Comput. Sci.*, vol. 1, no. 12, pp. 2616–2626, 1999.

[40] K. Kitayama, “Architectural considerations of radio-on-fiber millimeter-wave wireless access systems,” *1998 URSI Int. Symp. Signals, Syst. Electron. Conf. Proc. (Cat. No.98EX167)*, pp. 378–383, 1998.

[41] K. Ikeda, J. Abdul, S. Namiki, and K.-I. Kitayama, “Optical quantizing and coding for ultrafast A/D conversion using nonlinear fiber-optic switches based on Sagnac interferometer.,” *Opt. Express*, vol. 13, no. 11, pp. 4296–302, May 2005.

[42] N. Kataoka, N. Wada, X. Wang, G. Cincotti, A. Sakamoto, Y. Terada, T. Miyazaki, and K. Kitayama, “Field Trial of Duplex , 10 Gbps x 8-User DPSK-OCDMA System Using a Single 16 x 16 Multi-Port Encoder / Decoder and 16-Level Phase-Shifted SSFBG Encoder/decoders,” *J. Light. Technol.*, vol. 27, no. 3, pp. 299–305, 2009.

[43] I. Glesk, M. Sorel, A. E. Kelly, and P. R. Prucnal, “Enhancing Performance of Optical Communication Systems with Advanced Optical Signal Processing,” *J. Networks*, vol. 5, no. 11, pp. 1328–1334, Nov. 2010.

[44] I. Glesk, P. R. Prucnal, and I. Andonovic, “Incoherent Ultrafast OCDMA Receiver Design With 2 ps All-Optical Time Gate to Suppress Multiple-Access Interference,” *J. Sel. Top. Quantum Electron.*, vol. 14, no. 3, pp. 861–867, 2008.

[45] C. S. Bres, Y. K. Huang, D. Rand, I. Glesk, P. R. Prucnal, T. Bazan, C. Michie, D. Harle, and I. Andonovic, “On the Experimental Characterization of Beat Noise in 2D Time Spreading Wavelength Hopping OCDMA Systems,” *IEEE Photonic Technol. Lett.*, vol. 18, no. 21, pp. 2314–2316, 2006.

[46] N. T. Dang and A. T. Pham, “Performance analysis of incoherent multi-wavelength OCDMA systems under the impact of four-wave mixing.,” *Opt. Express*, vol. 18, no. 10, pp. 9922–33, May 2010.

[47] C.-S. Brès, I. Glesk, and P. R. Prucnal, “Tunable 2D time-wavelength optical CDMA encoder for differentiated service provisioning,” *Opt. Commun.*, vol. 271, no. 1, pp. 116–118, Mar. 2007.

[48] L. R. Chen and P. W. E. Smith, “Demonstration of Incoherent wavelength-encoding/time-spreading optical CDMA using chirped Moire gratings,” *IEEE Photonic Technol. Lett.*, vol. 12, no. 9, pp. 1281–1283, 2000.

[49] Y.-K. Huang, K. Kravtsov, I. Glesk, and P. R. Prucnal, “Integration of Dual-Code Optial CDMA Encoder and Decoder by Holographic Bragg Reflectors,” in *Proc. Opt. Fiber Commun. Nat. Fiber Opt. Eng. Conf., Anaheim, CA, Mar. 2007*, 2007, pp. 1–3.

[50] Y. Huang, V. Baby, I. Glesk, C. Bres, C. M. Greiner, D. Iazikov, T. W. Mossberg, and P. R. Prucnal, “Novel Multicode-Processing Platform for Wavelength-Hopping Time-Spreading Optical CDMA : A Path to Device Miniaturization and Enhanced Network Functionality,” *IEEE J. Sel. Top. Quantum Electron.*, vol. 13, no. 5, pp. 1471–1479, 2007.

[51] F. B. Mezger and M. Brandt-Pearce, “Dispersion limited fiber-optic CDMA systems with overlapped signature sequences,” in *Conference Proceedings LEOS’96 9th Annual Meeting IEEE Lasers and Electro-Optics Society*, 1996, vol. 2, pp. 408–409.

[52] J. Capmany and G. Mallea, “Autocorrelation pulse distortion in optical fiber CDMA systems employing ladder networks,” *J. Light. Technol.*, vol. 17, no. 4, pp. 570–578, Apr. 1999.

[53] E. K. H. Ng, G. E. Weichenberg, and E. H. Sargent, “Dispersion in multiwavelength optical code-division multiple-access systems: impact and remedies,” *IEEE Trans. Commun.*, vol. 50, no. 11, pp. 1811–1816, Nov. 2002.

[54] N. T. Dang, A. T. Pham, and Z. Cheng, “Impact of GVD on the Performance of 2-D WH/TS OCDMA Systems Using Heterodyne Detection Receiver,” *IEICE Trans. Fundam. Electron. Commun. Comput. Sci.*, vol. E92-A, no. 4, pp. 1182–1191, 2009.

[55] N. T. Dang and A. T. Pham, “Reducing the Dispersion Effects in Multiwavelength Optical CDMA Systems by Using MCM Signaling,” *J. Opt. Commun. Netw.*, vol. 2, no. 11, p. 967, Oct. 2010.

[56] C. Johnson, K. Demarest, C. Allen, R. Hui, K. V Peddanarappagari, and B. Zhu, “Multiwavelength All-Optical Clock Recovery,” *IEEE Photonic Technol. Lett.*, vol. 11, no. 7, pp. 895–897, 1999.

[57] K. Kravtsov, Y. Deng, and P. R. Prucnal, “Self-Clocked All-Optical Add / Drop Multiplexer for Asynchronous CDMA Ring Networks,” *IEEE J. Quantum Electron.*, vol. 45, no. 4, pp. 396–401, 2009.

[58] N. Karafolas and D. Uttamchandani, “Optical Fiber Code Division Multiple Access Networks : A Review,” *Opt. Fiber Technol.*, vol. 2, pp. 149–168, 1996.

[59] G. Yang and W. C. Kwong, “Two-Dimensional Spatial Signature Patterns,” *IEEE Trans. Commun.*, vol. 44, no. 2, pp. 184–191, 1996.

[60] T. B. Osadola, S. K. Idris, I. Glesk, and W. C. Kwong, “Network Scaling Using OCDMA Over OTDM,” *IEEE Photonics Technol. Lett.*, vol. 24, no. 5, pp. 395–397, 2012.

[61] V. Jyoti and R. S. Kaler, “Design and implementation of 2-dimensional wavelength/time codes for OCDMA,” *Opt. - Int. J. Light Electron Opt.*, vol. 122, no. 10, pp. 851–857, May 2011.

[62] C. H. Chua, F. M. Abbou, H. T. Chuah, and S. P. Majumder, “Performance Analysis on Phase-Encoded OCDMA Communication System in Dispersive Fiber Medium,” *IEEE Photonics Technol. Lett.*, vol. 16, no. 2, pp. 668–670, Feb. 2004.

[63] J. Yang, L. Zhang, X. Wu, O. F. Yilmaz, B. Zhang, and A. E. Willner, “All-Optical Chromatic Dispersion Monitoring for Phase-Modulated Signals Utilizing Cross-Phase Modulation in a Highly Nonlinear Fiber,” *IEEE Photonic Technol. Lett.*, vol. 20, no. 19, pp. 1642–1644, 2008.

[64] S. K. Idris, T. B. Osadola, and I. Glesk, “Investigation of All-Optical Switching OCDMA Testbed Under the Influence of Chromatic Dispersion and Timing Jitter,” *J. Eng. Technol.*, vol. 4, no. 1, 2013.

[65] S. K. Idris, T. B. Osadola, and I. Glesk, “OCDMA receiver with built-in all-optical clock recovery,” *Electron. Lett.*, vol. 49, no. 2, pp. 143–144, Jan. 2013.

[66] S. Idris, T. B. Osadola, and I. Glesk, “Towards self-clocked gated OCDMA receiver,” *J. Eur. Opt. Soc. Rapid Publ.*, vol. 8, no. 13013, pp. 13013–1 – 13013–6, 2013.

[67] G. R. Cooper and R. W. Nettleton, “A SpreadSpectrum Technique for High capacity Mobile Communications,” *IEEE Trans. Veh. Technol.*, vol. VT27, no. 4, pp. 264–275, 1978.

[68] H. J. Kochever, “Spread Spectrum Multiple Access Communications Experiment Through a Satellite,” *IEEE Trans. Commun.*, vol. COM-25, no. 8, pp. 853–856, 1977.

[69] K. S. Gilhousen, I. M. Jacobs, R. Padovani, A. J. Viterbi, L. A. Weaver, and C. E. Wheatley, “On the Capacity of a Cellular CDMA System,” *IEEE Trans. Veh. Technol.*, vol. 40, no. 2, pp. 303–312, 1991.

[70] L. B. Milstein, “Interference rejection techniques in spread spectrum communications,” *Proc. IEEE*, vol. 76, no. 6, pp. 657–671, Jun. 1988.

[71] H. Yin and D. J. Richardson, *Optical Code Division Multiple Access Communication Networks*, 1st ed. Beijing & New York: Tsinghua University Press & Springer Berlin Heidelberg, 2008, p. 382.

[72] M. Sust, “Code division multiple access for commercial communciations in Review of Radio Science,” *International Union of Radio Science (URSI)*, pp. 155–179.

[73] H. Sotobayashi, W. Chujo, and K. Kitayama, “Highly Spectral-Efficient Optical Code-Division Multiplexing Transmission System,” *IEEE J. Sel. Top. Quantum Electron.*, vol. 10, no. 2, pp. 250–258, 2004.

[74] X. Wang and K. Kitayama, “Analysis of Beat Noise in Coherent and Incoherent time-spreading OCDMA,” *J. Light. Technol.*, vol. 22, no. 10, pp. 2226–2235, 2004.

[75] A. Stok and E. H. Sargent, “The Role of Optical CDMA in Access Networks,” *IEEE Communications Magazine*, no. September, pp. 83–87, 2002.

[76] M. S. Ab-rahman, B. C. Ng, N. M. Ibrahim, and S. Shaari, “Development of Low-cost OCDMA Encoder based on Arrayed Waveguide Gratings (AWGs) and Optical Switches,” in *Worls Academy of Science and Technology 46*, 2008, pp. 657–660.

[77] K. Ohara, A. Tagami, H. Tanaka, M. Suzuki, T. Miyaoka, T. Kodate, T. Aoki, K. Tanaka, H. Uchinao, S. Aruga, H. Ohnishi, H. Akita, Y. Taniguchi, and K. Arai, “Traffic Analysis of Ethernet-PON in FTTH trial service,” in *OFC 2003*, 2003, vol. 2, pp. 607–608.

[78] S. Park, B. K. Kim, and B. W. Kim, “An OCDMA scheme to reduce multiple access interference and enhance performance for optical subscriber access networks,” *ETRI J.*, vol. 26, no. 1, pp. 1–8.

[79] E. Marom and O. G. Ramer, “Encoding-decoding Optical Fibre Network,” *Electron. Lett.*, vol. 14, no. 3, pp. 48–49, 1978.

[80] D. Zaccarin and M. Kavehrad, “An Optical CDMA System Based on Spectral Encoding of LED,” *IEEE Photonic Technol. Lett.*, vol. 4, no. 4, pp. 479–482, 1993.

[81] N. Wada and K. Kitayama, “A 10 Gb / s Optical Code Division Multiplexing Using 8-Chip Optical Bipolar Code and Coherent Detection,” *J. Light. Technol.*, vol. 17, no. 10, pp. 1758–1765, 1999.

[82] P. C. Teh, P. Petropoulos, M. Ibsen, and D. J. Richardson, “A Comparative Study of the Performance of Seven- Encoders and Decoders Based on Superstructured fiber Bragg gratings,” *IEEE J. Light. Technol.*, vol. 19, no. 9, pp. 1352–1365, 2001.

[83] C. Tian, Z. Zhang, M. Ibsen, P. Petropoulos, and D. J. Richardson, “A 16-Channel Reconfigurable OCDMA/DWDM System Using Continuous Phase-Shift SSFBGs,” *IEEE J. Sel. Top. Quantum Electron.*, vol. 13, no. 5, pp. 1480–1486, 2007.

[84] X. Wang, N. Wada, G. Cincotti, T. Miyazaki, and K. Kitayama, “Demonstration of Over 128-Gb / s-Capacity OCDMA Using FEC and AWG-Based Multiport Optical Encoder / Decoders,” *IEEE Photonic Technol. Lett.*, vol. 18, no. 15, pp. 1603–1605, 2006.

[85] J. Y. Hui, “Pattern Code Modulation and Optical Decoding-A Novel Code-Division Multiplexing Technique for Multifiber Networks,” *IEEE J. Sel. Areas Commun.*, vol. SAC-3, no. 6, pp. 916–927, 1985.

[86] M. R. Kumar, P. Ganguly, S. S. Pathak, and N. B. Chakrabarti, “Construction and Generation of OCDMA Code Families using a Complete Row-Wise Orthogonal Pairs Algorithm,” *Int. J. Electron. Commun.*, vol. 67, no. 868–874, pp. 1–8, 2013.

[87] C.-S. Bres, V. Baby, I. Glesk, L. Xu, D. Rand, and P. R. Prucnal, “Scalability of frequency-Hopping time-spreading OCDMA code matrix,” in *Conference in Laser and Electro Optics (CLEO)*, 2004, p. CWH7.

[88] I. Glesk, V. Baby, C. Bres, L. Xu, D. Rand, and R. P. Paul, “Experimental demonstration of a 2 . 5Gbps incoherent 2D OCDMA system,” *Acta Phys. Slovaca*, vol. 54, no. 3, pp. 245–250, 2004.

[89] L. Xu, I. Glesk, V. Baby, and P. R. Prucnal, “Multiple access interference (MAl) noise reduction in a 2D optical CDMA system using ultrafast optical thresholding,” in *Lasers and Electro-Optics Society,. LEOS 2004*, 2004, pp. 591–592.

[90] C. F. Lam, “To spread or not to spread: The myths of Optical CDMA,” in *IEEE LEOS annual meeting*, 2000, pp. 810–811.

[91] I. Glesk, V. Baby, C.-S. Bres, Y.-K. Huang, and P. R. Prucnal, “Performance enhancement of optical CDMA systems using ultrafast all-optical sampling,” *IEEE Conf. Avion. Fiber-Optics Photonics, 2005.*, pp. 58–59, 2005.

[92] V. Baby, D. Rand, C. Brès, I. Glesk, and P. R. Prucnal, “Incoherent Optical CDMA Systems,” in *optical code division multiple access : fundamental and applications*, 1st ed., P. R. Prucnal, Ed. Boca Raton: Taylor & Francis and CRC Press, 2006, pp. 199–240.

[93] N. Minato, H. Tamai, A. Iwamura, K. Satoko, S. Kobayashi, K. Sasaki, and A. Nishiki, “Demonstration of 10 Gbit/s-Based Time-Spreading and Wavelength-Hopping Optical-Code-Division-Multiplexing Using Fiber-Bragg-Grating En/Decoder,” *IEICE Trans Commun (Inst Electron Inf Commun Eng)*, vol. E88-B, no. 10, pp. 3848–3854, 2005.

[94] Y. Zhang, H. Chen, Z. Si, H. Ji, and S. Xie, “Design of FBG En / Decoders in Coherent 2-D Time-Wavelength OCDMA Systems,” *IEEE Photonic Technol. Lett.*, vol. 20, no. 11, pp. 891–893, 2008.

[95] V. Baby, D. Rand, C.-S. Brès, L. Xu, I. Glesk, and P. R. Prucnal, “Incoherent Optical CDMA Systems,” in *optical code division multiple access : fundamental and applications*, Boca Raton, 2006, pp. 199–240.

[96] G. P. Agrawal, *Fiber optic communication systems*, 3rd ed. New York: John Wiley & Sons, 2002, p. 546.

[97] M. K. Smit and C. Van Dam, “PHASAR-Based WDM-Devices :,” *IEEE J. Sel. Top. Quantum Electron.*, vol. 2, no. 2, pp. 236–250, 1996.

[98] C. Dragone, “Efficient Techniques for Widening the Passband of a Wavelength Router,” *J. Light. Technol.*, vol. 16, no. 10, pp. 1895–1906, 1998.

[99] Stamatios V. Kartalopoulos, *Introduction to DWDM Technology : Data in a rainbow*. Piscataway, New Jersey: SPIE Optical Engineering Press & IEEE Press, 2000, p. 252.

[100] S. Yegnanarayanan, A. S. Bhushan, and B. Jalali, “Fast Wavelength-Hopping Time-Spreading Encoding / Decoding for Optical CDMA,” *IEEE Photonic Technol. Lett.*, vol. 12, no. 5, pp. 573–575, 2000.

[101] Z. Knittl, *Optics of Thin Films*. Prague, Czechoslovakia: John Wiley & Sons, 1976, p. 551.

[102] H A Macleod, *Thin-Film Optical Filters*, 3rd ed. Bristol, UK: Institute of Physics Publishing Bristo; and Philadelphia, 2001, p. 667.

[103] S. Sumriddetchkajorn and K. Chaitavon, “A reconfigurable thin film filter-based 2x2 add-drop fiber-optic switch structure,” *IEEE Photonic Technol. Lett.*, vol. 15, no. 930–932, 2003.

[104] L. H. Domash, “Thin Films Sing a New Tune (Photonics Spectra | Nov 2004 | Features),” *Photonic spectra*, pp. 70–74, 2004.

[105] K. O. Hill and G. Meltz, “Fiber Bragg grating technology fundamentals and overview,” *J. Light. Technol.*, vol. 15, no. 8, pp. 1263–1276, 1997.

[106] Raman Kashyap, *Fibre Bragg Gratings*, 2nd editio. Montreal Canada: Academic Press, 2009, p. 614.

[107] J. Magné, D. Wei, S. Ayotte, L. A. Rusch, and S. Larochelle, "Experimental Demonstration of Frequency-Encoded Optical CDMA using Superimposed Fiber Bragg Gratings," in *Proc. OSA Top. Mtg. on Bragg gratings, photosensitivity, and poling*, 2003, pp. 10–12.

[108] A. Grunnet-Jepsen, A. E. Johnson, E. S. Maniloff, T. W. Mossberg, M. J. Munroe, and J. N. Sweetser, "Fibre Bragg grating based spectral encoder/ decoder for lightwave CDMA," *Electron. Lett.*, vol. 35, no. 13, pp. 1096–1097, 1999.

[109] J. H. Lee, P. C. Teh, P. Petropoulos, M. Ibsen, and D. J. Richardson, "A Grating-Based OCDMA Coding – Decoding System Incorporating a Nonlinear Optical Loop Mirror for Improved Code Recognition and Noise Reduction," *IEEE J. Light. Technol.*, vol. 20, no. 1, pp. 36–46, 2002.

[110] L. R. Chen, "flexible fiber bragg grating encoder/ decoder for hybrid wavelength-time optical CDMA," *photonic Technol. Lett.*, vol. 13, no. 11, pp. 1233–1235, 2001.

[111] N. Minato, S. Kutsuzawa, K. Sasaki, S. Kobayashi, A. Nishiki, T. Ushikubo, T. Kamijoh, Y. Kamio, N. Wada, and F. Kubota, "Field trial of time-spreading and wavelength- hopping OCDM transmission using FBG en / decoders," *Opt. Express*, vol. 14, no. 13, pp. 5853–5859, 2006.

[112] A. Othonos and K. Kalli, *Fiber Bragg Gratings: fundamentals and applications in telecommunications and sensing.*, 1st ed. Norwood: Artech House, 1999, p. 422.

[113] L. R. Chen, "Optical Code-Division Multiple-Access Enabled by Fiber Bragg Grating Technology," in *optical code division multiple access : fundamental and applications*, 1st ed., P. R. Prucnal, Ed. Boca Raton: CRC Press, 2006, pp. 111–164.

[114] H. Ben Jaafar, S. LaRochelle, P.-Y. Cortes, and H. Fathallah, "1 . 25 Gbit / s transmission of optical FFH-OCDMA signals over 80 km with 16 users," in *Proc. Opt. Fiber Commun. Conf. (OFC '01)*, 2001, pp. 8–10.

[115] N. Wada, H. Sotobayashi, and K. Kitayama, "2.5 Gbit/s time-spread/wavelength-hop Optical Code Division Multiplexing Using fiber Bragg grating with supercontinuum light source," *Electron. Lett.*, vol. 36, no. 9, pp. 815–817.

[116] A. Scherer, O. Painter, J. Vuckovic, M. Loncar, and T. Yoshie, "Photonic Crystals for Confining , Guiding , and Emitting Light," *IEEE Trans. Nanotechnol.*, vol. 1, no. 1, pp. 4–11, 2002.

[117] T. W. Mossberg, “Planar holographic optical processing devices.,” *Opt. Lett.*, vol. 26, no. 7, pp. 414–6, Apr. 2001.

[118] C. Greiner, D. Iazikov, and T. W. Mossberg, “Lithographically Fabricated Planar Holographic Bragg Reflectors,” *J. Light. Technol.*, vol. 22, no. 1, pp. 136–145, 2004.

[119] Y.-K. Huang, I. Glesk, C. M. Greiner, D. Iazkov, T. W. Mossberg, T. Wang, and P. R. Prucnal, “Single integrated device for optical CDMA code processing in dual-code environment.,” *Opt. Express*, vol. 15, no. 12, pp. 7327–34, Jun. 2007.

[120] X. Wang, T. Hamanaka, N. Wada, and K.-I. Kitayama, “Dispersion-flattened-fiber based optical thresholder for multiple-access-interference suppression in OCDMA system.,” *Opt. Express*, vol. 13, no. 14, pp. 5499–505, Jul. 2005.

[121] T. Morioka, H. Takara, S. Kawanishi, O. Kamatani, K. Takiguchi, K. Uchiyama, M. Saruwatari, H. Takahashi, M. Yamada, T. Kanamori, and H. Ono, “1 Tbit/s (100Gbit/s x 10 channel) OTDM/WDM transmission using a single supercontinuum WDM source,” *Electron. Lett.*, vol. 32, no. 10, pp. 906–907, 1996.

[122] S. Kawanishi, H. Takara, K. Uchiyama, I. Shake, and K. Mori, “3Tbit/s (160Gbit/s x 19 channel) optical TDM and WDM transmission experiment,” *Electron. Lett.*, vol. 35, no. 10, pp. 826–827, 1999.

[123] M. Gagnaire and S. Zahr, “Impairment-aware routing and wavelength assignment in translucent networks: State of the art,” *IEEE Communications Magazine*, vol. 47, no. 5, pp. 55–61, May-2009.

[124] M. Yannuzzi, E. Marin-Tordera, R. Serral-Gracia, X. Masiip-Bruin, O. González, J. Jiménez, and D. Verchere, “Modeling Physical-Layer Impairments in Multi-domain Optical Networks,” in *15th International Conference on Optical Network Design and Modeling (ONDM), 2011*, 2011, pp. 1–6.

[125] C. V. Saradhi, S. Subramaniam, and S. Member, “Physical Layer Impairment Aware Routing (PLIAR) In WDM Optical Networks : Issues and Challenges,” *IEEE Commun. Surv. Tutor.*, vol. 11, no. 4, pp. 109–130, 2009.

[126] B. Mukherjee, “All-Optical Impairment-Aware Routing,” in *Optical Network series: Optical WDM Networks*, B. Mukherjee, Ed. Springer USA, 2006, pp. 723–749.

[127] G. Keiser, *Optical communication essentials*. McGraw-Hill, 2003, p. 372.

[128] J. Liu, *Photonic devices*. Cambridge University Press, 2005, p. 1052.

[129] B. Mukherjee, *Optical WDM Network*. New York, USA: Springer New York, 2006, p. 973.

[130] R. L. Lachance, Y. Painchaud, and A. Doyle, “Fiber Bragg Gratings and Chromatic Dispersion,” in *Proc. SPIE 4833, Applications of Photonic Technology 5*, no. 418, pp. 1–8.

[131] B. Max and E. Wolf, *Principles of Optics: Electromagnetic Theory of Propagation, Interference and Diffraction of Light*, 7th ed. Cambridge University Press, 1999.

[132] B. Chomycz, *Planning Fibre Optic Networks*. New York: McGrawHill, 2009, p. 401.

[133] Govind P. Agrawal, *Nonlinear Fiber Optics*, 3rd ed. San Diego, California: CRC Press, 2001, p. 466.

[134] Casimer M. DeCusatis Carolyn J. Sher DeCusatis, *Fiber Optic Essentials*, 1st ed. San Diego, California: Elsevier Academic Press, 2006, p. 271.

[135] R. Paschotta, *Encyclopedia of Laser Physics and Technology*, 1st ed. Berlin: Wliey-VCH, 2008, p. 844.

[136] A. Sahin and A. E. Willner, “System limitations due to chromatic dispersion and receiver bandwidth for 2-D time-wavelength OCDMA systems,” in *Lasers and Electro-Optics Society,2003. LEOS 2003. The 16th Annual Meeting of the IEEE*, 2003, pp. 551–552.

[137] S. P. Majumder, a. Azhari, and F. M. Abbou, “Impact of fiber chromatic dispersion on the BER performance of an optical CDMA IM/DD transmission system,” *IEEE Photonics Technol. Lett.*, vol. 17, no. 6, pp. 1340–1342, Jun. 2005.

[138] Y. Igarashi and H. Yashima, “Dispersion Compensation for Ultrashort Light Pulse CDMA Communication Systems.,” *EICE Trans Commun (Inst Electron Inf Commun Eng)*, vol. E85-B, no. 12, pp. 2776–2784, 2002.

[139] T. Pfeiffer, M. Witte, and B. Deppisch, “High-speed transmission of broad-band thermal light pulses over dispersive fibers,” *IEEE Photonics Technol. Lett.*, vol. 11, no. 3, pp. 385–387, Mar. 1999.

[140] H. P. Sardesai and A. M. Weiner, “A Femtosecond Code-Division Multiple-Access,” *J. Light. Technol.*, vol. 16, no. 11, pp. 1953–1964, 1998.

[141] L. Grüner-nielsen, M. Wandel, P. Kristensen, C. Jørgensen, L. V. Jørgensen, B. Edvold, B. Pálsdóttir, and D. Jakobsen, “Dispersion-Compensating Fibers,” *J. Light. Technol.*, vol. 23, no. 11, pp. 3566–3579, 2005.

[142] E. A. Sharma, E. S. Singh, and E. B. Sharma, “Dispersion Compensation In Optical Communication - A Review .,” *Int. J. Comput. Technol.*, vol. 4, no. 3, pp. 742–754, 2013.

[143] S. Spolitis, V. Bobrovs, and G. Ivanovs, “Realization of Combined Chromatic Dispersion Compensation Methods in High Speed WDM Optical Transmission Systems,” *Electron. Electr. Eng.*, vol. 10, no. 116, pp. 33–38, 2011.

[144] Y. Danziger and D. Askegard, “High-ordermode fiber– an innovative approach tochromatic dispersion management that enables optical networking in longhaul high-speed transmission systems,” *Optical Networks Magazine January/February 2001*, pp. 40–50, 2001.

[145] S. L. Jansen, D. van den Borne, P. M. Krummrich, S. Spalter, G.-D. Khoe, and H. de Waardt, “Long-haul DWDM transmission systems employing optical phase conjugation,” *IEEE J. Sel. Top. Quantum Electron.*, vol. 12, no. 4, pp. 505–520, Jul. 2006.

[146] M.-J. Li and D. a. Nolan, “Optical Transmission Fiber Design Evolution,” *J. Light. Technol.*, vol. 26, no. 9, pp. 1079–1092, May 2008.

[147] M. Nishimura, “Optical fibers and fiber dispersion compensators for high-speed optical communication,” *J. Opt. Fiber Commun. Reports*, vol. 2, no. 2, pp. 115–139, Jun. 2005.

[148] B. Collings, F. Heismann, and G. Lietaert, *Reference Guide to Fiber Optic Testing*, 2nd ed., vol. 2. JDSU, 2010, p. 146.

[149] C. Corporation, “Corning ® SMF-28e + ® Photonic Optical Fiber Applications : Features :,” 2010.

[150] J. Peerlings, “Agilent: From Loss Test to Fiber Certification Fiber Characterization Today Part I: Chromatic Dispersion.”

[151] J. M. Dugan, A. J. Price, M. Ramadan, D. L. Wolf, E. F. Murphy, A. J. Antos, D. K. Smith, and D. W. Hall, “All-optical, fiber-based 1550 nm dispersion compensation in a 10 Gbit/s, 150km transmission experiment over 1310 nm optimized fiber,” in *Technical Digest of Optical Fiber Communication Conference (OFC’92),*, p. paper PD–14, pp. 367–370.

[152] C. O. Alford, T. S. Floyd, T. R. Collins, A. M. Henshaw, and E. L. Sanders, “KEW testbed simulation facility,” 1987.

[153] J C Diels, *Ultrashort Laser Pulse Phenomena*. San Diego, California: Academic Press, 1996.

[154] D. T. Reid, W. Sibbett, J. M. Dudley, L. P. Barry, B. C. Thomsen, and J. D. Harvey, “Commercial Semiconductor Devices for Two Photon Absorption Auto- correlation of Ultrashort Light Pulses,” *Appl. Opt.*, vol. 37, pp. 8142–44, 1998.

[155] Femtochrome Research, “Femtochrome Rapid scanning autocorrelator/crosscorrelator manual.” pp. 1–6.

[156] E. L. Wooten, K. M. Kissa, A. Yi-yan, E. J. Murphy, D. A. Lafaw, P. F. Hallemeier, D. Maack, D. V Attanasio, D. J. Fritz, G. J. Mcbrien, and D. E. Bossi, “A Review of Lithium Niobate Modulators for Fiber-Optic Communications Systems,” *J. Sel. Top. Quantum Electron.*, vol. 6, no. 1, pp. 69–82, 2000.

[157] I. Djordjevic, W. Ryan, and B. Vasic, “Fundamentals of Optical Communication,” in *Coding for Optical Channels*, 1st ed., no. 1, New York, USA: Springer New York, 2010, p. 433.

[158] C. Peucheret, “Direct and External Modulation of Light,” 2009.

[159] Govind P. Agrawal, *Lightwave technology : components and devices*, 1st ed. New York: Willey, 2004.

[160] Lucent Technologies, “Using the Lithium Niobate Modulator : Electro-Optical and Mechanical Connections,” 1998.

[161] R. R. Alfano, *The Supercontinuum Laser Source : fundamentals with updated references*, 2nd ed. New York: Springer-Verlag, 2006, p. 537.

[162] B. Gross and J. T. Manassah, “Supercontinuum in the anomalous group-velocity dispersion region,” *J. Opt. Soc. Am. B*, vol. 9, no. 10, p. 1813, Oct. 1992.

[163] Y. Takushima, F. Futami, and K. Kikuchi, “Generation of over 140-nm-wide super-continuum from a normal dispersion fiber by using a mode-locked semiconductor laser source,” *IEEE Photonics Technol. Lett.*, vol. 10, no. 11, pp. 1560–1562, Nov. 1998.

[164] Y. Takushima and K. Kikuchi, “10-GHz, Over 20 Channel Multiwavelength Pulse Source by Slicing Super-Continuum Spectrum Generated in Normal-Dispersion Fiber,” *IEEE Photonic Technol. Lett.*, vol. 11, no. 3, pp. 322–324, 1999.

[165] H. Sotobayashi and K. Kitayama, “325nm Bandwidth Supercontinuum generation at 10Gbit/s using dispersion flattened and non-decreasing normal dispersion fibre with pulse compression technique,” *IEEE Electron. Lett.*, vol. 34, no. 13, pp. 1336–1337, 1998.

[166] H. Sotobayashi and K. Kitayama, “Observation of phase conservation in multiwavelength binary phase shift-keying pulse-sequence generation at 10 Gbits/s by use of a spectrum-sliced supercontinuum in an optical fiber,” *Opt. Lett.*, vol. 24, no. 24, pp. 1820–2, Dec. 1999.

[167] N. S. Kim, M. Prabhu, C. Li, J. Soug, K. Ueda, and C. Allen, “100nm supercontinuum generation centered at 1483.4nm from Brilloi/Raman fiber laser,” in *Conference in Laser and Electro Optics (CLEO)*, 2000, vol. 889, no. 1995, p. 263.

[168] K. Mori, H. Takara, S. Kawanishi, M. Saruwatari, and T. Morioka, “Flatly broadened supercontinuum spectrum generated in a dispersion decreasing fiber with convex dispersion profile,” *Electron. Lett.*, vol. 33, no. 21, pp. 1806–1808, 1997.

[169] T. Okuno, M. Onishi, and M. Nishimura, “Generation of ultra-broad-band supercontinuum by dispersion-flattened and decreasing fiber,” *IEEE Photonics Technol. Lett.*, vol. 10, no. 1, pp. 72–74, Jan. 1998.

[170] J. Kim, G. A. Nowak, O. Boyraz, and M. N. Islam, “Low energy, enhanced supercontinuum generation in high nonlinearity dispersion shifted fibers,” in *Proc. Conf. Lasers and Electro-Optics (CLEO’99)*, 1999, vol. 3, pp. 224–225.

[171] J. Herrmann, U. Griebner, N. Zhavoronkov, A. Husakou, D. Nickel, J. C. Knight, W. J. Wadsworth, P. S. J. Russell, and G. Korn, “Experimental evidence for supercontinuum generation by fission of higher-order solitons in photonic fibers.,” *Phys. Rev. Lett.*, vol. 88, no. 17, p. 173901, Apr. 2002.

[172] T. Von Lerber, S. Honkanen, A. Tervonen, H. Ludvigsen, and F. Küppers, “Optical clock recovery methods: Review (Invited),” *Opt. Fiber Technol.*, vol. 15, no. 4, pp. 363–372, Aug. 2009.

[173] K. Vlachos, G. Theophilopoulos, A. Hatziefremidis, and H. Avramopoulos, “30 Gb/s all-optical clock recovery circuit,” *IEEE Photonics Technol. Lett.*, vol. 12, no. 6, pp. 705–707, Jun. 2000.

[174] Y. Su, L. Wang, A. Agarwal, and P. Kumar, “Wavelength-tunable all-optical clock recovery using a ® ber- optic parametric oscillator,” vol. 184, no. October, pp. 151–156, 2000.

[175] L. F. K. Lui, L. Xu, C. C. Lee, P. K. A. Wai, H. Y. Tam, and C. Lu, “All-Optical Clock Recovery Using Erbium-Doped Fiber Laser Incorporating an Electroabsorption Modulator and a Linear Optical Amplifier,” *IEEE Photonic Technol. Lett.*, vol. 19, no. 10, pp. 720–722, 2007.

[176] L. F. K. Lui, P. K. a. Wai, H. Y. Tam, and M. S. Demokan, “40 Gb/s all optical clock recovery based on an optical parametric oscillator with photonic

crystal fiber," *OECC/ACOFT 2008 - Jt. Conf. Opto-Electronics Commun. Conf. Aust. Conf. Opt. Fibre Technol.*, pp. 1–2, Jul. 2008.

[177] S. Zhang, F. Gomez-agis, Y. Liu, N. Calabretta, E. Tangdiongga, and H. J. S. Dorren, "Fast-synchronization and low-timing-jitter self-clocking concept for 160 Gbit/s optical time-division multiplexing transmissions," *Opt. Lett.*, vol. 35, no. 1, pp. 37–39, 2010.

[178] Y. Deng, K. Kravtsov, M. P. Fok, P. R. Prucnal, K. Sasaki, G. C. Gupta, and S. Kobayashi, "All-Optical Asynchronous Detection for a Compact Integrable Incoherent Optical CDMA System," *J. Eur. Opt. Soc. Rapid Publ.*, vol. 27, no. 23, pp. 5370–5375, 2009.

[179] J. Faucher, S. Ayotte, L. A. Rusch, S. Larochelle, and D. V Plant, "Experimental BER performance of 2D Lamda-t OCDMA with recovered clock," *Electron. Lett.*, vol. 41, no. 12, pp. 713–715, 2005.

[180] H. Takara, S. Kawanishi, T. Morioka, K. Mori, and M. Saruwatari, "100Gbit/s optical waveform measurement with 0.6ps resolution optical sampling using subpicosecond supercontinuum pulses," *Electron. Lett.*, vol. 30, no. 14, pp. 1152–1153, 1994.

[181] K. L. Hall and K. A. Rauschenbach, "All-optical bit pattern generation and matching," *Electron. Lett.*, vol. 32, no. 13, pp. 1214–1215, 1996.

[182] K. L. Hall, "40-Gbit/s optical packet buffering," in *OFC 97*, 1995, pp. 3–4.

[183] N. S. Patel, K. L. Hall, J. D. Moores, and B. S. K A Rauschenbach, Robinson, "All-optical rate conversion," in *OFC 97*, 1997, pp. 1–2.

[184] J. D. Moores, "80-Gbit/s 9-kbit optical pulse storage loop," in *OFC 97*, 1997, pp. 2–3.

[185] P. E. Barnsley, H. J. Wickes, G. E. Wickens, and D. M. Spirit, "All-optical clock recovery from 5Gb/s RZ data using a self-pulsating 1.56um laser diode," *IEEE Photonic Technol. Lett.*, vol. 3, no. 10, pp. 942–945, 1991.

[186] A. D. Ellis, K. Smith, and D. M. Patrick, "All optical clock recovery at bit rates up to 40Gbit/s," *Electron. Lett.*, vol. 29, no. 15, pp. 1323–1324, 1993.

[187] B. Sartorius, C. Bornholdt, S. Bauer, M. Mohrle, P. Brindel, and O. Leclerc, "System application of 40 GHz All-Optical Clock in a 40 Gbit/s optical 3R Regenerator," in *OFC 2000*, 2000, pp. 199–201.

[188] H. K. Lee, J. T. Ahn, M.-Y. Jeon, K. H. Kim, D. S. Lim, and C.-H. Lee, "All-optical clock recovery from NRZ data of 10 Gb/s," *IEEE Photonics Technol. Lett.*, vol. 11, no. 6, pp. 730–732, Jun. 1999.

[189] R. C. J. Smets, “All-Optical Time-Domain Demultiplexing and Signal Regeneration using 1300 nm Semiconductor Optical Amplifiers,” Universiteit Eindhoven, 1999.

[190] L. Tancevski and L. A. Rusch, “Impact of the Beat Noise on the Performance of 2-D Optical CDMA Systems,” *IEEE Comm. Lett.*, vol. 4, no. 8, pp. 264–266, 2000.

[191] T. B. Osadola, S. K. Idris, and I. Glesk, “Novel method for multi access interference suppression in multiwavelength FBG-encoded OCDMA,” in *2012 20th Telecommunications Forum (TELFOR)*, 2012, pp. 907–910.

[192] C. Brès, I. Glesk, and P. R. Prucnal, “Demonstration of an Eight-User 115-Gchip / s Incoherent OCDMA System Using Supercontinuum Generation and Optical Time Gating,” *IEEE Photonic Technol. Lett.*, vol. 18, no. 7, pp. 889–891, 2006.

[193] I. Glesk, I. Andonovic, C. Michie, P. R. Prucnal, K. Sasaki, and G. Gupta, “Improving Performance of FBG-based OCDMA System Employing All-optical Signal Processing,” in *IEEE Photonics Global (IPGC 2008) Singapore*, 2008, pp. 1–4.

[194] I. Glesk, I. Andonovic, and C. Michie, “Increasing transmission efficiency with advanced signal processing,” in *International Conference on Renewable Energies and Power Quality (ICREPQ’10) Granada*, 2010, pp. 1–4.

[195] C. Zhang, K. Qiu, and B. Xu, “Passive optical networks based on optical CDMA: Design and system analysis,” *Chinese Sci. Bull.*, vol. 52, no. 1, pp. 118–126, Jan. 2007.

[196] W. C. Kwong and G.-C. Yang, “Optical CDMA Codes,” in *optical code division multiple access : fundamental and applications*, 1st ed., P. R. Prucnal, Ed. Boca Raton: CRC Press, 2006, pp. 55–80.

[197] K. Tajima, S. Nakamura, and Y. Ueno, “Ultrafast all-optical signal processing with Symmetric Mach ± Zehnder type all-optical switches,” *Opt. Quantum Electron.*, vol. 33, no. 33, pp. 875–897, 2001.

[198] S. Nakamura, Y. Ueno, and K. Tajima, “Ultrahigh-speed optical signal processing with Symmetric-Mach-Zehnder-type all-optical switches,” in *Proceedings of All-Optical Networking: Existing and Emerging Architecture and Applications/Dynamic Enablers of Next-Generation Optical Communications Systems/Fast Optical Processing in Optical Transmission/VCSEL 2002, (IEEE/LEOSST, Quebec,Canada*, 2002, vol. 4, pp. 27–28.

[199] P. Bakopoulos, D. Tsiokos, O. Zouraraki, and H. Avramopoulos, “Compact all-optical clock and data recovery for variable length asynchronous data

packets based on integrated MZI switches," *Opt. Express*, vol. 13, no. 17, pp. 6401–6406, 2005.

[200] P. Bakopoulos, D. Tsiokos, O. Zouraraki, H. Avramopoulos, G. Maxwell, and A. Poustie, "Compact all-optical clock and data recovery for variable length asynchronous data packets based on integrated MZI switches," *Opt. Express*, vol. 13, pp. 6401–6406, 2005.

[201] I. Glesk, P. J. Bock, P. Cheben, J. H. Schmid, J. Lapointe, and S. Janz, "All-optical switching using nonlinear subwavelength Mach-Zehnder on silicon.," *Opt. Express*, vol. 19, no. 15, pp. 14031–9, Jul. 2011.

[202] H. Le Minh, Z. Ghassemlooy, and W. P. Ng, "Ultrafast All-optical Self Clock Extraction Based on Two Inline Symmetric Mach-Zehnder Switches," in *International Conference of Transparent Optical Networks 2006, (ICTON, Nottingham,*, 2006, pp. 64–67.

[203] I. Andonovic, L. Tancevski, M. Shabeer, and L. Bazgaloski, "Incoherent All-Optical Code Recognition with Balanced Detection," *J. Light. Technol.*, vol. 12, no. 6, pp. 1073–1080, 1994.

[204] S. K. Idris, T. B. Osadola, S. F. Shaukat, I. Glesk, and S. Member, "All-optical Clock Recovery for OCDMA Systems with Optical Time Gating," in *20th Telecommunications Forum TELFOR 2012*, 2012, pp. 903–906.

[205] S. Ramachandran, *Optical and Fiber Communications Reports 5: Fiber Based Dispersion Compensation*. New York, New York, USA: Springer USA, 2007.

[206] R. Jones, J. Doylend, P. Ebrahimi, S. Ayotte, O. Raday, and O. Cohen, "Silicon photonic tunable optical dispersion compensator.," *Opt. Express*, vol. 15, no. 24, pp. 15836–41, Nov. 2007.

[207] A. Rahim, S. Schwarz, J. Bruns, K. Voigt, D. I. Kroushkov, T. Mohammed, L. Zimmermann, C. G. Schäffer, and K. Petermann, "Tunable Residual Dispersion Compensator using Generalized MZIs in Silicon-on-Insulator," in *OFC/NFOEC 2012 - Conference on Optical Fiber Communication and the National Fiber Optic Engineers Conference*, 2012, pp. 11–13.

[208] S. Ramachandran, S. Ghalmi, S. Chandrasekhar, I. Ryazansky, M. F. Yan, F. V. Dimarcello, W. a. Reed, and P. Wisk, "Tunable dispersion compensators utilizing higher order mode fibers," *IEEE Photonics Technol. Lett.*, vol. 15, no. 5, pp. 727–729, May 2003.

[209] H. Kawashima and K. Nara, "Wideband Tunable Dispersion Compensator Using a 25-Stage PLC-MZI," *Furukawa Review*, no. 35, pp. 6–11, 2009.

[210] N. M. Litchinitser, M. Sumetsky, and P. S. Westbrook, “Fiber-based tunable dispersion compensation,” *J. Opt. Fiber Commun. Reports*, vol. 4, no. 1, pp. 41–85, Jan. 2007.

[211] G. Lee, “Demonstration of Optical Tunable Dispersion Compensation with a Virtually-Imaged Phased-Array Based Pulse Shaper,” university of Purdue, 2006.

[212] C. K. Madsen, “Integrated Waveguide all pass filter tunable dispersion compensators,” in *OFC 2002*, 2002, pp. 1–2.

[213] C. R. Doerr, L. W. Stulz, S. Chandrasekhar, and R. Pafchek, “Colorless tunable dispersion compensator with 400-ps/nm range integrated with a tunable noise filter,” *IEEE Photonics Technol. Lett.*, vol. 15, no. 9, pp. 1258–1260, Sep. 2003.

[214] K. Seno, “Tunable dispersion compensator consisting of simple optics with arrayed-waveguide grating and flat mirror,” *LEOS 2008 - 21st Annu. Meet. IEEE Lasers Electro-Optics Soc.*, no. 2, pp. 447–448, Nov. 2008.

[215] K. Seno, K. Suzuki, N. Ooba, K. Watanabe, M. Ishii, H. Ono, and S. Mino, “Demonstration of channelized tunable optical dispersion compensator based on arrayed- waveguide grating and liquid crystal on silicon,” *Opt. Express*, vol. 18, no. 18, pp. 777–778, 2010.

[216] B. J. Vakoc, W. V. Sorin, and B. Y. Kim, “A tunable dispersion compensator comprised of cascaded single-cavity etalons,” *IEEE Photonics Technol. Lett.*, vol. 17, no. 5, pp. 1043–1045, May 2005.

[217] G.-H. Lee, S. Xiao, and A. M. Weiner, “Optical Dispersion Compensator With > 4000-ps / nm Tuning Range Using a Virtually Imaged Phased Array,” *IEEE Photonic Technol. Lett.*, vol. 18, no. 17, pp. 1819–1821, 2006.

[218] B. J. Eggleton, A. Ahuja, P. S. Westbrook, J. A. Rogers, P. Kuo, T. N. Nielsen, and B. Mikkelsen, “Integrated tunable fiber gratings for dispersion management in high-bit rate systems,” *J. Light. Technol.*, vol. 18, no. 10, pp. 1418–1432, Oct. 2000.

[219] OSAKI, “Specifications for MZI Typed Tunable Optical Dispersion Compensating Modules,” 2008.

[220] B. HU, W. Jing, W. Wei, and R. Zhao, “Analysis Disperson Compensation with DCF based on Optisystem,” in *International Conference on Industrial and Information Systems*, 2010, vol. 6, pp. 40–43.